MOLECULAR MECHANISMS REGULATING COPPER BALANCE IN HUMAN CELLS

by
Nesrin M. Hasan

A dissertation submitted to Johns Hopkins University in conformity with the requirements for the degree of Doctor of Philosophy

Baltimore, Maryland
August 2014

Intended to be blank

ABSTRACT

Precise copper balance is essential for normal growth, differentiation, and function of human cells. Loss of copper homeostasis is associated with heart hypertrophy, liver failure, neuronal de-myelination and other pathologies. The copper-transporting ATPases ATP7A and ATP7B maintain cellular copper homeostasis. In response to copper elevation, they traffic from the *trans*-Golgi network (TGN) to vesicles where they sequester excess copper for further export. The mechanisms regulating activity and trafficking of ATP7A/7B are not well understood. Our studies focused on determining the role of kinase-mediated phosphorylation in copper induced trafficking of ATP7B, and identifying and characterizing novel regulators of ATP7A. We have shown that Ser-340/341 region of ATP7B plays an important role in interactions between the N-terminus and the nucleotide-binding domain and that mutations in these residues result in vesicular localization of the protein independent of the intracellular copper levels. We have determined that structural changes that alter the inter-domain interactions initiate exit of ATP7B from the TGN and that the role of copper-induced kinase-mediated hyperphosphorylation might be to maintain an open interface between the domains of ATP7B. In a separate study, seven proteins were identified, which upon knockdown result in increased intracellular copper levels. We performed an initial characterization of the knock-downs and obtained intriguing results indicating that these proteins regulate ATP7A protein levels, post-translational modifications, and copper-dependent trafficking. None of these proteins has been previously linked to copper homeostasis. Our studies have pointed to novel kinase inhibitors (IBTK and CAMK2N2), a novel relationship between copper transport and organic anion/bile acid transport (ABCC3), a

likely mechanism of ATP7A regulation through changes in glycosylation levels, and identified an adaptor protein (ankyrin repeat domain protein 9 (ANKRD9)) that might be involved in stabilizing the Golgi structure. ANKRD9 depletion led to increase of intracellular copper levels, Golgi fragmentation, and defects in protein glycosylation. Additionally, the mRNA and protein levels of the human copper uptake protein Ctr1 were increased significantly despite high copper levels in the cells. We are facing challenging questions related to Golgi fragmentation and copper homeostasis. Further characterization of the above-mentioned novel regulatory modes will greatly expand our understanding of copper metabolism in human cells.

Thesis advisor: Svetlana Lutsenko, Ph.D.

Thesis reader: Rajini Rao, Ph.D.

Committee Members: Ann Hubbard, Ph.D.; Rajini Rao, Ph.D.; Steven Claypool, Ph.D.

ACKNOWLEDGMENTS

Undertaking Ph.D. studies was a life changing experience for me and I would like to thank everybody who has encouraged, guided and supported me during this period.

First and foremost, I would like to thank my advisor, Dr. Svetlana Lutsenko, for accepting me to her lab and her constant support. She has been a great mentor and under her guidance I learned a lot. Her comments were of great help and her optimistic view always made me carry on with confidence. Her advice on research as well as career-related topics has been invaluable. I am grateful to her for always guiding me in the right direction and preparing me to be a good scientist.

I would like to thank my thesis committee members Dr. Ann Hubbard, Dr. Rajini Rao and Dr. Steven Claypool for their insightful comments, suggestions and advice. Special thanks to Dr. Rajini Rao for being my thesis reader and reviewing it in a short time frame.

In addition, I would like to thank past and present Lutsenko lab members that I had the chance to work together for creating a positive lab atmosphere and a collaborative environment. I truly appreciate your friendship.

Furthermore, I would like to thank the CMP program director Dr. Jan Hoh and CMP program coordinator Madeline McLaughlin for their support and assistance.

Finally, I would like to thank my parents and other family members for supporting me in all my pursuits and encouraging me throughout this experience. Since childhood, my

parents have instilled in me the importance of determination, education and hard work; which motivated me to pursue a graduate study. Special thanks to my mother for always being there for me, being understanding during stressful times and her constant encouragement.

With that, I would like to conclude with a thank you to everybody who has been a part of my Ph.D. journey.

TABLE OF CONTENTS

LIST OF TABLES

Chapter-I

Chapter-III

Chapter-VI

LIST OF FIGURES

Chapter -I

Chapter -II

Chapter -III

Chapter -IV

Chapter -VI

Chapter -VII

I. Introduction: Regulation of Copper Transporters in Human Cells

This research was originally published in Curr Top Membr. 2012;69:137-61, Regulation of copper transporters in human cells., and all text and figures in this chapter have been adapted from it.

Contributing Authors: Hasan NM, Lutsenko S.

I. Copper auto regulates its cytoplasmic levels by modulating the amounts of high affinity transporter CTR1 at the plasma membrane.

1.1. Acute regulation of CTR1 through binding and signaling.

Copper enters human cells through at least two independent pathways. The high affinity copper transporter hCTR1 is responsible for the 60-70% of total copper influx, while the remaining uptake is mediated through a low affinity transport mechanism (Lee et al., 2002). The identity of the low affinity transporter(s) remains unknown. Several candidates have been proposed (Arredondo et al., 2003; Zimnicka et al., 2011); the role of divalent metal transporter DMT1 in copper acquisition in the brain has recently been questioned (Zheng et al., 2012). Human CTR1, hCTR1, is a homotrimer with a relatively long His/Met-rich N-terminal tail exposed at the extracellular side, three transmembrane (TM) segments, and a very short cytosolic C-terminus containing the His-Cys-His motif (Kaplan and Lutsenko, 2009; Puig et al., 2007). In the vast majority of cells, hCTR1 is responsible for acquisition of copper from the blood; in intestine, it plays an essential role in a dietary copper absorption (Nose et al., 2006). Copper uptake by hCTR1 is tightly controlled: the short-term regulation is mediated via copper dependent changes in the abundance of hCTR1 at the plasma membrane (PM). Copper depletion increases the amount of hCTR1 at the PM through the recruitment from the intracellular pools (Kuo et al., 2006), whereas elevated copper induces rapid endocytosis of the transporter from the PM to vesicles (Guo et al., 2004) (Fig. 1-1).

The mechanisms through which copper triggers hCTR1 internalization and, reciprocally, the loss of copper initiates the return of hCTR1 to the PM, are unclear. Biochemical and

molecular modeling experiments revealed the presence of copper binding sites at both the extracellular and cytosolic portions of hCTR1 (De Feo et al., 2009; Haas et al., 2011; Tsigelny et al., 2012). Mutations to Ala of residues at the entrance of the transmembrane copper translocation pathway (Met150 and Met154 in the TM2) eliminate copper uptake. In contrast, mutations/deletions of Met, His, or Cys residues in the N-terminal or C-terminal tails of hCTR1, respectively, change the rates of transport (Du et al., 2012), but do not fully abolish the transport activity, pointing to the regulatory functions for the N-terminal and C-terminal copper-binding sites. The binding of copper to one or more of such regulatory sites and subsequent conformational changes in the protein (Eisses and Kaplan, 2002) are likely to be the first steps towards hCTR1 internalization. Further steps involve a clathrin-dependent pathway, as suggested by a co-localization of hCTR1 with the transferrin receptor and the inhibition of hCTR1 endocytosis by chlorpromazine and methyl-β-cyclodextrin (Petris et al., 2003).

1.2. Does low or high copper serve as a physiologically relevant signal for CTR1 trafficking?

It should be noted that most of the current evidence for hCTR1 internalization and recycling has been obtained using the recombinant over-expressed protein. There is little doubt that the recombinant hCTR1 traffics to the intracellular compartments upon exposure to copper, whereas treatment with the copper chelator (or cisplatin) stabilizes protein levels at the plasma membrane (Guo et al., 2004). Given these observations, it might be worth considering why the results of early experiments on the endogenous hCTR1 are distinctly different from those with the overexpressed protein. In cells of

various origin, the location of the endogenous hCTR1 was found to be predominantly intracellular. In addition to vesicles, the plasma membrane location was observed in HEK293 cells (Eisses et al., 2005), Caco-2 cells (Klomp et al., 2002)and in polarized Jeg-3 cells (Hardman et al., 2006). High copper did not affect the plasma membrane localization of CTR1 in any of these cells, and no obvious internalization was observed. More recently, endocytosis of recombinant and endogenous hCTR1 was examined using surface biotinylation (Molloy and Kaplan, 2009). In these experiments, partial endocytosis (20-60%) was detected for both the recombinant and endogenous hCTR1 in some, but not all cell types. Internalization of endogenous CTR1 was seen in polarized MDCK cells and in HepG2 cells; no significant internalization of hCTR1 in response to extracellular copper was detected in HeLa and T47D cells (Molloy and Kaplan, 2009).

In mouse tissues, mCTR1 is also predominantly intracellular (with a notable exception of the liver where it was immuno-detected at the plasma membrane (Hardman et al., 2006; Kuo et al., 2006; Ralle et al., 2010). In copper deficient tissues, there is a distinct upregulation and recruitment of mCTR1 to the plasma membrane, especially in the intestine (Kuo et al., 2006). High copper has an opposite effect on protein localization, but not under all circumstances. The decreased levels of mCTR1 at the PM were observed in the liver tissue with a prolonged (20 weeks) intracellular accumulation of copper (Ralle et al., 2010), whereas high dietary copper did not seem to have such an effect (Araya et al., 2012). Altogether, these observations raise an interesting possibility that under physiologically relevant conditions the distribution of CTR1 between the intracellular and PM pools is controlled by the metabolic demands of a cell (i.e. by the

need for copper for biosynthetic purposes) rather than by extracellular copper. This hypothesis would be consisted with a repeatedly observed increase in the CTR1 levels (total and at the PM) in response to copper deprivation. (Hardman et al., 2006) have also found decreased intracellular staining of CTR1 in the insulin treated Jeg-3 cells and proposed that insulin influenced the recruitment of hCTR1 to the PM through the mechanism resembling that of the glucose transporter GLUT4.

1.3. Copper sensors sites in CTR1 are probably cytosolic.

How copper levels are sensed by hCTR1 and then transferred into a signal for redistribution between cellular compartments is an interesting unresolved problem. The fact that the endogenous hCTR1 in HEK293 cells does not traffic in response to extracellular additions of copper, whereas a stably transfected hCTR1 does, suggests that the rate of copper entry and accumulation in the cytosol (which is higher in cells overexpressing hCTR1) may play an important role in triggering the internalization of the transporter. Consistent with this hypothesis, the recombinant CTR1, which lost its transport activity due to mutations of critical Met150 and Met154 (see above), does not traffic from the plasma membrane to vesicles despite the presence of the extracellular copper binding sites at the N-terminal tail (Guo et al., 2004). Finally, since hCTR1 internalization is a reversible process (i.e. copper depletion triggers the return of CTR1 to the PM) it seems that a "copper sensing" site is present at the cytosolic face of the molecule, where copper can be easily exchanged. Consistent with this idea, exposure of cells to higher copper delays the return of internalized hCTR1 to the PM (Molloy and

Kaplan, 2009), although this phenomenon could also be due to time needed to clear extra copper by the efflux systems.

1.4. Regulation of copper uptake by modulation of total levels of CTR1

The long-term regulation of hCTR1 is achieved through transcriptional/translational changes. The basal levels of CTR1 are influenced by the HIF2α transcription factor (Pourvali et al., 2012), however which proteins directly control expression of hCTR1 in response to changing copper levels or other metabolic needs is not entirely clear. Furthermore, similar to studies on CTR1 trafficking, there is some discrepancy in the literature on whether an elevated copper influences levels of CTR1 mRNA. Recent studies demonstrating that regulation of the CTR1 abundance could be affected by various metabolic factors offer potential explanation for such inconsistencies between the reports. For example, incubation of HepG2 cells in high copper results in decreased amounts of CTR1 mRNA and protein, whereas treatment with estradiol alleviates this copper effect (Arredondo et al., 2010). It is also interesting that overexpression of the exogenous CTR1 is associated with down-regulation of the endogenous CTR1 mRNA indicating a tight homeostatic control of the total hCTR1 levels (Liang et al., 2012).

The role of glutathione in regulating copper transport machinery is another intriguing finding. Overexpression of recombinant *γ*- GCSht0090, a rate-limiting enzyme in the biosynthesis of glutathione, in human lung cancer cell line is associated with a 2-3 fold increase in cellular levels of glutathione (Yamane et al., 1998). This, in turn, coincides

with an increase in the CTR1 mRNA and protein level as well as increased copper uptake (Chen et al., 2008). In another set of experiments, the expression of CTR1 was shown to be up-regulated upon copper depletion and down-regulated under replete conditions. These changes in CTR1 paralleled changes in the levels of the transcription factor Specificity protein 1 (Sp1) leading to the suggestion that Sp1 oscillations in response to copper availability regulate hCTR1 expression (Liang et al., 2012; Song et al., 2008).

Increases in the hCTR1 mRNA and protein have also been observed in a cell model of inflammation. Treatment of BV-2 microglial cells with γ-interferon resulted in a two-fold increase of the CTR1 mRNA levels, increased rates of copper uptake, and higher copper accumulation (Zheng et al., 2010). Very similar phenomena, i.e. an increase in the CTR1 mRNA along with higher copper accumulation was observed in RAW264.7 cells exposed to hypoxic conditions (4% oxygen) (White et al., 2009b). The mechanisms behind these interesting and potentially important regulatory events remain largely unexplored; however, the role of a kinase-mediated signaling appears increasingly likely. Recent study revealed an unexpected requirement for the CTR1-mediated copper uptake in signaling via the Ras/mitogen-activated protein (MAP) kinase pathway (Turski et al., 2012). In these studies, genetic inactivation of CTR1 in flies and in mouse cells as well as copper deficiency induced by metal chelation were shown to reduce the ability of the MAP kinase kinase Mek1 to phosphorylate the MAP kinase Extracellular signal regular Kinases ERK1/2, whereas Akt kinase remained unaffected (Turski et al., 2012). Surprisingly, silver (which would be expected to mimic the effects of copper) had effect similar to copper chelation, i.e. it decreased cells response to insulin, as evidenced by the

diminished ERK1/2 phosphorylation. An important finding in this set of experiments was the observation that the addition of copper to the CTR1+/+ cells did not potentiate insulin signaling, whereas the same treatment of the copper-deficient CTR1-/- cells partially restores the ability of insulin to signal via the ERK1/2 phosphorylation pathway. These results seem to imply that the CTR1 function in insulin signaling is to maintain normal cell metabolism, rather than directly deliver copper to a copper dependent kinase(s), although there is a convincing evidence for the direct Cu^{2+} binding to Mek1 kinase in vitro (Turski et al., 2012).

II. Regulation of copper export via protein trafficking and kinase-mediated phosphorylation

2.1. ATP7A and ATP7B are copper-transporting ATPases important for maintaining cellular copper homeostasis.

Human cells express two homologous copper-exporting ATPases, ATP7A and ATP7B, that transport copper across a membrane bilayer by using the energy derived from ATP hydrolysis. Both ATP7A and ATP7B belong to the P-type ATPases family, i.e. during their catalytic cycle they form a transient phosphorylated intermediate (catalytic phosphorylation) that is stimulated by binding of the exported ion, copper. ATP7A/B contains eight TM domains and several cytosolic domains (Fig. 1-2). The cytosolic N-terminal domain is composed of six metal binding domains (MBDs) that are connected by flexible loops. Each MBD binds one copper (Lutsenko et al., 1997); the binding induces conformational changes within the domain (DiDonato et al., 2000) that are

accompanied by the rearrangements of loops connecting MBD's (Bartee et al., 2009). The nucleotide binding domain (NBD), the phosphorylation (P) domain and the actuator (A) domain are central for the P-type ATPase function. The NBD and the P-domain are involved in ATP binding and hydrolysis, whereas the A-domain is required for conformational changes during ATP hydrolysis. Both the N-terminal domain and C-terminal tails of ATP7A/B are important for proper targeting of the protein. The 1-63 region of the N-terminal domain of ATP7B contains a region (F^{37}AFDNVGYE^{45}) which is involved in trans-Golgi network (TGN) retention/apical targeting (Braiterman et al., 2009), whereas the C-terminal tail contains domains/motifs important for endocytosis (Cater et al., 2006; Francis et al., 1999; Stephenson et al., 2005) and copper-responsive trafficking to apical membrane (Braiterman et al., 2011).

2.2. Localization of human copper efflux transporters is regulated.

ATP7A and ATP7B have two main localizations within cells. One compartment is the TGN where these copper-ATPases supply the copper cofactor to cuproenzymes; the other compartment is vesicles-PM, to which copper-ATPases traffic in order to remove excess copper out of the cells (Gupta and Lutsenko, 2009). Copper regulates the distribution of ATP7A and ATP7B between these two locations. In basal or low copper, the TGN is the primary site for the localization and function of copper-ATPases; in high copper the transporters exit the TGN and relocate to vesicles, which eventually fuse with the PM. This copper regulated trafficking of ATP7A/7B is important for maintaining a cellular copper homeostasis. Despite its central role, the exact mechanism of ATP7A/7B trafficking between cellular compartments remains only partially characterized. It has

been established that both ATP7A/7B undergo kinase-mediated phosphorylation and the level of phosphorylation is copper-dependent and reversible. Therefore, the kinase-mediated phosphorylation of ATP7A/7B is likely an important regulatory step for trafficking of ATP7A/7B and/or for modulation of their copper-transport function.

2.3. *Both copper-ATPases are phosphorylated on multiple sites.*

Biochemical and mass-spectrometry (MS) experiments suggest that both ATP7A and ATP7B are phosphorylated by kinases on serine residues (Vanderwerf et al., 2001; Vanderwerf and Lutsenko, 2002; Voskoboinik et al., 2003). The level of kinase-mediated phosphorylation is linked to the intracellular localization of copper-ATPases. Under basal conditions, while in TGN, ATP7A/B are basally phosphorylated. Upon copper elevation, the kinase mediated phosphorylation increases, and this coincides with the trafficking of ATP7A/B to vesicles. Return to the basal media or copper depletion with chelators triggers trafficking back to the TGN. In parallel, the regulatory phosphorylation of ATP7A/7B reverts to its basal levels; suggesting that copper-dependent phosphorylation might be required for either exit from the TGN or retention in vesicles (Vanderwerf et al., 2001; Voskoboinik et al., 2003).

The identification of phosphorylation sites is necessary for determining the precise physiological role of ATP7A/7B phosphorylation. The in-cell and in vitro studies indicate that more than one residue is phosphorylated in either ATP7A or ATP7B (Pilankatta et al., 2009; Vanderwerf et al., 2001; Voskoboinik et al., 2003). For ATP7B, it has been shown that the copper-responsive phosphorylation occurs at different site(s) than the

basal phosphorylation site(s) and different regions of the protein are involved in these events (Vanderwerf et al., 2001). The C-terminal tail and the N-terminal domain of ATP7B are not required for basal phosphorylation, indicating that at least some of the basal phosphorylation site(s) are located in the Ser 796-Tyr 1384 region of ATP7B. On the other hand, the copper-induced phosphorylation requires the presence of the N-terminal domain (Vanderwerf et al., 2001), which is a target of phosphorylation both in vitro and in cells. MS analysis of the in vitro phosphorylated N-terminal domain of ATP7B pointed to the loop connecting MBD3-MBD4 as a site for the kinase mediated phosphorylation (Bartee et al., 2009). Other putative copper-responsive phosphorylation sites were identified by MS analysis of the full-length ATP7B expressed in mammalian cells (Table 1-1): these sites are located in the N-terminal domain (Ser 478 and Ser 481), the nucleotide-binding domain (Ser 1121) and the C-terminal tail (Ser 1453) (Pilankatta et al., 2009; Pilankatta et al., 2011).

Similar to ATP7B, ATP7A has multiple phosphorylation sites. Residues associated with basal and copper-induced phosphorylation have been mapped to the N-terminal domain and the C-terminal tail of ATP7A (Veldhuis et al., 2009). Several other phosphosites/phosphopeptides have been identified by the MS analysis and the results are summarized in Table 1-2 (Fedjaev et al., 2012; Huttlin et al., 2010; Lundby et al., 2012; Monetti et al., 2011). Despite these important advances, it remains unclear which, if any, of these sites represent primary targets of phosphorylation, and how stoichiometry of phosphorylation is regulated in response to changing copper levels. Mutation of two putative phosphorylation sites revealed that the corresponding ATP7A variants,

ATP7A^{S1469A} and ATP7A^{S1432A}, have different intracellular localization, indicating that phosphorylation may have different consequences even when residues are located in the same domain (Veldhuis et al., 2009). At the same time, different signaling events may yield phosphorylation of the same region/sites triggering trafficking response similar to that induced by copper. For example, treatment of placental Jeg-3 cells with insulin stimulates ATP7A exit from the TGN and, interestingly, down-regulates the ATP7B protein levels resulting in lower copper levels in cells (Hardman et al., 2006). In those earlier studies, the mechanism of insulin action was not explored. However, more recent studies using the large-scale mass-spectrometry identified numerous liver proteins phosphorylated following insulin signaling, including ATP7A and ATP7B. The residues phosphorylated in response to insulin were found in regions that were also known to be phosphorylated in response to changing copper level (Tables 1-1 and 1-2). How different signaling pathways intersect and interact with each other is a complex and fascinating question for further studies.

Several studies have been done to identify the kinases involved in the phosphorylation of ATP7A and ATP7B. Protein kinase D (PKD) (Pilankatta et al., 2011) and casein kinase II (Vanderwerf et al., 2001) were suggested to be involved in kinase mediated phosphorylation of ATP7B. In contrast, PKD does not seem to affect ATP7A, whereas Protein Kinase A and Rho GTPase Cdc 42 were implicated in ATP7A anterograde trafficking (Cobbold et al., 2002).

2.4. Copper-induced trafficking of ATP7B depends on the conformational state of the transporter.

The cytosolic copper chaperone Atox1 was shown to transfer copper to the regulatory metal binding domains (MBDs) of the Cu-ATPases and regulate their occupancy (Walker et al., 2004). Current data indicate that copper binding to N-terminal domain of both ATP7A and ATP7B is necessary for their copper-responsive phosphorylation (Vanderwerf et al., 2001; Veldhuis et al., 2009; Voskoboinik et al., 2003). Upon binding, copper induces rearrangements of the loops connecting MBDs in the N-terminal domain of ATP7B and also facilitates phosphorylation by a kinase; suggesting that conformational changes due to copper binding might be important in the exposure of additional phosphorylation sites (Bartee et al., 2009). An ATP7A mutant which can not bind copper (due to mutation of CxxC in MBDs to SxxS) (Strausak et al., 1999) has a basal level of phosphorylation, but shows no increase in phosphorylation upon copper treatment and no trafficking (Voskoboinik et al., 2003).

The Wilson disease causing mutant $ATP7B^{G591D}$ is mislocalized to the endoplasmic reticulum (ER) under basal conditions (de Bie et al., 2007) and has a basal level of phosphorylation but no copper-induced phosphorylation (Vanderwerf et al., 2001). Similarly, the $ATP7B^{R875}$ variant is also localized in ER under basal/copper-depleted conditions and is basally phosphorylated (Hasan et al., 2012). These findings indicate that the basal phosphorylation of ATP7B occurs early in the secretory pathway (presumably in the ER). The difference between $ATP7B^{G591D}$ and $ATP7B^{R875}$ is that $ATP7B^{R875}$ binds copper and under elevated copper conditions traffics to vesicles, which

is also coupled with the increase in the kinase mediated phosphorylation (Hasan et al., 2012).

2.5. The sequence of events associated with the TGN exit/trafficking of copper-ATPases

It is not yet clear how hyperphosphorylation and trafficking are linked, or which occurs first. Copper binding to the regulatory N-terminal domain of ATP7A/7B might expose additional phosphorylation sites and the addition of a negative charge (hyperphosphorylation) may induce further structural changes necessary for the exit from the TGN. Alternatively, copper binding to the ATPase and the subsequent structural changes may enable protein sorting within the TGN/interaction with the trafficking machinery, whereas hyperphosphorylation may be a result of the relocalization of ATP7A/7B to the correct compartment in which kinase(s) might be present.

Several sets of data support the important role of copper induced structural changes in the initiation of ATP7B exit from the TGN. Copper binding not only influences the rearrangement of the N-terminal domain of ATP7B, but also alters the domain-domain interactions within the entire ATP7B molecule. Relative to the copper-free form, copper-bound N-terminal domain interacts poorly with the NBD (Tsivkovskii et al., 2001), but strongly with the A-domain (Gupta et al., 2011). Since copper binding to the N-terminus of ATP7B alters the inter-domain contacts, the increased phosphorylation might be a result of the exposure of additional phosphorylation sites in more than one domain.

An alternative model is that the stabilization of ATP7B in a distinct conformational state is sufficient to cause its trafficking from TGN to vesicles. This model is supported by the observation that mutating residues that are not directly involved in copper binding may significantly alter the targeting and trafficking of ATP7B. The mutant ^{858}TGE^{860}>AAA, which is catalytically inactive, is found in vesicles under basal copper conditions (Cater et al., 2007). This targeting is associated with the stabilization of this mutant protein in the so-called E2 conformational state, as was demonstrated by the high level of catalytic phosphorylation (whether this hyperphosphorylation caused by the loss of phosphatase activity by the mutant is also coupled to the increase in regulatory kinase-mediated phosphorylation has not been explored). Mutating the six N-terminal MBDs and/or the TM Cys-Proc-Cys(CPC) motif individually results in a non-trafficking ATP7B; however, simultaneous mutation of all sites produces protein targeted to vesicles even in basal conditions (Cater et al., 2007). The fact that the conformation acquired by ATP7B$^{TGE>AAA}$ was sufficient to trigger its trafficking to vesicles suggests that trafficking is driven by structural changes in ATP7B, rather than interactions with other copper-binding proteins or phosphorylation by copper-dependent kinases.

Similar results were obtained by mutating S340/341 residues of the N-terminal domain of ATP7B. The ATP7B mutants with S340/341 mutations are found in vesicles under basal conditions. Metabolic labeling in cells with inorganic phosphate directly demonstrated that mutation of S340/341 residues significantly decreased the level of ATP7B phosphorylation, indicating that these residues were important for ATP7B modification by a kinase (Hasan et al., 2012). Therefore, vesicular localization of the

ATP7B$^{Ser340/341Gly}$ protein was not due to mutation-induced hyperphosphorylation of some other residues, but rather due to conformational changes in ATP7B. Further studies revealed weakened interactions between the N-terminal and NBD domains in ATP7B$^{S340/341A}$ compared to the control ATP7B (Hasan et al., 2012). Thus, the role of kinase mediated phosphorylation might be to keep the N-terminal and NBD domains apart and stabilize the protein in a particular confirmation that can be recognized by the trafficking machinery, rather than acting as a recognition sequence for such machinery (Hasan et al., 2012). Although ^{858}TGE^{860} and S340/341 residues are located in different domains of ATP7B, the mutation of these sites may have similar effects on the overall conformation of ATP7B and thus produce similar trafficking response.

2.6. Copper binding to the regulatory N-terminal sites and catalytically important trans-membrane (TM) sites has different effect on the kinase mediated phosphorylation of ATP7B.

Mutating the N-terminal copper-binding site in MBD6 (ATP7B$^{C575/578A}$) interferes with a kinase mediated phosphorylation, whereas mutating the intramembrane TM6 copper-binding site (ATP7B$^{C983/985A}$) does not have such an effect. Thus, copper binding to the MBD6 of N-terminal domain might be important for inducing the conformational changes within the domain so the phosphorylation sites can be accessed by the kinase. Neither mutant traffics in response to copper, i.e. the kinase-mediated phosphorylation of ATP7B$^{C983/985A}$ is not sufficient for triggering its relocalization. At the same time, the ATP7B$^{C983/985A}$ mutant has a lower phosphorylation level (or possibly a slower rate of phosphorylation) compared to the wildtype (WT) ATP7B, suggesting that the extent of

phosphorylation might be important for ATP7B exit from the TGN or that this mutation indirectly altered other sites (Pilankatta et al., 2011).

2.7. The catalytic and kinase mediated phosphorylation occur through different mechanisms and are independent events.

Both catalytic and kinase mediated phosphorylation are stimulated by copper, but through different mechanisms (Pilankatta et al., 2011). Supporting the model that both phosphorylations are independent events, inhibition of the kinase mediated phosphorylation using a kinase inhibitor does not affect the formation of catalytic phosphorylation by ATP7B (Pilankatta et al., 2011). Reciprocally, the catalytically inactive ATP7B^{D1027A} and ATP7B^{D1027N} mutants are phosphorylated indicating that the catalytic transfer of phosphate from ATP to D1027 is not necessary for their kinase mediated phosphorylation (Bartee et al., 2009; Pilankatta et al., 2011). The same phenomenon was observed for the ATP7B$^{C983/985A}$ mutant, which had no catalytic phosphorylation, but showed kinase mediated phosphorylation (Pilankatta et al., 2011). In the cases of ATP7B^{D1027N} and ATP7B$^{C983/985A}$ mutants the kinase mediated phosphorylation level was lower (or the phosphorylation rate was slower compared to the WT), suggesting that the overall phosphorylation level of ATP7B might be altered as a result of catalytic impairment (Pilankatta et al., 2011).

In summary, both ATP7A and ATP7B undergo kinase mediated phosphorylation, which is a regulatory post-translational modification coupled to the intracellular localization of the protein. Copper binding to the N-terminal domain and/or trafficking to the post-Golgi

compartments (vesicular/PM) is associated with hyperphosphorylation, but in some cases ($ATP7B^{S340/341G}$ or $ATP7B^{TGE>AAA}$) the conformational state attained by the protein determines its localization irrespective of copper binding. Several putative phosphorylation sites have been identified, however it remains unclear whether the stoichiometry of phosphorylation or phosphorylation of distinct residues are important for the copper-responsive trafficking of ATP7A/B.

III. Redox control of copper uptake and efflux from human cells.

As described in section I, copper deficiency is associated with the increase of cellular glutathione levels, which in turn stimulate production of hCTR1 (Tennant et al., 2002). Recent studies indicate that the cellular glutathione status and the intracellular redox potential may also have a significant effect on the copper export activity of ATP7A and ATP7B. It has been suggested that under basal conditions, the copper ATPases can be glutathionylated, presumably at their metal-binding sites, and that the glutathionylation of ATP7A/7B and their interaction with glutaredoxin 1 are affected by changes in copper levels (Singleton et al., 2010). The down-regulation of glutaredoxins by small interfering RNA (siRNA) resulted in increased intracellular copper accumulation (Singleton et al., 2010), which was interpreted as evidence for direct regulation of copper export by glutaredoxin 1. While the data are compelling, it remains to be established more firmly whether the diminished copper export is due to a direct oxidation of copper-ATPases or due to effect on cellular redox environment and interference with the copper delivery system. Recent data suggest that copper export can be controlled at the stage of copper transfer to copper-ATPases.

The copper ATPases receive copper from a copper chaperone Atox1. This small cytosolic protein has a characteristic copper-binding site CxxC, which is maintained in the reduced state by glutathione (Hatori et al., 2012). Decrease in the cellular ratio of reduced to oxidized glutathione (GSH:GSSG) results in Atox1 oxidation and a diminished delivery of copper to the secretory pathway, as evidenced by decreased levels of secreted holo-ceruloplasmin (Hatori et al., 2012). The redox potential of Atox1 is estimated at approximately -220 mV and, in resting cells, Atox1 is expected to be fully reduced. However, upon cell proliferation and differentiation, the intracellular environment changes significantly (Dong-Yun et al., 2003; Markovic et al., 2009; Ranjan et al., 2006). In Caco-2 cells, where both ATP7A and ATP7B are expressed, the redox state of cellular GSH/GSSG pair changes towards a 40-mV oxidation when cells progress from proliferation to contact inhibition and differentiation (Nkabyo et al., 2002). This shift would be sufficient to produce partial oxidation of Atox1 and presumably influence copper excretion. The direct testing of these predictions would greatly expand our understanding between copper transport and cellular redox balance.

Overall, the current results suggest that copper transport in and out of cells is likely to fluctuate depending on cellular metabolic status, the stage of cell division, or differentiation. An example of significant changes in the routes of copper distribution is provided by the effects of hypoxia in macrophages (White et al., 2009a). Oxygen limitation in RAW264.7 macrophage cells stimulates copper uptake likely due to increased expression of hCTR1. Under these conditions, copper transfer to the secretory pathway is also enhanced, as evidenced by the trafficking of ATP7A to vesicles. At the

same time, the activities of cytosolic superoxide dismutase and mitochondria cytochrome c oxidase are reduced in response to hypoxia (White et al., 2009a). Thus, under hypoxic conditions copper delivery to the secretory pathway becomes the primary pathway of copper distribution, presumably to facilitate copper incorporation into ceruloplasmin.

In conclusion, the human copper transporters are subject of a complex multi-layer regulation by various metabolic signals. Recent success in understanding the structure and biochemistry of these transporters provide strong foundation for trying to link the molecular characteristics of the transporters to their behavior in cells.

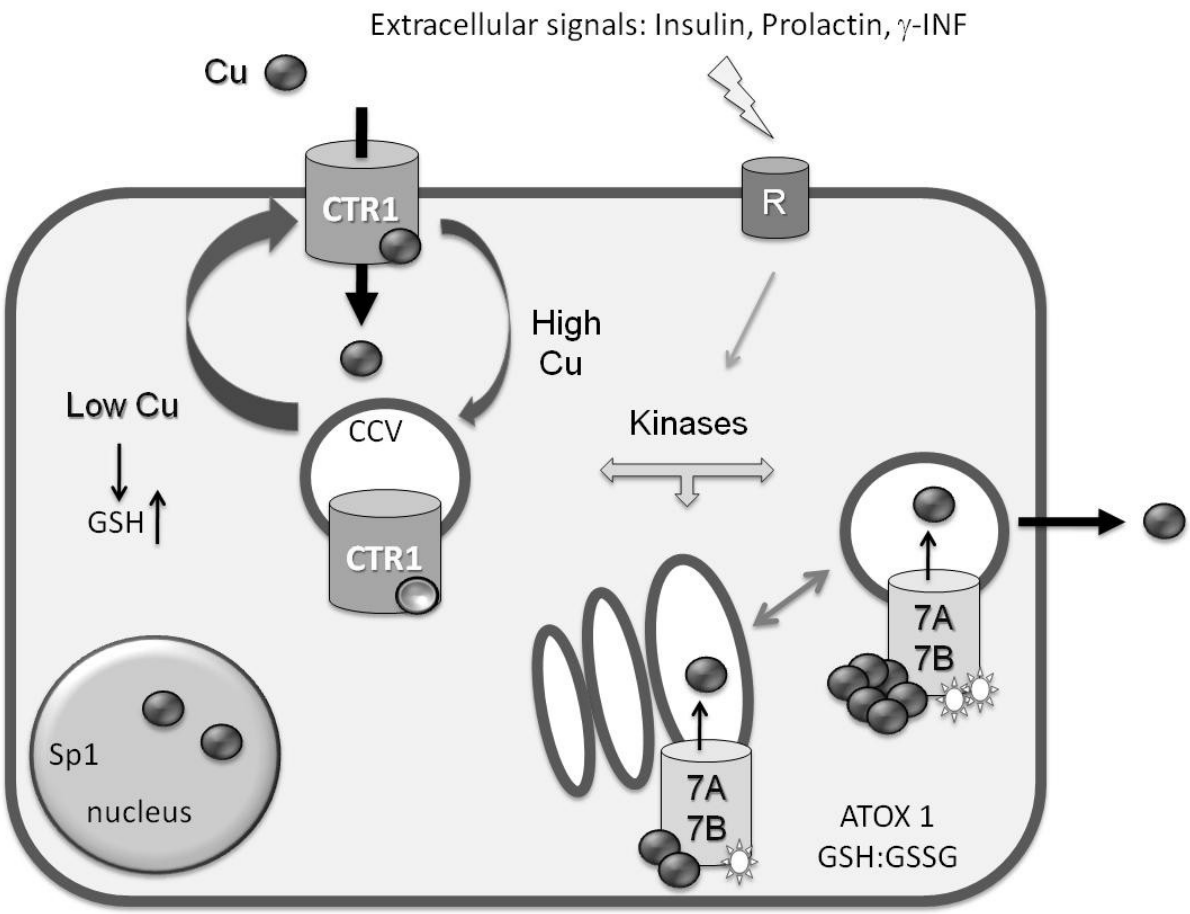

Figure 1-1. Main regulation modes of copper transporters in human cells. The high affinity copper transporter hCTR1 is located at the PM, where it facilitates copper entry into the cell. It is currently unknown whether hCTR1 is functional in the intracellular compartments. The cycling between two compartments may be constitutive and involves the clathrin-dependent pathway (CCV, clathrin-coated vesicles). Copper binding to "sensor" sites favors the redistribution of hCTR1 toward intracellular vesicles, whereas copper depletion facilitates the delivery of hCTR1 to the PM. Copper-transporting ATPases 7A and 7B are located in the TGN under basal conditions where they have basal level of phosphorylation (indicated by a star). In response to copper elevation and hormonal signaling, the Cu-ATPases become hyperphosphorylated and traffic to vesicles, where they sequester excess copper. The return to the TGN is linked to the decrease in copper levels and return to a basal level of phosphorylation. Changes in glutathione (GSH) levels and/or alterations of the cellular redox balance GSH:GSSG influence the levels and activity of copper transporters.

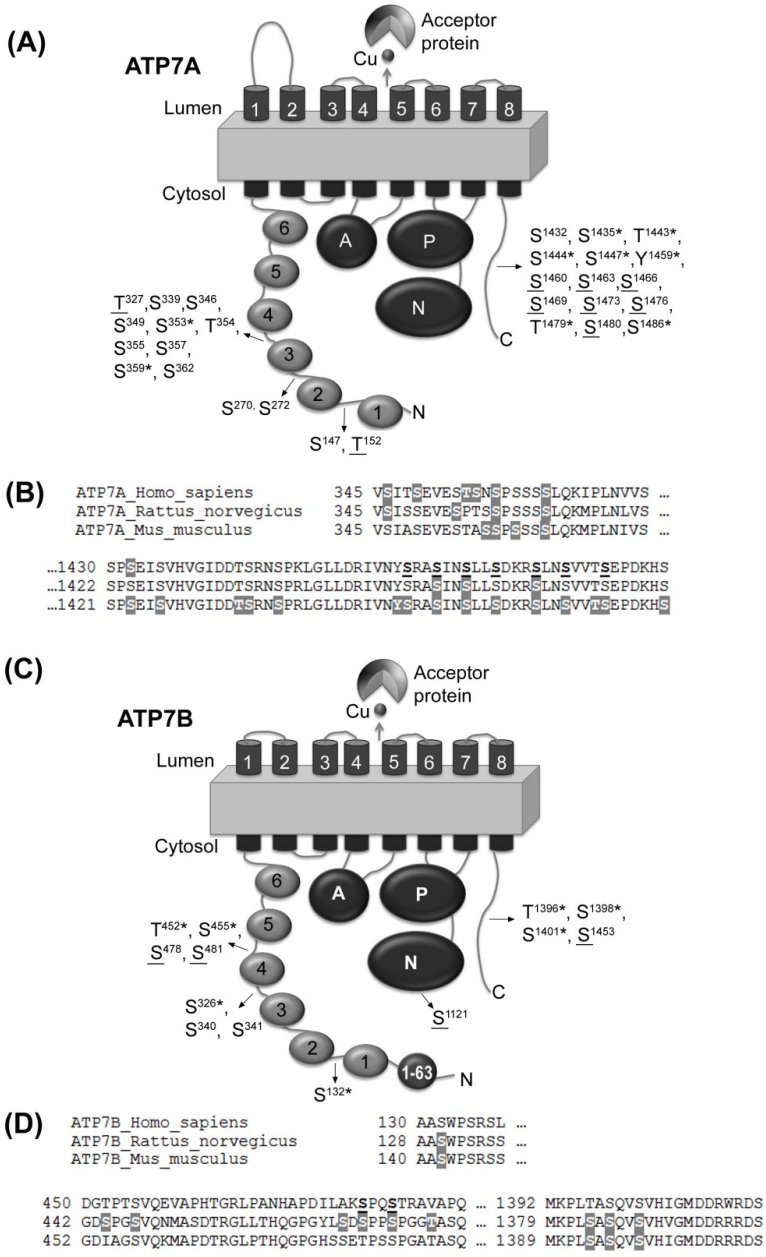

Figure 1-2. The location of phosphorylated sites in ATP7A and ATP7B. (A, C) Schematic presentation of the domain organization of ATP7A (A) and ATP7B (C). Filled circles represent the N-terminal MBDs and are numbered 1–6. TM domains are numbered 1–8. The other domains are as follows: A: actuator domain; P: phosphorylation domain; N: NBD. The 1–63 region of ATP7B contains a region (F^{37}AFDNVGYE^{45}) important for TGN retention/apical targeting (Braiterman et al., 2009b). The positions of identified phosphosites are shown. Underlined residues are putative copper-responsive phosphosites; the star (*) labels the putative phosphosites identified in other species and aligned with human ATP7A or ATP7B. (B,D) Sequence alignment of ATP7A (B) and ATP7B (D) orthologs in the regions with identified phosphosites. Sites for basal/constitutive phosphorylation identified by MS are in gray background. Copperresponsive phosphosites are in bold and underlined.

Table 1-1. Predicted Phosphorylation Sites in ATP7B. Species: m-mouse; r-rat; h-human; N-N-terminal; C-C-terminal; ND: not determined. *The identified phosphopeptide has different phosphorylated residue combinations identified by MS, and different phospho-occupancy.

Phosphosites/ Phosphopeptides	Type of phosphorylation	Effect of mutation	Ref.
[Ser 478 (N-terminal), Ser 481(N-terminal), Ser 1121 (NBD), Ser 1453 (C-terminal)] [h]	Copper-responsive	Quadruple S>A mutant is not trafficking in response to copper.	(Pilankatta et al., 2009; Pilankatta et al., 2011)
[340 SSSSHSPGSPPR] [N, h]	Basal/constitutive	S340/341 mutants are localized in vesicles.	(Bartee et al., 2009)
[270 SCVLNIEENIGQLLGVQSIQVSLENK] [N, h] [352 NQVQGTCSTTL] [N, h] [407 VISPEELR] [N, h] [415 AIEDMGFEASVVSESCSTNP LGNHSAGN] [N, h] [439 HSAGNSMVQTTDGTPTSVQEV APHTGR] [N, h] [444 SMVQTTDGTPTSVQEVAPHTGR] [N, h] [496 GMTCASCVSNIER] [N, h] [512 EAGVLSVLVALMAGK] [N, h] [589 TNGITYASVALATSK] [N, h] [595 ASVALATSK] [N, h]	Basal/constitutive	ND	(Bartee et al., 2009)
[140 AAS^{142}WPSR] [N, m]	Basal/constitutive	ND	(Huttlin et al., 2010)
[1389 MKPLS^{1393}AS^{1395}QVS^{1398}VHIGMDDR] [*, C, m]	Basal/constitutive	ND	(Huttlin et al., 2010)
[1389 MKPLSAS^{1395}QVSVHI] [C, m]	Insulin dependent	ND (putative kinase motif: NEK6)	(Monetti et al., 2011)
[458 GLLTHQGPGYLSDSPPS^{474}PGGTASQ] [N, r]	Insulin dependent	ND	(Fedjaev et al., 2012)
[128 AAS^{130}WPSR] [N, r]	Basal/constitutive	ND	(Lundby et al., 2012)
[323 VS^{324}LPDGLEK] [N, r]	Basal/constitutive	ND	(Lundby et al., 2012)
[431 VSSGNSVPQAVGDS^{444}PGS^{447}VQNMA SDTR] [*, N, r]	Basal/constitutive	ND	(Lundby et al., 2012)
[457 GLLTHQGPGYLS^{468}DS^{470}PPS^{473}PGGT^{477}ASQ] [*, N, r]	Basal/constitutive	ND	(Lundby et al., 2012)
[1381 PLS^{1383}AS^{1385}QVS^{1388}VHVGMDDR] [*, C, r]	Basal/constitutive	ND	(Lundby et al., 2012)
[1439 WSLLLS^{1444}DR] [*, C, r]	Basal/constitutive	ND	(Lundby et al., 2012)

Table 1-2. Predicted Phosphorylation Sites in ATP7A. Species: m-mouse; r-rat; h-human; N-N-terminal; C-C-terminal; ND: not determined. *The identified phosphopeptide has different phosphorylated residue combinations identified by MS, and different phospho-occupancy.

Phosphosites/ Phosphopeptides	Type of phosphorylation	Effects of mutation	Ref.
[141 ELVPELS^{147}LDTGT^{152}LEKK] $^{*, N, h}$	Ser 147- Basal/constitutive Thr 152- Copper-responsive	ND	(Veldhuis et al., 2009)
[270 S^{270}PS^{272}YTNDSTATFIID] $^{*, N, h}$	Basal/constitutive	ND	(Veldhuis et al., 2009)
[321 YNASSVT^{327}PESLR] $^{N, h}$	Copper-responsive	ND	(Veldhuis et al., 2009)
[334 AIEAVS^{339}PGLYR] $^{N, h}$	Basal/constitutive	ND	(Veldhuis et al., 2009)
[345 VS^{346}ITS^{349}EVEST^{354}S^{355}NS^{357}P SSSS^{362}LQK] $^{*, N, h}$	Basal/constitutive	ND	(Veldhuis et al., 2009)
[1430 SPS^{1432}EISVHVGIDDTSR] $^{C, h}$	Basal/constitutive	S1432A is mislocalized (vesicles in high Cu, proximal to basolateral PM)	(Veldhuis et al., 2009)
[1456 IVNYS^{1460}RAS^{1463}INS^{1466}LL S^{1469}DK] $^{*, C, h}$	Copper-responsive	S1469A is mislocalized (vesicles in high Cu, but no PM localization)	(Veldhuis et al., 2009)
[1473 S^{1473}LNS^{1476}VVTS^{1480}EPDK] $^{*, C, h}$	Copper-responsive	S1473A; basal localization and Cu-induced trafficking similar to WT.	(Veldhuis et al., 2009)
[345 VSIASEVESTAS^{356}S^{357}PS^{359}SS S^{362}LQK] $^{*, N, m}$	Basal/constitutive	ND	(Huttlin et al., 2010)
[1421 SPS^{1423}EIS^{1426}VHVGIDDT^{1434} S^{1435}RNS^{1438}PR] $^{*,C, m}$	Basal/constitutive	ND	(Huttlin et al., 2010)
[1447 IVNY^{1450}S^{1451}RAS^{1454}INS^{1457}LL S^{1460}DKR] $^{*, C, m}$	Basal/constitutive	ND	(Huttlin et al., 2010)
[1464 S^{1464}LNS^{1467}VVT^{1470}S^{1471}EPDKH S^{1477} LLVGDFREDDDTTL] $^{*, C, m}$	Basal/constitutive	ND	(Huttlin et al., 2010)
[1446 DRIVNYS^{1452}RAS^{1455}INS^{1458}L LS^{1461}DKRSLN] $^{*, C, m}$	Insulin dependent	ND; (putative kinase motifs: AURORA; AURORA-1; CK1; PKA; GSK3)	(Monetti et al., 2011)
[345 VS^{346}ISSEVES^{353}PTSS^{357}P SSSSLQK] $^{*, C, r}$	Basal/constitutive	ND	(Lundby et al., 2012)
[1454 AS^{1455}INS^{1458}LLSDK] $^{*, C, r}$	Basal/constitutive	ND	(Lundby et al., 2012)
[1465 S^{1465}LNSVVTSEPDK] $^{C, r}$	Basal/constitutive	ND	(Lundby et al., 2012)

Reference List

Araya, M., Nunez, H., Pavez, L., Arredondo, M., Mendez, M., Cisternas, F., Pizarro, F., Sierralta, W., Uauy, R., and Gonzalez, M. (2012). Administration of high doses of copper to capuchin monkeys does not cause liver damage but induces transcriptional activation of hepatic proliferative responses. J. Nutr. *142,* 233-237.

Arredondo, M., Munoz, P., Mura, C.V., and Nunez, M.T. (2003). DMT1, a physiologically relevant apical Cu1+ transporter of intestinal cells. Am. J. Physiol. Cell. Physiol. *284,* C1525-30.

Arredondo, M., Nunez, H., Lopez, G., Pizarro, F., Ayala, M., and Araya, M. (2010). Influence of estrogens on copper indicators: in vivo and in vitro studies. Biol. Trace Elem. Res. *134,* 252-264.

Bartee, M.Y., Ralle, M., and Lutsenko, S. (2009). The loop connecting metal-binding domains 3 and 4 of ATP7B is a target of a kinase-mediated phosphorylation. Biochemistry *48,* 5573-5581.

Braiterman, L., Nyasae, L., Guo, Y., Bustos, R., Lutsenko, S., and Hubbard, A. (2009). Apical targeting and Golgi retention signals reside within a 9-amino acid sequence in the copper-ATPase, ATP7B. Am. J. Physiol. Gastrointest. Liver Physiol. *296,* G433-44.

Braiterman, L., Nyasae, L., Leves, F., and Hubbard, A.L. (2011). Critical roles for the COOH terminus of the Cu-ATPase ATP7B in protein stability, trans-Golgi network

retention, copper sensing, and retrograde trafficking. Am. J. Physiol. Gastrointest. Liver Physiol. *301,* G69-81.

Cater, M.A., La Fontaine, S., and Mercer, J.F. (2007). Copper binding to the N-terminal metal-binding sites or the CPC motif is not essential for copper-induced trafficking of the human Wilson protein (ATP7B). Biochem. J. *401,* 143-153.

Cater, M.A., La Fontaine, S., Shield, K., Deal, Y., and Mercer, J.F. (2006). ATP7B mediates vesicular sequestration of copper: insight into biliary copper excretion. Gastroenterology *130,* 493-506.

Chen, H.H., Song, I.S., Hossain, A., Choi, M.K., Yamane, Y., Liang, Z.D., Lu, J., Wu, L.Y., Siddik, Z.H., Klomp, L.W., Savaraj, N., and Kuo, M.T. (2008). Elevated glutathione levels confer cellular sensitization to cisplatin toxicity by up-regulation of copper transporter hCtr1. Mol. Pharmacol. *74,* 697-704.

Cobbold, C., Ponnambalam, S., Francis, M.J., and Monaco, A.P. (2002). Novel membrane traffic steps regulate the exocytosis of the Menkes disease ATPase. Hum. Mol. Genet. *11,* 2855-2866.

de Bie, P., van de Sluis, B., Burstein, E., van de Berghe, P.V., Muller, P., Berger, R., Gitlin, J.D., Wijmenga, C., and Klomp, L.W. (2007). Distinct Wilson's disease mutations in ATP7B are associated with enhanced binding to COMMD1 and reduced stability of ATP7B. Gastroenterology *133,* 1316-1326.

De Feo, C.J., Aller, S.G., Siluvai, G.S., Blackburn, N.J., and Unger, V.M. (2009). Three-dimensional structure of the human copper transporter hCTR1. Proc. Natl. Acad. Sci. U. S. A. *106,* 4237-4242.

DiDonato, M., Hsu, H.F., Narindrasorasak, S., Que, L.,Jr, and Sarkar, B. (2000). Copper-induced conformational changes in the N-terminal domain of the Wilson disease copper-transporting ATPase. Biochemistry *39,* 1890-1896.

Dong-Yun, S., Yu-Ru, D., Shan-Lin, L., Ya-Dong, Z., and Lian, W. (2003). Redox stress regulates cell proliferation and apoptosis of human hepatoma through Akt protein phosphorylation. FEBS Lett. *542,* 60-64.

Du, X., Wang, X., Li, H., and Sun, H. (2012). Comparison between copper and cisplatin transport mediated by human copper transporter 1 (hCTR1). Metallomics *4,* 679-685.

Eisses, J.F., Chi, Y., and Kaplan, J.H. (2005). Stable plasma membrane levels of hCTR1 mediate cellular copper uptake. J. Biol. Chem. *280,* 9635-9639.

Eisses, J.F., and Kaplan, J.H. (2002). Molecular characterization of hCTR1, the human copper uptake protein. J. Biol. Chem. *277,* 29162-29171.

Fedjaev, M., Parmar, A., Xu, Y., Vyetrogon, K., Difalco, M.R., Ashmarina, M., Nifant'ev, I., Posner, B.I., and Pshezhetsky, A.V. (2012). Global analysis of protein phosphorylation networks in insulin signaling by sequential enrichment of phosphoproteins and phosphopeptides. Mol. Biosyst *8,* 1461-1471.

Francis, M., Jones , E., Levy, E., Martin, R., Ponnambalam, S., and Monaco, A. (1999). Identification of a dileucinemotif within the C terminus domain of the Menkes disease protein that mediates endocytosis from the plasma membrane. J Cell Sci *112,* 1721–1732.

Guo, Y., Smith, K., Lee, J., Thiele, D.J., and Petris, M.J. (2004). Identification of methionine-rich clusters that regulate copper-stimulated endocytosis of the human Ctr1 copper transporter. J. Biol. Chem. *279,* 17428-17433.

Gupta, A., Bhattacharjee, A., Dmitriev, O.Y., Nokhrin, S., Braiterman, L., Hubbard, A.L., and Lutsenko, S. (2011). Cellular copper levels determine the phenotype of the Arg875 variant of ATP7B/Wilson disease protein. Proc. Natl. Acad. Sci. U. S. A. *108,* 5390-5395.

Gupta, A., and Lutsenko, S. (2009). Human copper transporters: mechanism, role in human diseases and therapeutic potential. Future Med. Chem. *1,* 1125-1142.

Haas, K.L., Putterman, A.B., White, D.R., Thiele, D.J., and Franz, K.J. (2011). Model peptides provide new insights into the role of histidine residues as potential ligands in human cellular copper acquisition via Ctr1. J. Am. Chem. Soc. *133,* 4427-4437.

Hardman, B., Manuelpillai, U., Wallace, E.M., Monty, J.F., Kramer, D.R., Kuo, Y.M., Mercer, J.F., and Ackland, M.L. (2006). Expression, localisation and hormone regulation of the human copper transporter hCTR1 in placenta and choriocarcinoma Jeg-3 cells. Placenta *27,* 968-977.

Hasan, N.M., Gupta, A., Polishchuk, E., Yu, C.H., Polishchuk, R., Dmitriev, O.Y., and Lutsenko, S. (2012). Molecular Events Initiating Exit of a Copper-transporting ATPase ATP7B From the Trans-Golgi Network. J. Biol. Chem.

Hatori, Y., Clasen, S., Hasan, N.M., Barry, A.N., and Lutsenko, S. (2012). Functional partnership of the copper export machinery and glutathione balance in human cells. J. Biol. Chem. *287,* 26678-26687.

Huttlin, E.L., Jedrychowski, M.P., Elias, J.E., Goswami, T., Rad, R., Beausoleil, S.A., Villen, J., Haas, W., Sowa, M.E., and Gygi, S.P. (2010). A tissue-specific atlas of mouse protein phosphorylation and expression. Cell *143,* 1174-1189.

Kaplan, J.H., and Lutsenko, S. (2009). Copper transport in mammalian cells: special care for a metal with special needs. J. Biol. Chem. *284,* 25461-25465.

Klomp, A.E., Tops, B.B., Van Denberg, I.E., Berger, R., and Klomp, L.W. (2002). Biochemical characterization and subcellular localization of human copper transporter 1 (hCTR1). Biochem. J. *364,* 497-505.

Kuo, Y.M., Gybina, A.A., Pyatskowit, J.W., Gitschier, J., and Prohaska, J.R. (2006). Copper transport protein (Ctr1) levels in mice are tissue specific and dependent on copper status. J. Nutr. *136,* 21-26.

Lee, J., Petris, M.J., and Thiele, D.J. (2002). Characterization of mouse embryonic cells deficient in the ctr1 high affinity copper transporter. Identification of a Ctr1-independent copper transport system. J. Biol. Chem. *277,* 40253-40259.

Liang, Z.D., Tsai, W.B., Lee, M.Y., Savaraj, N., and Kuo, M.T. (2012). Specificity protein 1 (sp1) oscillation is involved in copper homeostasis maintenance by regulating human high-affinity copper transporter 1 expression. Mol. Pharmacol. *81,* 455-464.

Lundby, A., Secher, A., Lage, K., Nordsborg, N.B., Dmytriyev, A., Lundby, C., and Olsen, J.V. (2012). Quantitative maps of protein phosphorylation sites across 14 different rat organs and tissues. Nat. Commun. *3,* 876.

Lutsenko, S., Petrukhin, K., Cooper, M.J., Gilliam, C.T., and Kaplan, J.H. (1997). N-terminal domains of human copper-transporting adenosine triphosphatases (the Wilson's and Menkes disease proteins) bind copper selectively in vivo and in vitro with stoichiometry of one copper per metal-binding repeat. J. Biol. Chem. *272,* 18939-18944.

Markovic, J., Mora, N.J., Broseta, A.M., Gimeno, A., de-la-Concepcion, N., Vina, J., and Pallardo, F.V. (2009). The depletion of nuclear glutathione impairs cell proliferation in 3t3 fibroblasts. PLoS One *4,* e6413.

Molloy, S.A., and Kaplan, J.H. (2009). Copper-dependent recycling of hCTR1, the human high affinity copper transporter. J. Biol. Chem. *284,* 29704-29713.

Monetti, M., Nagaraj, N., Sharma, K., and Mann, M. (2011). Large-scale phosphosite quantification in tissues by a spike-in SILAC method. Nat. Methods *8,* 655-658.

Nkabyo, Y.S., Ziegler, T.R., Gu, L.H., Watson, W.H., and Jones, D.P. (2002). Glutathione and thioredoxin redox during differentiation in human colon epithelial (Caco-2) cells. Am. J. Physiol. Gastrointest. Liver Physiol. *283,* G1352-9.

Nose, Y., Kim, B.E., and Thiele, D.J. (2006). Ctr1 drives intestinal copper absorption and is essential for growth, iron metabolism, and neonatal cardiac function. Cell. Metab. *4,* 235-244.

Petris, M.J., Smith, K., Lee, J., and Thiele, D.J. (2003). Copper-stimulated endocytosis and degradation of the human copper transporter, hCtr1. J. Biol. Chem. *278,* 9639-9646.

Pilankatta, R., Lewis, D., Adams, C.M., and Inesi, G. (2009). High yield heterologous expression of wild-type and mutant Cu+-ATPase (ATP7B, Wilson disease protein) for functional characterization of catalytic activity and serine residues undergoing copper-dependent phosphorylation. J. Biol. Chem. *284,* 21307-21316.

Pilankatta, R., Lewis, D., and Inesi, G. (2011). Involvement of protein kinase D in expression and trafficking of ATP7B (copper ATPase). J. Biol. Chem. *286,* 7389-7396.

Pourvali, K., Matak, P., Latunde-Dada, G.O., Solomou, S., Mastrogiannaki, M., Peyssonnaux, C., and Sharp, P.A. (2012). Basal expression of copper transporter 1 in intestinal epithelial cells is regulated by hypoxia-inducible factor 2alpha. FEBS Lett. *586,* 2423-2427.

Puig, S., Mira, H., Dorcey, E., Sancenon, V., Andres-Colas, N., Garcia-Molina, A., Burkhead, J.L., Gogolin, K.A., Abdel-Ghany, S.E., Thiele, D.J.*, et al.* (2007). Higher plants possess two different types of ATX1-like copper chaperones. Biochem. Biophys. Res. Commun. *354,* 385-390.

Ralle, M., Huster, D., Vogt, S., Schirrmeister, W., Burkhead, J.L., Capps, T.R., Gray, L., Lai, B., Maryon, E., and Lutsenko, S. (2010). Wilson's disease at a single cell level:intracellular copper trafficking activates compartment-specific responses in hepatocytes. J. Biol. Chem.

Ranjan, P., Anathy, V., Burch, P.M., Weirather, K., Lambeth, J.D., and Heintz, N.H. (2006). Redox-dependent expression of cyclin D1 and cell proliferation by Nox1 in mouse lung epithelial cells. Antioxid. Redox Signal. *8,* 1447-1459.

Singleton, W.C., McInnes, K.T., Cater, M.A., Winnall, W.R., McKirdy, R., Yu, Y., Taylor, P.E., Ke, B.X., Richardson, D.R., Mercer, J.F., and La Fontaine, S. (2010). Role of glutaredoxin1 and glutathione in regulating the activity of the copper-transporting P-type ATPases, ATP7A and ATP7B. J. Biol. Chem. *285,* 27111-27121.

Song, I.S., Chen, H.H., Aiba, I., Hossain, A., Liang, Z.D., Klomp, L.W., and Kuo, M.T. (2008). Transcription factor Sp1 plays an important role in the regulation of copper homeostasis in mammalian cells. Mol. Pharmacol. *74,* 705-713.

Stephenson, S.E., Dubach, D., Lim, C.M., Mercer, J.F., and La Fontaine, S. (2005). A single PDZ domain protein interacts with the Menkes copper ATPase, ATP7A. A new protein implicated in copper homeostasis. J. Biol. Chem. *280,* 33270-33279.

Strausak, D., La Fontaine, S., Hill, J., Firth, S.D., Lockhart, P.J., and Mercer, J.F. (1999). The role of GMXCXXC metal binding sites in the copper-induced redistribution of the Menkes protein. J. Biol. Chem. *274,* 11170-11177.

Tennant, J., Stansfield, M., Yamaji, S., Srai, S.K., and Sharp, P. (2002). Effects of copper on the expression of metal transporters in human intestinal Caco-2 cells. FEBS Lett. *527,* 239-244.

Tsigelny, I.F., Sharikov, Y., Greenberg, J.P., Miller, M.A., Kouznetsova, V.L., Larson, C.A., and Howell, S.B. (2012). An all-atom model of the structure of human copper transporter 1. Cell Biochem. Biophys. *63,* 223-234.

Tsivkovskii, R., MacArthur, B.C., and Lutsenko, S. (2001). The Lys1010-Lys1325 fragment of the Wilson's disease protein binds nucleotides and interacts with the N-terminal domain of this protein in a copper-dependent manner. J. Biol. Chem. *276,* 2234-2242.

Turski, M.L., Brady, D.C., Kim, H.J., Kim, B.E., Nose, Y., Counter, C.M., Winge, D.R., and Thiele, D.J. (2012). A novel role for copper in Ras/mitogen-activated protein kinase signaling. Mol. Cell. Biol. *32,* 1284-1295.

Vanderwerf, S.M., Cooper, M.J., Stetsenko, I.V., and Lutsenko, S. (2001). Copper specifically regulates intracellular phosphorylation of the Wilson's disease protein, a human copper-transporting ATPase. J. Biol. Chem. *276,* 36289-36294.

Vanderwerf, S.M., and Lutsenko, S. (2002). The Wilson's disease protein expressed in Sf9 cells is phosphorylated. Biochem. Soc. Trans. *30,* 739-741.

Veldhuis, N.A., Valova, V.A., Gaeth, A.P., Palstra, N., Hannan, K.M., Michell, B.J., Kelly, L.E., Jennings, I., Kemp, B.E., Pearson, R.B., Robinson, P.J., and Camakaris, J.

(2009). Phosphorylation regulates copper-responsive trafficking of the Menkes copper transporting P-type ATPase. Int. J. Biochem. Cell Biol. *41,* 2403-2412.

Voskoboinik, I., Fernando, R., Veldhuis, N., Hannan, K.M., Marmy-Conus, N., Pearson, R.B., and Camakaris, J. (2003). Protein kinase-dependent phosphorylation of the Menkes copper P-type ATPase. Biochem. Biophys. Res. Commun. *303,* 337-342.

Walker, J.M., Huster, D., Ralle, M., Morgan, C.T., Blackburn, N.J., and Lutsenko, S. (2004). The N-terminal metal-binding site 2 of the Wilson's Disease Protein plays a key role in the transfer of copper from Atox1. J. Biol. Chem. *279,* 15376-15384.

White, C., Kambe, T., Fulcher, Y.G., Sachdev, S.W., Bush, A.I., Fritsche, K., Lee, J., Quinn, T.P., and Petris, M.J. (2009a). Copper transport into the secretory pathway is regulated by oxygen in macrophages. J. Cell. Sci. *122,* 1315-1321.

White, C., Lee, J., Kambe, T., Fritsche, K., and Petris, M.J. (2009b). A role for the ATP7A copper-transporting ATPase in macrophage bactericidal activity. J. Biol. Chem. *284,* 33949-33956.

Yamane, Y., Furuichi, M., Song, R., Van, N.T., Mulcahy, R.T., Ishikawa, T., and Kuo, M.T. (1998). Expression of multidrug resistance protein/GS-X pump and gamma-glutamylcysteine synthetase genes is regulated by oxidative stress. J. Biol. Chem. *273,* 31075-31085.

Zheng, G., Chen, J., and Zheng, W. (2012). Relative contribution of CTR1 and DMT1 in copper transport by the blood-CSF barrier: implication in manganese-induced neurotoxicity. Toxicol. Appl. Pharmacol. *260,* 285-293.

Zheng, Z., White, C., Lee, J., Peterson, T.S., Bush, A.I., Sun, G.Y., Weisman, G.A., and Petris, M.J. (2010). Altered microglial copper homeostasis in a mouse model of Alzheimer's disease. J. Neurochem. *114,* 1630-1638.

Zimnicka, A.M., Ivy, K., and Kaplan, J.H. (2011). Acquisition of dietary copper: a role for anion transporters in intestinal apical copper uptake. Am. J. Physiol. Cell. Physiol. *300,* C588-99.

II. Molecular Events Initiating Exit of a Copper-transporting ATPase ATP7B From the Trans-Golgi Network

This research was originally published in J Biol Chem. 2012 Oct 19;287(43):36041-50., Molecular events initiating exit of a copper-transporting ATPase ATP7B from the trans-Golgi network., and all text and figures in this chapter have been adapted from it.

Contributing Authors: Hasan NM*, Gupta A*, Polishchuk E, Yu CH, Polishchuk R, Dmitriev OY, Lutsenko S.

(*equal contribution)

Introduction

Copper homeostasis plays an important role in human physiology. Copper is both a catalytic and a structural cofactor for a variety of enzymes essential for human cellular metabolism (cytochrome c oxidase, superoxide dismutase, dopamine-β-hydroxylase, etc). Under physiologic conditions, copper cycles between two oxidation states, Cu(I) and Cu(II); and copper levels must be tightly regulated to avoid participation in unwanted reactions affecting an intracellular redox status (Gupta and Lutsenko, 2009). Copper homeostasis is primarily maintained by the copper-transporting ATPases ATP7A and ATP7B. Both ATP7A and ATP7B are P-type ATPases that use the energy of ATP hydrolysis to transport copper across membranes; mutations in these proteins result either in copper accumulation in the body (Wilson's disease) or copper deficiency (Menkes disease) (Bull et al., 1993; La Fontaine et al., 1998; Payne et al., 1998; Tanzi et al., 1993; Voskoboinik et al., 1998; Vulpe et al., 1993).

ATP7B is highly expressed in the liver and has a dual function in hepatocytes. Under basal conditions, it transports copper into the TGN, where copper is incorporated into cuproenzymes. Elevation of intracellular copper triggers ATP7B trafficking from the TGN to vesicles, which accumulate copper and then fuse with the apical plasma membrane to excrete copper out of the cell. Thus, ATP7B trafficking is essential for regulation of cellular copper levels. Mechanistic link between copper sensing by ATP7B and recognition of ATP7B by trafficking machinery is not yet understood, although involvement of such proteins as COMMD1, dynactin, clusterin and glutaredoxin have been proposed (Bartee and Lutsenko, 2007; Guo et al., 2005; Hung et al., 1997; Lim et

al., 2006a; Lim et al., 2006b; Materia et al., 2012; Roelofsen et al., 2000; Tao et al., 2003).

In addition to regulating ATP7B localization, copper modulates ATP7B phosphorylation by kinases. In low copper, ATP7B has a basal level of phosphorylation. Copper elevation results in a hyperphosphorylation of ATP7B, and this event is coupled to trafficking of ATP7B from the TGN to vesicles, whereas dephosphorylation is associated with the return of ATP7B from vesicles to the TGN (Vanderwerf et al., 2001). The basal and copper-induced phosphorylation sites are different and involve different kinases (Vanderwerf et al., 2001). Mass-spectrometry studies revealed a large number of potential phosphorylation sites (Bartee et al., 2009; Pilankatta et al., 2009); simultaneous mutation of four such sites disrupts ATP7B trafficking (Pilankatta et al., 2011). However, the cumulative effects of this multi-site mutation on either ATP7B structure, activity, or phosphorylation level have not been explored, thus specific reason for the disrupted trafficking remains uncertain.

Biochemical and cellular studies also revealed the important role of the cytosolic N-terminal domain of ATP7B (N-ATP7B) in both copper sensing and kinase-mediated phosphorylation. N-ATP7B is composed of six metal binding domains (MBDs) that are connected by flexible loops. Each MBD binds one copper (Fig. 2-1a) (Lutsenko et al., 1997; Lutsenko et al., 2007). Copper binding to all 6 sites induces significant conformational changes in N-ATP7B (DiDonato et al., 2000) that are accompanied by the rearrangements of the loops connecting MBD's (Bartee et al., 2009) and decreased

interactions with the nucleotide-binding domain, NBD (Tsivkovskii et al., 2001). The recombinant N-ATP7B is phosphorylated *in vitro* and in cells (Bartee et al., 2009), and in the full-length ATP7B, deletion of the N-terminal region results in the loss of copper-dependent phosphorylation (Vanderwerf et al., 2001). Together, these observations suggested that copper binding to N-ATP7B induces structural changes favorable for kinase mediated phosphorylation and led to the hypothesis that phosphorylation may act as a signal for ATP7B exit from the TGN.

However, other reports indicate that ATP7B exit from the TGN can be induced by mutation of residues that are not directly involved in either copper binding or phosphorylation. The N41S mutation results in a poor TGN retention and mis-targeting to the basolateral membrane even when copper is low (Braiterman et al., 2009). A triple mutant ^{858}TGE^{860}>AAA is found in vesicles in either basal or high copper (Cater et al., 2007). This latter mutant is catalytically inactive and trapped in a hyperphosphorylated state (although in this case the increased phosphorylation could be due to increased stability of a catalytic *acyl*-phosphate intermediate (Cater et al., 2007). These observations suggest an alternative model according to which stabilization of ATP7B in a distinct conformational state is sufficient to cause its traffic from the TGN (Cater et al., 2007).

To gain insight into the mechanism of ATP7B exit from the TGN, we have focused on the Ser-rich region in N-ATP7B, which we previously identified as a region of a kinase-mediated phosphorylation (Bartee et al., 2009). We demonstrate that mutating S340/341

in this region results in ATP7B acquiring conformation that resembles its copper saturated state. Although S340/341 mutant has reduced levels of kinase-mediated phosphorylation, it shows poor retention in the TGN and preferential localization to vesicles. Our data suggest that exit of ATP7B from the TGN is predominantly governed by a conformational state of the protein and requires copper transfer from the cytosol.

Results

The loop connecting MBD3 and MBD4 of ATP7B has several putative sites for kinase-mediated phosphorylation.

To test whether inhibiting phosphorylation would affect the ATP7B exit from the TGN we examined the Ser-rich cluster in the loop between MBD3 and MBD4, which we previously identified as a region of kinase-mediated phosphotylation (Bartee et al., 2009). This cluster is conserved between human ATP7A and ATP7B (Fig. 2-1b), and in ATP7A, several Ser residues in this region are phosphorylated (Huttlin et al., 2010). Bioinformatic analysis of ATP7B using NetPhos or GPS 2.1 program predicts 4-5 potential sites within that loop. Consistent with these predictions, mutating any single serine within the S^{340}-S^{348} region to alanine decreases the *in vitro* phosphorylation of a recombinant N-ATP7B by 25-40%, however none of these mutations completely abolishes phosphorylation (our data, not shown). To determine if any of the serines was more important than the others we compared the ATP7B orthologs (Fig. 2-1c). None of the residues was invariant, however S340 and S341 showed highest conservation; consequently, we focused our studies on these residues.

Mutating S340 and/or S341 shifts the steady-state localization of ATP7B towards vesicles.

The $S^{340/341}$>A mutation was introduced into Flag-ATP7B cloned into the pcDNA5/FRT-TO plasmid to allow for a tet-regulated expression (We have previously observed that high expression often leads to ATP7B mis-localization. Consequently, expression of the Flag-ATP7B or the $S^{340/341}$A mutant was controlled by doxicycline and only cells with a low/medium Flag signal were imaged). As expected, in basal conditions the wild-type Flag-ATP7B was localized to TGN (Fig. 2-2a and 2-2b, upper panels). We expected that Flag-$ATP7B^{S340/341A}$ would also be targeted to the TGN but might be unable to traffic. Instead, the mutant showed predominantly vesicular localization (Fig. 2-2a and 2-2b, lower panels). In cell with high expression, the TGN localization was partially retained, resulting in both vesicular and TGN staining of Flag-$ATP7B^{S340/341A}$ (Fig. 2-2c).

In hepatocytes, ATP7B traffics from TGN to vesicles in response to 10 μM copper, and copper chelation with BCS causes the ATP7B return to TGN. In renal cells and in HEK 293 cells, ATP7B does not traffic in response to 10 μM copper (Barnes et al., 2009). Trafficking can only be seen upon treatment with very high copper (100 μM) and only small fraction of protein leaves the TGN under these conditions (data not shown). Therefore, finding the S340/341A mutant in vesicles in Hek293TRex cells was particularly striking and suggested that this mutation facilitated conversion of ATP7B from a "TGN retained" form to a "trafficking-compatible" state. This phenotype also argued against the essential role of Ser340/341 phosphorylation in ATP7B exit from the TGN.

ATP7B$^{S340/341A}$ does not return to the TGN in response to copper depletion.

One reason for vesicular localization of Flag-ATP7B$^{S340/341A}$ could be an increased sensitivity to basal copper levels induced by the mutation. If this were the case, then decreasing intracellular copper using the chelator BCS would induce trafficking of the Flag-ATP7B$^{S340/341A}$ back to the TGN. However, after prolonged treatment with 100 μM of BCS, the localization of mutant was unchanged, i.e. Flag-ATP7B$^{S340/341A}$ remained in vesicles (low expression) (Fig. 2-3a) or in vesicles and TGN (higher expression). We generated and observed similar results for single mutants S340A, S340T, and S341A (Fig. 2-3c illustrates the results for ATP7B^{S340A}. Other single mutants had similar vesicular localization).

The differences in the compartmentalization of wt ATP7B, the S340/341A mutant, and the S340A mutant were verified by immuno-EM. Gold labeling showed the wt ATP7B to be distributed along cisterns and tubular profiles at the *trans* face of the Golgi, whereas little of S340/341A mutant was detected in similar structures (Fig. 2-3b; arrows). Instead, the mutant was primarily localized in large vesicles (300 - 1000 nm in size). Reciprocally, wt ATP7B was almost completely excluded from such vesicular profiles (Fig. 2-3b; arrowheads). Similar to ATP7B$^{S340/341A}$, the single mutant GFP-ATP7B^{S340A} appeared in large "vesicles" (arrowheads) (Fig. 2-3c, right panel). Thus, the presence of serine residues in positions 340/341 is important for ATP7B retention in the TGN, whereas modification of these residues facilitates exit.

Mutation of S340/341 mimics consequences of copper binding.

The shift in the steady-state distribution of the S340/341A mutant from TGN to vesicles in low copper suggested that the mutant acquired a conformation resembling that of ATP7B under high copper conditions. To test this hypothesis, we took advantage of a naturally occurring ATP7B variant ATP7B^{R875}, which has a low apparent affinity to copper compared to a common ATP7B^{G875} variant and a very distinct cellular behavior. In basal or low copper, ATP7B^{R875} localizes in the endoplasmic reticulum (ER), but it traffics to the TGN and then to vesicles when copper is increased in a step-wise fashion (Gupta et al., 2011). Stabilizing the "copper-bound" state for the ATP7B^{R875} variant is expected to change its localization from ER to TGN and/or vesicles under basal conditions. To test this prediction we mutated S340/341 to A340/341 in ATP7B^{R875} and examined the localization of this mutant in Hek293TRex cells. In basal medium, the control ATP7B^{R875} showed expected ER localization, and it trafficked to vesicles upon copper treatment (Fig. 2-4a). In contrast, the mutant was localized exclusively to vesicles mimicking the behavior of ATP7B^{R875} in high copper (Fig. 2-4b). Copper chelation treatment did not alter the localization of ATP7B$^{R875,S340/341A}$ (Fig. 2-4b). To further minimize structural perturbations (side chains of glycine are smaller compared to alanine), we mutated S340/341 to G340/341 in ATP7B^{R875}. ATP7B$^{R875,S340/341G}$ was also localized exclusively to vesicles in both basal and copper depleted conditions (Fig. 2-4c).

To determine whether on its way to vesicles the S340/341 mutant follows a normal intracellular route of ATP7B trafficking via the TGN, we utilized the tyrosinase activation assay. The assay uses Menkes fibroblasts expressing the copper-dependent

enzyme tyrosinase (YSTT cells). The YSTT cells lack active copper ATPases and thus produce inactive tyrosinase. Transfection of YSTT cells with a wt ATP7B, which is targeted to the TGN, restores copper transport to the TGN lumen and activates tyrosinase resulting in a black chromogenic precipitate (Fig. 2-5, left panel) (Gupta et al., 2011). The negative control, Flag-ATP7B^{R875} localized in the ER, does not activate tyrosinase (Fig. 2-5, middle panel) (Gupta et al., 2011). Expression of Flag-ATP7B$^{R875,S340/341G}$ induces pigment formation, indicating that the mutant followed the normal trafficking itinerary and delivered copper to tyrosinase, presumably when passing through the TGN (Fig. 2-5, right panel).

ATP7B$^{R875,S340/341G}$ has a reduced kinase-mediated phosphorylation.

The exit of wt ATP7B from the TGN is stimulated by high copper, which also stimulates ATP7B phosphorylation by a kinase (Vanderwerf et al., 2001). Given our observations that the S340/340A mutation mimics behavior of ATP7B in elevated copper, we were wondering whether this mutation instead of eliminating phosphorylation induced structural changes that exposed sites critical for kinase mediated phosphorylation in high copper.

To clarify consequences of S340/341 mutation we compared kinase-mediated phosphorylation of ATP7B^{R875} and ATP7B$^{R875,S340/341G}$ using *in vivo* metabolic labeling with radioactive orthophosphate. (The ATP7B^{R875} variant was particularly useful for these studies because both ATP7B^{R875} and ATP7B$^{R875,S340/341G}$ have uniform intracellular localization, ER and vesicles, respectively). In low copper, the mutant had ~30% lower

phosphorylation compared to ATP7B^{R875} (Fig. 2-6). Copper treatment did not affect the phosphorylation level of the mutant and difference between ATP7B^{R875} and ATP7B$^{R875,S340/341G}$ became larger when metabolic labeling was carried out in the presence of copper (Fig. 2-6). Thus, Ser340/341 are important for normal phosphorylation of ATP7B, particularly in high copper, however the loss of phosphorylation caused by mutations is not detrimental for the ability of ATP7B to exit the TGN. To reconcile these observations, we hypothesized that in a wild-type ATP7B phosphorylation of S340 and/or S341 induces structural changes similar to those induced by Ser mutations. To test this prediction we generated and characterized a phospho-mimetic mutation S340/341D. This variant behaved indistinguishably from the S340/341A i.e. it was targeted to vesicles (Fig. 2-7a).

The effect of Ser340/341 mutations on trafficking is selective.

We were also curious whether vesicular targeting observed by mutating S340 and/or S341 was an effect specific for these sites or manipulating any phosphorylation site(s) in ATP7B would induce changes in localization. Consequently, using ATP7B^{R875} as a template we mutated to alanine S478, S481 and S1435, which were previously suggested as additional sites of phosphorylation in ATP7B (Pilankatta et al., 2009). No effect on localization was observed for all three mutants. Similarly to ATP7B^{R875}, these mutants were found in the ER in basal condition, were targeted to the TGN in low copper, and trafficked to vesicles in response to higher copper (Fig. 2-7b). We concluded that S340/341 play a specific role in the TGN retention/exit of ATP7B.

The S340/341A mutation does not markedly alter folding of N-ATP7B.

Our data suggested that the S340/341 substitution induced structural changes in ATP7B, which could either be local or transmitted via inter-domain interactions to affect entire ATP7B. S340/341 residues are located in the N-terminal domain of ATP7B (N-ATP7B). To evaluate potential structural effects, we first mutated S340/341 in a recombinant N-ATP7B. The folding of N-ATP7B and N-ATP7B$^{S340/341A}$ was compared using limited proteolysis with varying concentrations of trypsin at different time intervals. No difference in proteolytic patterns was detected under all tested conditions (Fig. 2-8a). Treatment with different protease, papain, yielded similar results (our data, not shown). We concluded that the S340/341A substitution did not markedly alter the N-ATP7B fold. To verify this conclusion, we examined the effect of Ser mutations on N-ATP7B structure in more detail. The recombinant N-ATP7B and N-ATP7B$^{S340/341A}$ were metabolically labeled with N15, purified in a non-tagged form, and their folding was compared by NMR at equal protein concentrations (Fig. 2-8b). The spectra of wt N-ATP7B and N-ATP7B$^{S340/341A}$ showed excellent chemical shift dispersion, characteristic of the well-folded proteins. The differences in spectra were very minor, demonstrating that the S340/341A mutation does not significantly change the fold of N-ATP7B.

Mutation of S340/341 induces conformational changes within ATP7B by reducing interactions between N-ATP7B and nucleotide-binding domain.

The lack of significant effects on N-ATP7B structure suggested that the Ser mutations may alter the inter-domain interactions in ATP7B. It was previously shown that N-ATP7B interacted with the nucleotide-binding domain (NBD) and that copper binding to

N-ATP7B decreased this interaction (Tsivkovskii et al., 2001). We hypothesized that the S340/341A mutation might mimic this effect and decrease interactions between N-ATP7B and NBD. To test this hypothesis, we performed a co-purification experiment, using cell lysates containing the recombinant maltose fusion N-ATP7B (WT and S340/341A) and the intein fusion of NBD. N-ATP7B$^{S340/341A}$ showed a ~50% reduction of inter-domain interaction compared to N-ATP7B (Fig. 2-9a). Thus, similarly to copper binding, S340/341 mutation decreases interactions between the N-terminal domain and NBD.

In the full-length ATP7B, the change of inter-domain interactions is expected to influence the kinetics and/or pattern of limited proteolysis. Consistent with this prediction, treatment with trypsin reproducibly yielded different rates of digestion for the membrane-bound Flag-ATP7B^{R875} and Flag-ATP7B$^{R875,S340/341G}$. This was evident from differences in the relative intensities of proteolytic bands (Fig. 2-9b). We concluded that Ser340/341 influences the interdomain interface and overall conformation of ATP7B.

Copper transport activity is necessary for the localization of ATP7B$^{R875,S340/341G}$ to vesicles.

Copper binds to ATP7B in at least 8 sites (6 in the cytosol and likely 2 sites in the trans-membrane portion). Occupation of the cytosolic MBDs with copper and changes in interdomain contacts may be sufficient to trigger trafficking of ATP7B to vesicles. Alternatively, binding of copper at both the cytosolic and membrane/lumenal sites of the transporter might be necessary to initiate ATP7B exit from the TGN. To discriminate

between these two possibilities, we generated a catalytically inactive mutant D1027A and a triple mutant D1027A,S340/341G (all on the R875 background). The D1027 mutation is expected to have no effect on the ability of ATP7B to bind copper at the cytosolic MBDs, but it would prevent transfer of copper to the lumenal side due to inability to hydrolyze ATP. Analysis of intracellular targeting showed that the control D1027A mutant had a mixed ER/TGN targeting; a higher proportion of TGN targeting compared to the ER-localized parent ATP7B^{R875} (Fig. 2-10) implied that the mutant might have increased protein stability. Significantly, the D1027A mutation completely blocked trafficking of the Ser340/341G variant, i.e. the localization of ATP7B$^{S340/341G,D1027A}$ mutant was no longer shifted towards vesicles (Fig. 2-10). We concluded that both domain/domain dissociation and copper transfer into the lumen are necessary for exiting the TGN and trafficking to vesicles.

Discussion

In this study, we demonstrate that the N-terminal Ser-rich region of ATP7B is an important regulator of protein exit from the TGN. The residues Ser340/341 contribute to a regulatory phosphorylation of ATP7B, particularly in high copper, and modulate the inter-domain interactions (Fig. 2-6, Fig. 2-9a). Significantly, mutations inhibiting phosphorylation (S>A, S>G) and mutation mimicking the phosphorylated state (S>D) all facilitate ATP7B trafficking from the TGN. Thus, the structural change that alters inter-domain contacts in ATP7B is a key trigger of ATP7B trafficking to vesicles. The role of copper-dependent phosphorylation is likely to maintain this "trafficking-compatible" state.

N-ATP7B acts as a copper sensor; and copper binding to MBDs alters the conformation of the entire N-ATP7B (Barnes et al., 2009; DiDonato et al., 2000). ATP7B with non-functional MBDs (which cannot bind copper) does not traffic in response to copper elevation (Cater et al., 2004). Residues S340/341 are located within the long loop connecting MBD3 and MBD4 and are not expected to have any effect on copper binding capacity of N-ATP7B, although this remains to be experimentally verified. It is also unlikely that S340/341 interact directly with the cellular trafficking machinery; because a deletion mutant of ATP7B that lacks the N-terminal residues 63-443 exhibits normal TGN localization and copper dependent trafficking (Guo et al., 2005). Instead, the S340/341 region appears to play an important role in interactions between N-ATP7B and the nucleotide-binding domain. This role could be direct because the effect of S340/341A mutation on overall structure of N-ATP7B is minimal (Fig. 2-8a, 2-8b), whereas the effect on inter-domain interaction is significant (Fig. 2-9a).

Phosphorylation of other membrane proteins was shown to expose sorting signals (Bonifacino and Traub, 2003) or itself serve as a signal for trafficking by facilitating interaction with the components of cellular trafficking machinery (Hinners and Tooze, 2003). Our data are more consistent with a scenario, where phosphorylation alone is not a required factor in the exit of ATP7B from the TGN; rather it stabilizes the 'trafficking ready' copper bound state of ATP7B. We speculate that in low copper S340/341 are protected from a kinase by inter-domain interactions. Domain dissociation in response to copper binding to N-ATP7B exposes S340/341 to phosphorylation by a kinase. The phosphorylation would then keep domains apart, thus stabilizing ATP7B is a state that has a poor TGN retention (Fig. 2-11).

The fact that even a mild mutation such as S340T produces the loss of TGN retention indicates that this region of ATP7B is not merely an exposed loop, but a site critical for the conformational state of entire ATP7B. From this perspective, it is interesting to consider that mutations in another N-terminal region $F^{37}AFDNVGYE^{45}$ also result in the loss of TGN retention (Braiterman et al., 2009). It is tempting to speculate that in a three-dimensional structure of ATP7B, the two N-terminal regions can be in vicinity to each other. Copper binding and subsequent structural rearrangements that expose S340/341 for phosphorylation may simultaneously expose the F37-E45 region for interaction with the apical trafficking machinery (Braiterman et al., 2009).

Mass-spectrometry analysis of the recombinant ATP7B demonstrated that S478, S481 and S1453 can be phosphorylated and that quadruple mutant (S478, 481, 1121, 1453A) fails to traffic in response to copper (Pilankatta et al., 2009; Pilankatta et al., 2011). In our studies, individual mutations of these residues do not alter trafficking pattern (Fig. 2-7b). Difference in the phenotypes could be due to global conformational changes induced by a quadruple mutation versus a single mutation. These observations emphasize the role of ATP7B structure in its localization.

Finally, the phenotype of the S340/341 mutant resembles a phosphatase deficient ATP7B mutant, $^{858}TGE^{860}$>AAA (Cater et al., 2007). This mutant is trapped in a so called E2P state (Cater et al., 2007). Similar E2P state would be stabilized under conditions of copper saturation, when copper release into the TGN lumen is diminished. Thus, although $^{858}TGE^{860}$ and S340/341 residues are located in different domains of ATP7B, the mutation of these sites are likely to have similar effects on the overall conformation of ATP7B.

The following model (Fig. 2-11) is consistent with our results as well as many experimental observations reported in the literature. Under basal conditions, N-ATP7B has a partial copper occupancy and ATP7B pumps copper into the lumen of TGN, where the released copper is incorporated into available apo-proteins. In high copper, more copper binds to N-ATP7B; the binding relieves the autoinhibitory interaction between N-ATP7B and the nucleotide-binding domain and activates the pump. Higher transport activity would saturate the copper-binding capacity of acceptor proteins and eventually inhibit copper release from ATP7B into the lumen. Altogether, these events would lead to ATP7B acquiring a "copper-saturated" conformation, which is a target of a kinase-mediated phosphorylation. Phosphorylation of serine residues may stabilize the "TGN-exit ready" conformation, which is posed to interact with the cellular machinery responsible for an anterograde trafficking of ATP7B. The mutations that stabilize this specific form would facilitate the TGN exit and result in vesicular localization of ATP7B.

Materials and Methods

Cell lines: Hek293TRex cells were maintained in MEM supplemented with 10 % FBS, 1 % pen/strep, 1 % non-essential amino acids, 12.5 µg/mL blasticidin and 100 µg/mL zeocin. During experiments media without blasticidin and zeocin was used. YSTT cells were maintained in DMEM supplemented with 10 % FBS, 1 % pen/strep, 1 % non essential amino acids, 200 µg/ml G418 and 0.5 µg/ml puromycin. Hek293 cells were cultured in DMEM containing 10 % FBS, 1 % pen/strep and 1 % non-essential amino acids.

Site-directed mutagenesis in ATP7B: The previously generated construct of N-terminally Flag-tagged ATP7B in pcDNA 5.1 FRT/TO vector was used as a template (Gupta et al., 2011). The Ser>Ala, Ser>Gly, Ser>Thr, and Ser>Asp mutations were introduced by PCR using the Quickchange XL mutagenesis kit (Stratagene). All primers were obtained from Invitrogen and the primer sequences are available upon request. The presence of the mutation and the fidelity of the cDNA sequence were verified by DNA sequencing of the coding region.

Tyrosinase activation assay: YSTT cells grown on glass coverslips were transfected with either 2 μg of pcTYR (a plasmid encoding apo-tyrosinase) or with 2 μg pcTYR and 2 μg Flag-ATP7B plasmids using Turbofect (Fermentas). Positive control (wt GFP-ATP7B, known as pYG7 (Guo et al., 2005)) and negative control (only pcTYR) were used to ensure the specificity of the assay. 24 h post-transfection, cells were washed with PBS and fixed in cold acetone-methanol for 30 sec. The cells were then incubated for 4 h at 37°C in 0.1 M Na-phosphate buffer (pH 6.8) containing 0.15% (wt/vol) levo-3,4-dihydroxy-L-phenylalanine (L-DOPA). Coverslips were mounted, and the formation of the black DOPA-chrome pigment was detected by phase microscopy. Pigment color intensity was quantified using Image J.

Analysis of kinase-mediated phosphorylation. Hek293TRex cells were grown in 6 cm dishes until confluent. The cells were transiently transfected with either wt Flag-ATP7B^{R875} or Flag-ATP7B$^{R875,S340/341G}$ plasmids using Turbofect (Fermentas). Protein expression was induced with 40 ng/ml DOX (Sigma) for 16 h in basal conditions. Cells were rinsed with PBS and kept in the phosphate-free DMEM for 3 h. Then, media was changed to fresh phosphate-free DMEM (Gibco) containing 0.3 mCi ^{32}P (Perkin Elmer).

After 3 h, media was removed and cells were treated with 100 μM BCS or 100 μM $CuCl_2$ (both pre-dissolved in FBS) added to a phosphate-free DMEM for 2 h. Cells were harvested, homogenized in a homogenizing buffer (25 mM imidazole, 0.25 M sucrose, 1 mM AEBSF and protease inhibitor tablets (Roche)) using a Dounce homogenizer with 40 strokes of a tight-fitting pestle. The lysate was centrifuged at 700 g for 10 min at 4°C to pellet cell debri and nuclei. The postnuclear supernatant was centrifuged at 3,000 g for 10 min at 4°C to pellet mitochondria. The resulting supernatant was then centrifuged at 20,000 g for 30 min at 4°C to pellet down the microsomal membranes. The pellet was resuspended in 100 μl of IP buffer (150 mM NaCl, 10 mM Tris-HCl, 2 mM EDTA (pH 7.5), 1 % *n*-Dodecyl β-D-maltoside (DDM) (Sigma), protease inhibitor tablets (Roche)). 200 μl of blocking buffer (3 % BSA in PBST) was added. After 5 min, 2.5 μl of anti-Flag antibody (Sigma) was added and rotated for 1 h at room temperature. 55 μl of pre-equilibrated protein G resin (Thermo Scientific) was added and rotated for 1 h at RT. The resin was washed with 20 column volumes of PBS and the bound protein was eluted using 60 μl of elution buffer (0.17 M Tris, pH 6.8, 6.8 % SDS, 2.7 M urea, 1:100 β-mercaptoethanol). 24 μl of the eluted protein was loaded to a 4-20% TGX gel (Bio-Rad) (2 gels were used). One of the gels was dried for determining the phosphorylation level. The proteins in the second gel were transferred to PVDF membrane using a 10 mM CAPS, pH 11 transfer buffer. Immunoblotting was done using rat polyclonal anti-N-ATP7B antibody (1:5000) as primary antibody, and HRP-conjugated goat anti-rat IgG (1:10,000) (Santa Cruz) The average intensity of protein bands was determined using densitometry (Alpha Imager 2200). The level of phosphorylation was normalized to protein levels detected in the immunoblot.

Cloning, expression, and purification of N-ATP7B variants: The cDNA fragment encoding the N-ATP7B in a pTYB12 vector was used for expression of N-ATP7B-intein fusion protein. The Ser>Ala replacement was introduced by PCR using the Quickchange XL mutagenesis kit. 1 L of *E. coli* BL21 (DE3) cells transformed with the appropriate plasmids were grown at 37°C to an A_{600} of 0.7. Protein expression was induced with 1 mM isopropyl 1-thio-β-D-galactopyranoside (IPTG). Protein was expressed at 25°C for 4 h. Cells were harvested by centrifugation, disrupted using French press, recombinant proteins were purified on chitin beads according to manufacturer's protocol (NEB) and eluted with 50 mM DTT for 36 hours at room temperature. The proteins were concentrated using ultracel-30K (Millipore) and the purity of recombinant N-ATP7B was verified by SDS-PAGE.

Limited proteolysis with trypsin: 5 µg of purified N-ATP7B was diluted to 1 µg/µl in 40 mM Na-phosphate, pH 7.5, containing 400 mM NaCl, 1 mM BCS and mixed with 0.05 µg TPCK-treated bovine pancreatic trypsin (Sigma) at RT in a total volume of 12 µl. The reaction was quenched for 10 min by adding 1.2 µl of 50 mM AEBSF. Proteins were precipitated using 1.2 µl of 20 % TCA, and mixed with a loading dye and 1 µl of 1 M NaOH. Digestion patterns were determined by using 12 % Tricine gels and staining of protein bands with Coomassie blue.

For limited proteolysis of Flag-ATP7B, confluent Hek293TRex cells in 10 cm dishes were transiently transfected with either wt Flag-ATP7B^{R875} or Flag-ATP7B$^{R875,S340/341G}$ plasmids using Turbofect. Protein expression was induced with 10 ng/ml DOX for 4 h in basal conditions and cells were kept overnight in media containing 50 µM BCS. Cells were harvested, homogenized in a homogenizing buffer (25 mM imidazole, 0.25 M

sucrose) and the microsomal fractions were isolated as described above. The pellet containing the microsomal membranes was resuspended in 100 µl of trypsin buffer containing 40 mM Na- phosphate, pH 7.5, 400 mM NaCl, and 0.25 M sucrose. Equal amounts of total protein were loaded (15 µg); when necessary levels of ATP7B were also equalized by using membranes from non-transfected cells. The microsomal fractions were treated with 0.15 µg TPCK-treated trypsin at 37°C in a total volume of 20 µl. The reaction was quenched by adding 2 µl of 100 mM AEBSF. Proteins were analyzed by 8 % SDS gel, transferred to PVDF membrane using a 10 mM CAPS transfer buffer, pH 11 and immunostained using rabbit polyclonal anti-NBD-ATP7B antibody (1:2500) as primary antibody, and HRP-conjugated goat anti-rabbit IgG (1:10,000) (Santa Cruz). The average intensity of protein bands was determined by densitometry (Alpha Imager 2200).

Domain-domain interactions: Nucleotide-binding domain (NBD) cloned in a pTYB12 vector (Dmitriev et al., 2006) was expressed in *E.coli* BL21 strain in 500 ml of culture medium using 1 mM IPTG. N-ATP7B (wt and S340/341A) fused with maltose binding protein (MBP) (~105kDa) was expressed as previously described (Lutsenko et al., 1997). Bacterial cells were harvested by centrifugation at 5000 rpm at 4°C, lysed by French press (3 passes) followed by centrifugation at 17,000 rpm at 4°C to remove cell debris and collect supernatants. 100 µl of supernatant were analyzed by 10 % SDS PAGE to quantitate amount of expressed recombinant proteins by densitometry. Supernatants were then mixed to reach an equimolecular ratio of NBD and N-ATP7B and incubated for 1 h in a rotator at 4°C. The mixture was applied to amylose beads and incubated for 1 h in the rotator at RT. The beads were then washed with 20 column volumes of 50 mM Na-

phosphate buffer containing 500 mM NaCl (pH 7.0) and complete EDTA free protease inhibitor cocktail (Roche). Interacting proteins were eluted with the same buffer containing 10 mM maltose. 10 µl of the eluate was ran on a 15% SDS-PAGE, transferred to PVDF membrane and the presence of NBD was detected with rabbit polyclonal anti-NBD antibody. To quantify N-ATP7B, the membrane was stripped with 10X PBS for 1 h and re-probed with rat polyclonal anti-N-ATP7B Ab. The bands intensity was quantified by densitometry using Alpha Imager 2200.

NMR analysis of N-ATP7B: The ^{15}N-isotopic labeling of N-ATP7B for NMR was performed using published protocol (Dmitriev et al., 2006). Following purification by chitin affinity chromatography, N-ATP7B was additionally purified by ion-exchange chromatography on a Hi Trap Q column (GE Healthcare) using linear concentration gradient of NaCl (0-0.5M) for elution, dialyzed to remove salt, and concentrated by membrane filtration. Samples for NMR contained 20-90 µM protein, 50 mM HEPES-Na, pH 7.4, 50 mM NaCl, 5 mM tris(2-carboxyethyl)phosphine, 5% (v/v) D_2O and 0.5 mM 2,2-dimethyl-2-sila-pentane-5-sulfonate (DSS) for chemical shift referencing. ^{1}N,^{15}N-TROSY (Pervushin et al., 1997) experiments were recorded on a 900 MHz Varian NMR spectrometer at 298K.

Immunofluorescence microscopy: Hek293TRex cells on coverslips were transiently transfected with the wt or mutant Flag-ATP7B using Turbofect. Protein expression was induced with 40 ng/ml DOX for 16 h in basal conditions. Cells were treated with 100 µM BCS or 100 µM $CuCl_2$ for 2 h, rinsed with PBS and fixed with in cold acetone-methanol mixture (1:1) for 30 sec. The cells were blocked in blocking buffer (1 % gelatin, 1 % BSA in PBS) and then incubated with appropriate primary and secondary

antibodies diluted in blocking buffer. (Primary antibody: mouse anti-Flag antibody 1:250 (Sigma) and rabbit anti-TGN38 1:100 (Santa Cruz). Secondary antibody: Alexa Fluor 488 Goat anti mouse antibody 1:500 (Invitrogen) and Alexa Fluor 555 goat anti rabbit 1:500 (Invitrogen)). Coverslips were mounted onto glass slides using Vectashield w/DAPI (Vector Laboratories). Images were taken using a Zeiss PALM confocal microscope and a 100x oil immersion objective.

Immuno-electron microscopy: HEK293 cells transfected with either wt or mutant Flag-ATP7B were fixed with a mixture of 4% paraformaldehyde and 0.05% glutaraldehyde, labeled with rabbit polyclonal anti-Flag antibody (Sigma) using the gold-enhance protocol as described previously (Polishchuk et al., 2003). Then, cells were fixed in uranyl acetate and in OsO_4, dehydrated through a graded series of ethanol and embedded in the epoxy resin (Epon 812). Thin sections were cut with Leica EM UC6 ultramicrotome (Leica Microsystems, Wetzlar, Germany). Images from sections were acquired using a JEM-1011 electron microscope (JEOL, Tokyo, Japan) equipped with an MORADA CCD digital camera (Soft Imaging Systems GmbH, Munster, Germany).

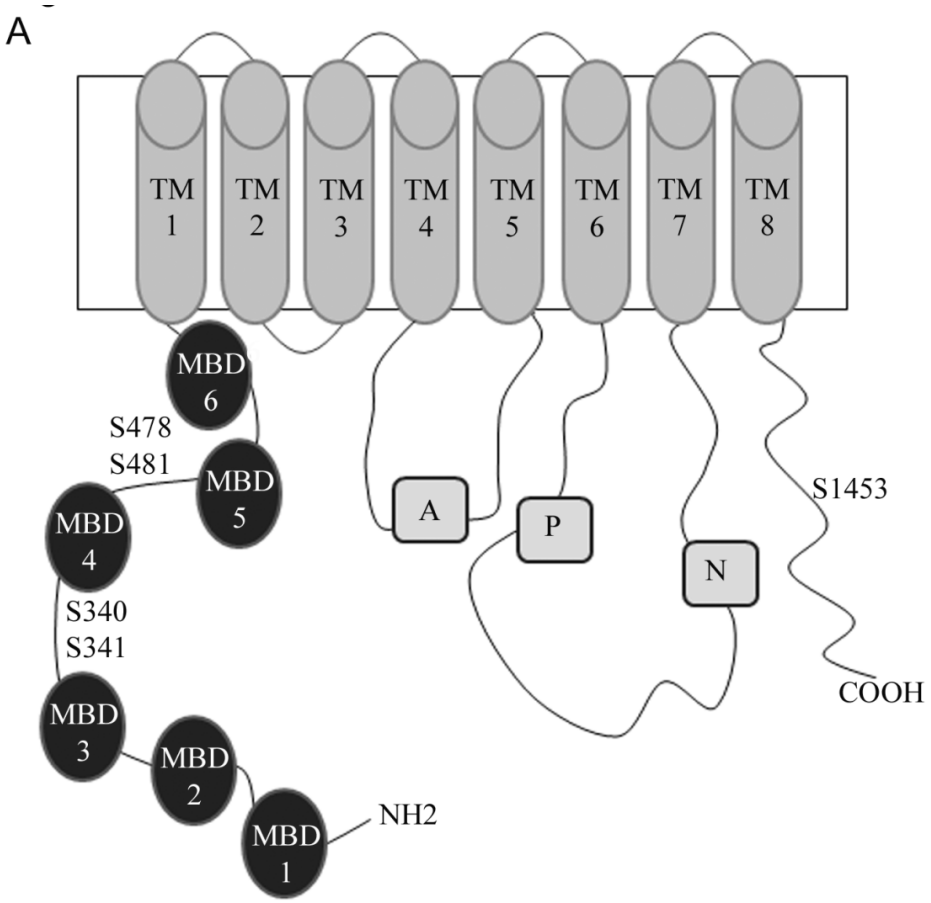

B

```
ATP7B_Homo_sapiens        GSGTDHRSSSSHSPGSPPRNQVQGTCS
ATP7A_Homo_sapiens        STSNSPSSSSLQK--IPLNVVSQPLTQ
ATP7A_Bos_taurus          STSNSPSSSSLQK--SPLNIVSQPLTQ
ATP7A_Mus_musculus        STASSPSSSSLQK--MPLNIVSQPLTQ
ATP7A_Rattus_norvegicus   SPTSSPSSSSLQK--PLNLVSQPLTQE
```

C

```
ATP7B_Homo_sapiens        GSGTDHRSSSSHSPGSPPRNQVQGTCS
ATP7B_Rattus_norvegicus   ---KESGSSSVPSLGSSQRQQEPGPCR
ATP7B_Bos_taurus          GSGPDSRS--------PPASSAP---C
ATP7B_Canis_lupus         GSETGNRFSACAAPAPAPRTPAPGRCD
ATP7B_Equus_caballus      GSGADNGSSTRHSPSPLQRTQVQGTCR
ATP7B_Gallus_gallus       --ANNQASPSPALVCDLFREPLKDTVC
```

Figure 2-1. (A) Schematic representation of ATP7B, (B) sequence alignment of ATP7B and ATP7A, or (C) ATP7B orthologs in the region containing Ser 340 and Ser 341 (A) Filled circles represent the N-terminal metal binding domains (MBDs) and are numbered 1 to 6. Transmembrane domains are numbered TM1 to TM8. The other domains are as follows: A: actuator domain; P: phosphorylation domain; N: nucleotide-binding domain. The positions of serine residues mutated in this study are shown. (B) The Ser rich cluster (shown in bold) in human ATP7B (S340-S343) is conserved in mammalian ATP7A orthologs. (C) Ser residues in ATP7B orthologs that align with human ATP7B Ser340 and Ser341 are shown in bold font. Ser340 and Ser341 show significant conservation.

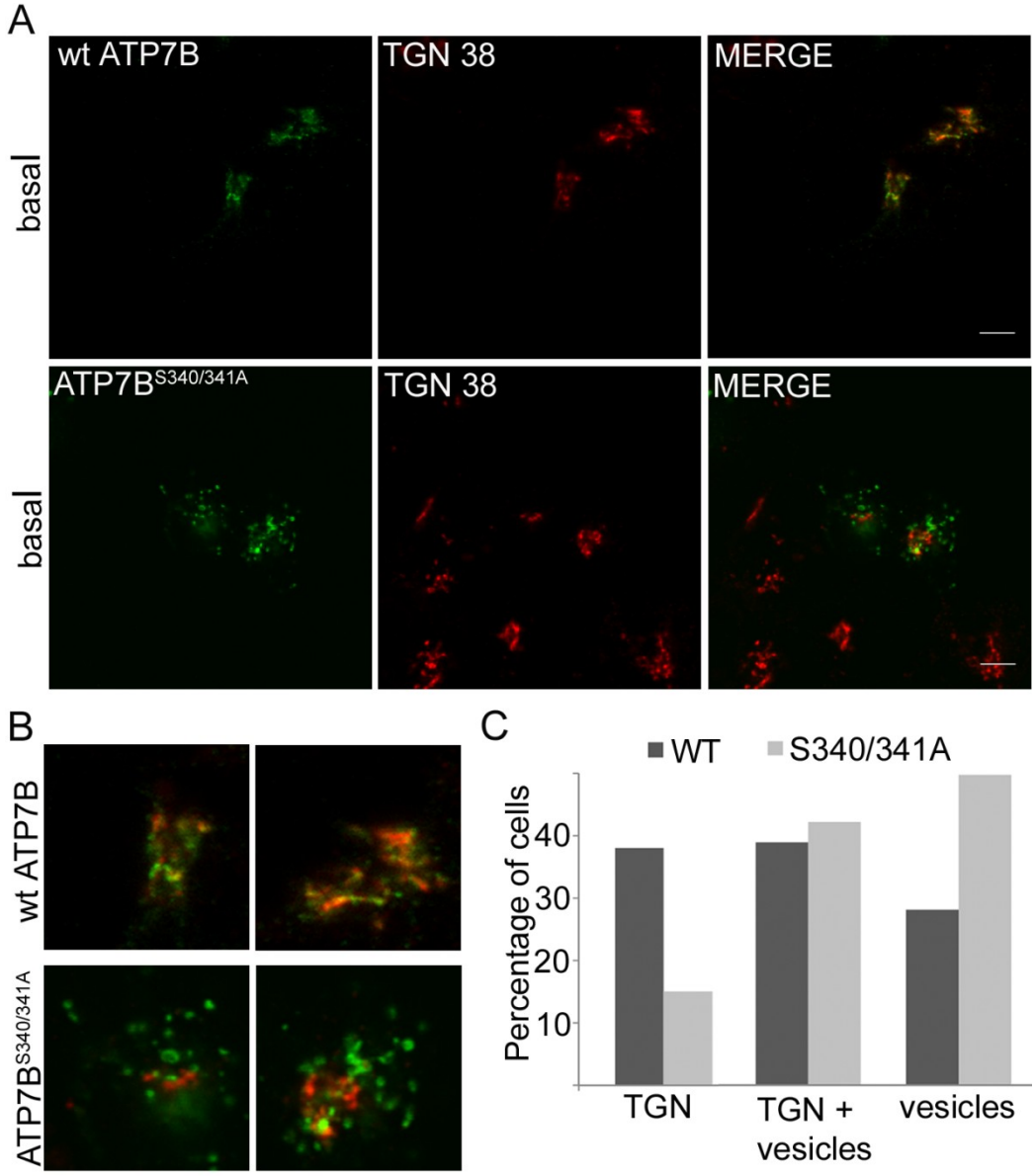

Figure 2-2. Mutating S340 and/or S341 shifts the steady-state localization of ATP7B towards vesicles in Hek293TRex cells. (A) Hek293TRex cells were transiently transfected with wt Flag-ATP7B or Flag-ATP7B$^{S340/341A}$. After doxycycline-induced expression in basal conditions, cells were immunostained with anti-Flag antibody (left, green) and anti-TGN38 (middle, red) and the patterns were compared (merge, right). Scale bar: 5 µm. (B) Magnified images demonstrating good colocalization between wt Flag-ATP7B and TGN 38 (upper panel), and vesicular localization of Flag-ATP7B$^{S340/341A}$ and the loss of colocalization with TGN38 (lower panel). (C) Random fields of view were chosen and the number of cells having different intracellular localizations of transfected ATP7B were counted. The graph shows the number of cells having wt Flag-ATP7B or Flag-ATP7B$^{S340/341A}$ in different localizations within the cells: TGN, TGN+vesicles, or vesicles.

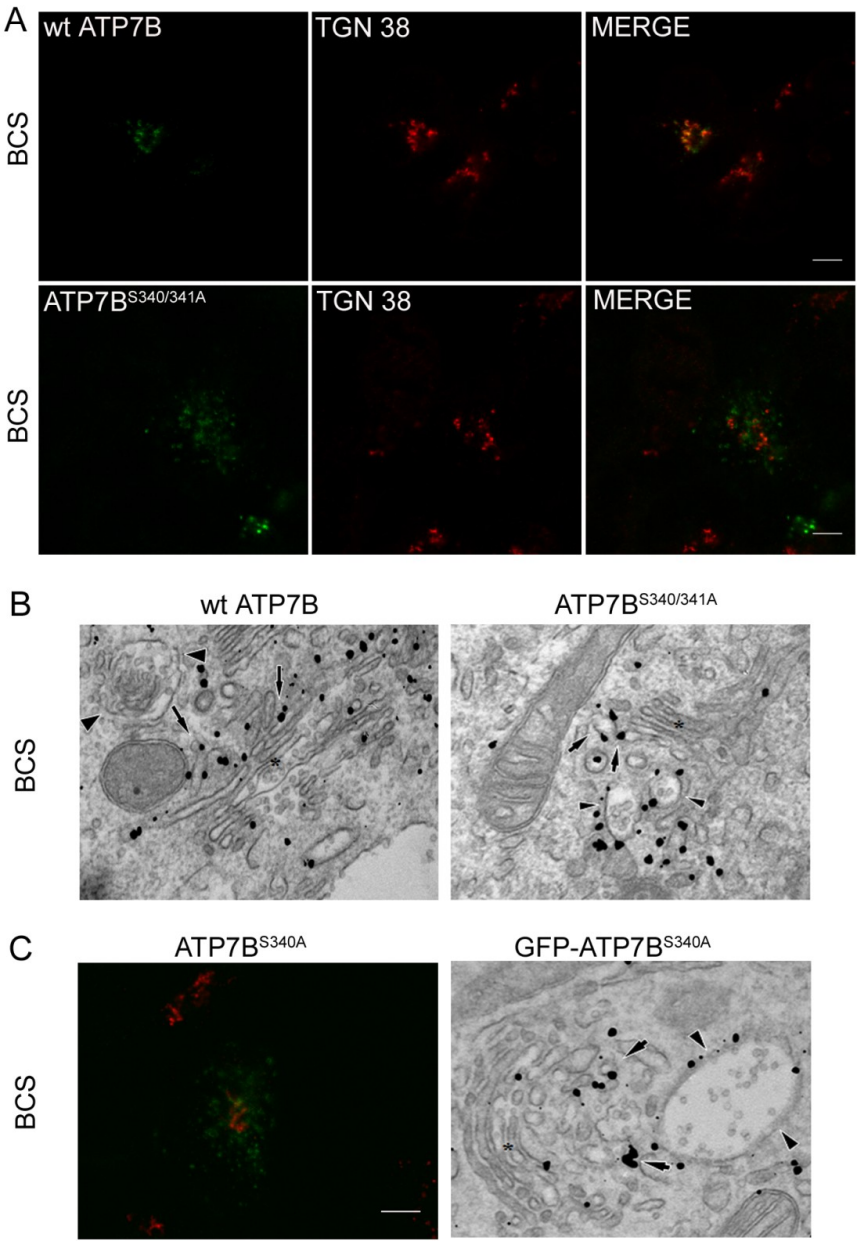

Figure 2-3. ATP7B$^{S340/341A}$ and ATP7B^{S340A} do not return to TGN with copper depletion. (A) Copper depletion of Hek293TRex cells transiently transfected with wt Flag-ATP7B or Flag-ATP7B$^{S340/341A}$ was done using 100 µM BCS for 2 h. Cells were immunostained using anti-Flag antibody (green) and TGN 38 (red). Merged image is located at the right panel. Scale bar: 5 µm. (B) Copper depletion treatment was done using 200 µM BCS for 3 h. Cells were processed for immuno-gold EM with anti-Flag antibody. The wt Flag-ATP7B (left panel) was detected over the tubular-vesicular profiles (arrows) at the *trans*-side of the Golgi stacks (asterisks). Arrowheads indicate large vesicles which were devoid of ATP7B signal. Flag-ATP7B$^{S340/341A}$ (right panel) decorated membrane profiles (arrows) at the *trans*-side of the Golgi stacks (asterisk) as well as large vesicles (arrowheads). (C) Representative confocal image (left panel) of Flag-ATP7B^{S340A} (green) with a TGN marker (red) in copper depleted conditions (100 µM BCS for 2 h). Electron microscopy (right panel) of GFP-ATP7B^{S340A} in Hek 293 cells under copper depleted conditions (200 µM BCS for 3 h) is shown. GFP-ATP7B^{S340A} is localized at the *trans*-side (arrows) of the Golgi complex (asterisk). In addition the mutant appeared also in large "vesicles" (arrowheads) which (in contrast to wt ATP7B) exhibited heavy gold labeling even at low Cu conditions.

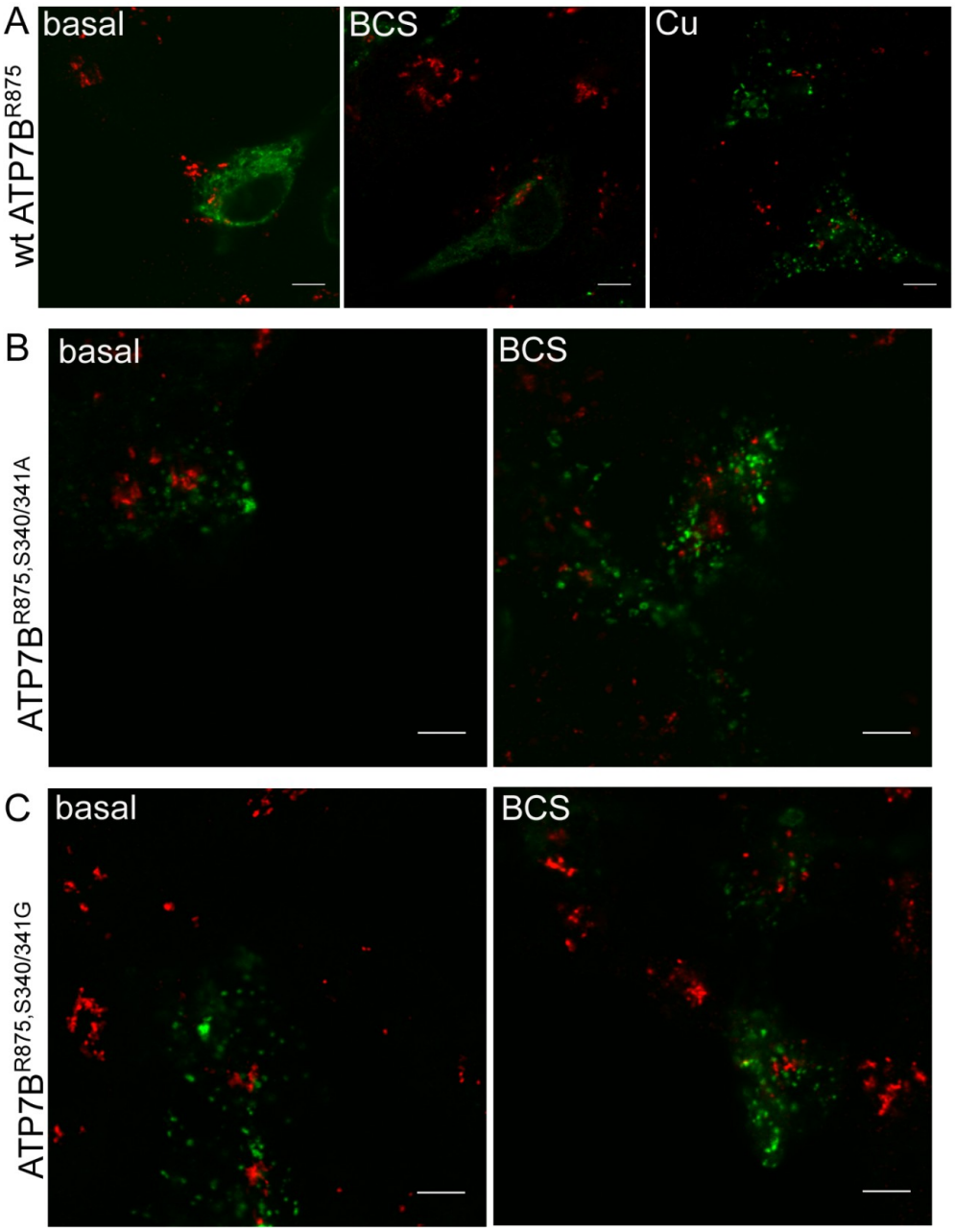

Figure 2-4. ATP7B$^{R875,S340/341A}$ and ATP7B$^{R875,S340/341G}$ mimic a copper saturated form and are localized in vesicles. Hek293TRex cells were transiently transfected with wt Flag-ATP7B^{R875}, Flag-ATP7B$^{R875,S340/341A}$ or Flag-ATP7B$^{R875,S340/341G}$. Cells were kept in basal media, copper depleted by treatment with 100 µM BCS for 2 h or copper treated by treatment with 100 µM $CuCl_2$ for 2 h. Cells were immunostained using Flag antibody (green) and TGN 38 (red); shown are merged images. (Scale bar: 5 µm) (A) wt Flag- ATP7B^{R875} is localized in ER in basal (left panel) and copper-depleted conditions (middle panel), and moves to vesicles upon copper treatment (right panel). (B) ATP7B$^{R875,S340/341A}$ is localized in vesicles in basal (left panel) and copper-depleted (right panel) conditions. (C) ATP7B$^{R875,S340/341G}$ is localized in vesicles in basal (left panel) and copper-depleted (right panel) conditions.

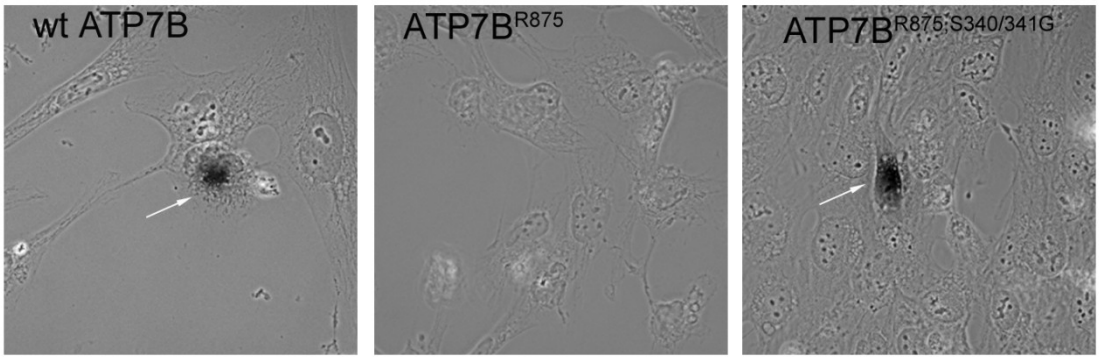

Figure 2-5. ATP7B$^{R875,S340/341G}$ has copper transport activity and pumps copper into the TGN of YSTT cells in basal conditions. Tyrosinase assay shows pigment formation for wt GFP-ATP7B (arrow, left panel) and Flag-ATP7B$^{R875,S340/341G}$ (arrow, right panel) but no pigment formation for wt Flag-ATP7B^{R875} (middle panel) in YSTT cells in basal copper conditions.

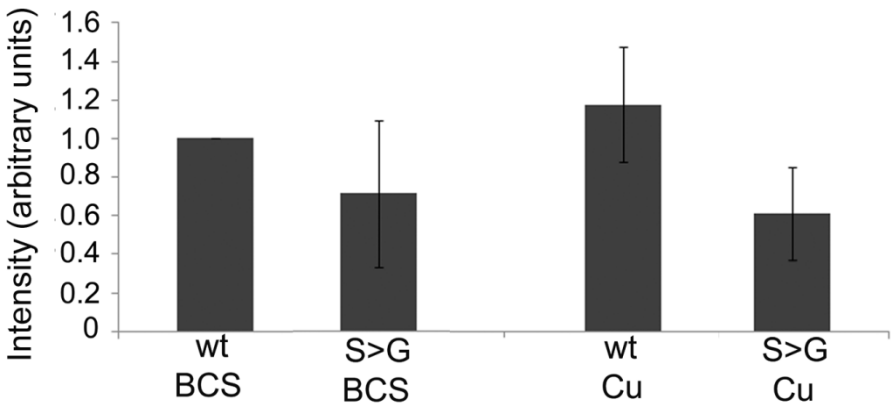

Figure 2-6. ATP7B$^{R875,S340/341G}$ has a decreased level of kinase mediated phosphorylation. Hek293TRex cells were transiently transfected with wt Flag-ATP7B^{R875} or Flag-ATP7B$^{R875,S340/341G}$, treated with 100 µM BCS or 100 µM $CuCl_2$ for 2 h and *in vivo* metabolically labeled with radioactive orthophosphate. The kinase mediated phosphorylation of Flag-ATP7B^{R875} (wt) and Flag-ATP7B$^{R875,S340/341G}$ (S>G) was compared following immunoprecipitation, gel-separation and densitometry. Error bars indicate S.D. across four independent experiments.

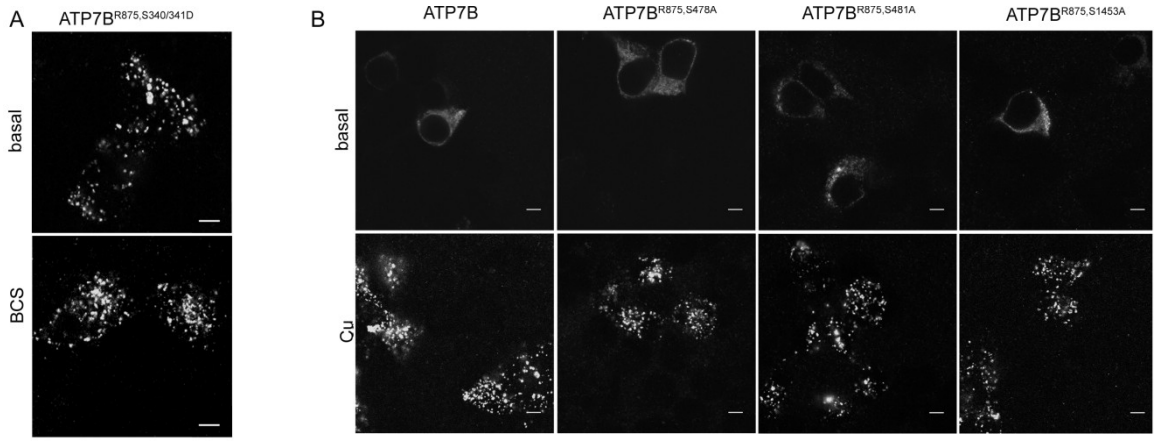

Figure 2-7. The phospho-mimetic mutant ATP7B$^{R875,S340/341D}$ is localized in vesicles and the effect of Ser340/341 mutations on trafficking is selective. Hek293TRex cells were transiently transfected with wt Flag-ATP7B^{R875}, Flag-ATP7B$^{R875,S340/341D}$, Flag-ATP7B^{R875,S478A}, Flag-ATP7B^{R875,S481A} or Flag-ATP7B^{R875,1453A}. Cells were kept in basal media, copper depleted by treatment with 100 µM BCS for 2 h or copper treated by treatment with 100 µM $CuCl_2$ for 2 h. Cells were immunostained using anti-Flag antibody. (A) Shown are representative confocal images of Flag-ATP7B$^{R875,S340/341D}$ in basal (upper panel) and copper depleted conditions (lower panel). Flag-ATP7B$^{R875,S340/341D}$ is localized in vesicles. (B) Representative confocal images of ATP7B mutants in Hek293TRex cells are shown. Flag-ATP7B^{R875,S478A}, Flag-ATP7B^{R875,S481A} and Flag-ATP7B^{R875,S1453A} behave as wild type. They are predominantly found in ER in basal conditions, and traffic to vesicles upon copper treatment. (Scale bar: 5µm).

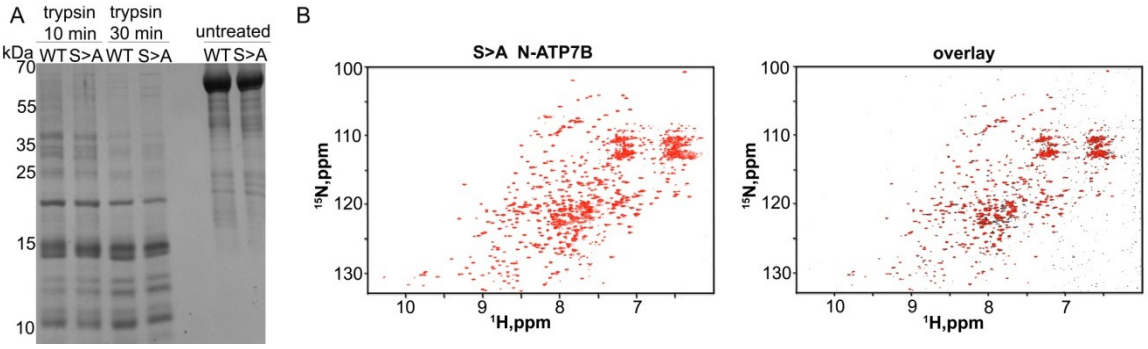

Figure 2-8. The Ser340/341A mutation does not disrupt protein folding of N-ATP7B. (A) Proteolytic patterns obtained following treatment of 5 µg purified recombinant N-ATP7B (WT) and N-ATP7B$^{S340/341A}$ (S>A) with 0.05 µg trypsin. Peptides were resolved using 12% Tricine gel and stained with Coomassie blue G. (B) 900 MHz $^{1}H,^{15}N$-TROSY spectra of the S340/341A mutant MBD1-6 (left panel), and an overlay (right panel) of the wild type (*black*) and the S340/341A mutant (*red*).

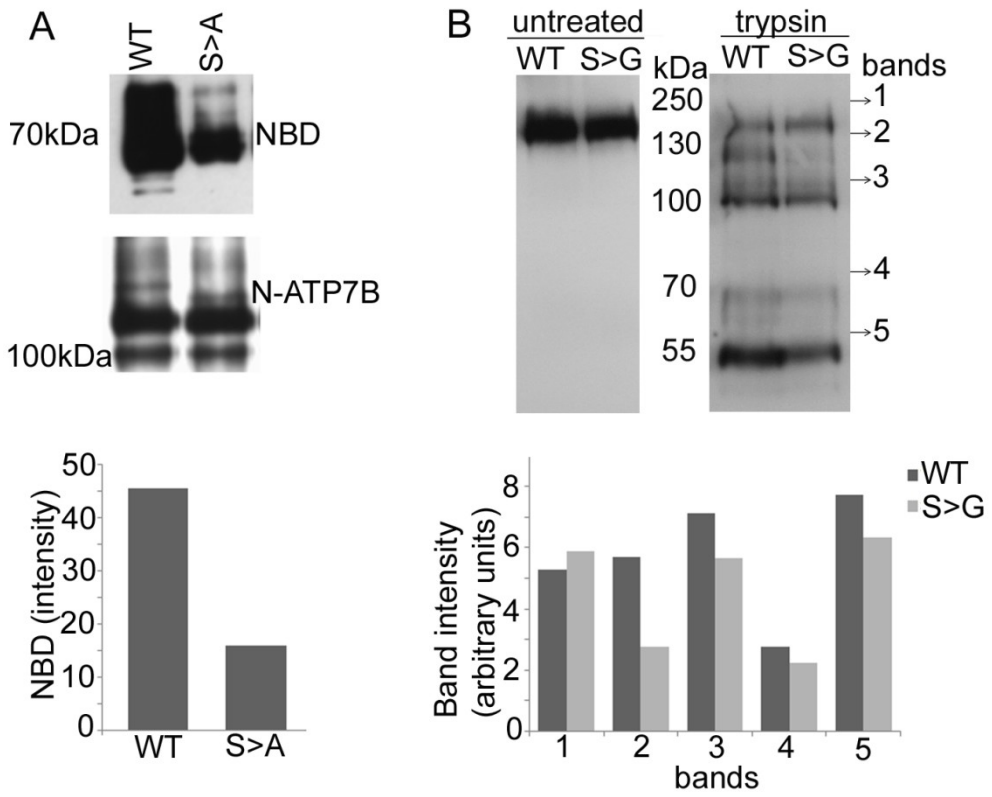

Figure 2-9. The Ser340/341A mutation reduces interactions between N-ATP7B and nucleotide-binding domain (NBD) resulting in an altered conformation of ATP7B. (A) Cell lysates containing maltose-binding fusions of N-ATP7B (WT) or N-ATP7B$^{S340/341A}$ (S>A) were mixed with lysates containing recombinant NBD and passed over amylose resins. NBD co-purified with the N-ATP7B was quantified in western blot using anti-NBD antibody (upper panel) and by densitometry (lower panel). Staining with anti-N-ATP7B antibody shows comparable amount of purified wt and mutant N-ATP7B (middle panel). (B) Proteolytic patterns obtained following treatment of 15 µg total membrane (from Flag-ATP7B^{R875} (WT) or Flag-ATP7B$^{R875,S340/341G}$ (S>G) transfected cells) with 0.15 µg trypsin for 15 min at 37°C. Peptides were resolved using 8% SDS gel and immunoblotted with NBD-ATP7B antibody. The bands were analyzed by densitometry and are represented in the bar graph.

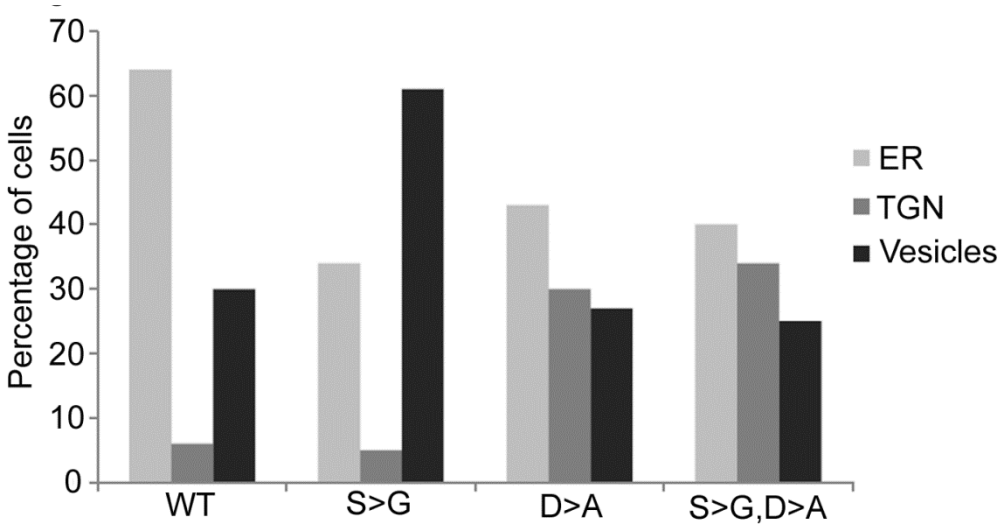

Figure 2-10. Copper transport activity is necessary for the shift of the intracellular localization of ATP7B$^{R875,S340/341G}$ to vesicles. Hek293TRex cells were transiently transfected with Flag-ATP7B^{R875} (WT), Flag-ATP7B$^{R875,\ D1027A}$ (D>A), Flag-ATP7B$^{R875,\ S340/341G}$ (S>G) or ATP7B$^{R875,\ S340/341G,\ D1027A}$ (S>G, D>A). Cells were kept in basal media. Cells were immunostained using Flag antibody and TGN 38. Random fields of view were chosen and the number of cells having different intracellular localizations of transfected ATP7B were counted. The graph shows the number of cells having WT, D>A, S>G and S>G, D>A ATP7B in different localizations within the cells: ER, TGN, or vesicles.

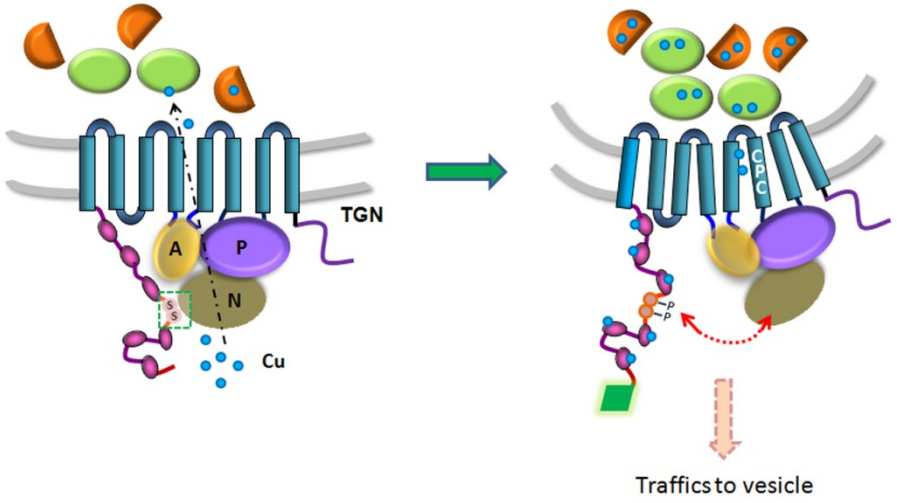

Figure 2-11. The proposed sequence of events that triggers ATP7B trafficking. In basal copper, N-ATP7B has a partial copper occupancy and ATP7B pumps copper into the lumen of TGN, where released copper is incorporated into available apo-proteins (green beads and brown half-spheres). In high copper, MBDs are saturated with copper and N-ATP7B dissociates from the N-domain resulting in pump activation. The S340/341 sites situated in the MBD3-MBD4 loop are phosphorylated and that keeps the domains apart (dotted red arrow). Due to higher pump activity, the acceptor proteins become saturated, copper release is diminished, and ATP7B is stabilized is a conformation favorable for TGN exit. In this conformation, ATP7B interacts with the trafficking machinery (green rhomboid). Similar effect on ATP7B conformation is achieved by mutating Ser340/341. The domains are denoted as, A: Actuator; N: Nucleotide-binding domain; P: Phosphorylation domain. The six metal-binding sites on N-ATP7B are shown in purple beads.

Reference List

Barnes, N., Bartee, M.Y., Braiterman, L., Gupta, A., Ustiyan, V., Zuzel, V., Kaplan, J.H., Hubbard, A.L., and Lutsenko, S. (2009). Cell-specific trafficking suggests a new role for renal ATP7B in the intracellular copper storage. Traffic *10,* 767-779.

Bartee, M.Y., and Lutsenko, S. (2007). Hepatic copper-transporting ATPase ATP7B: function and inactivation at the molecular and cellular level. Biometals *20,* 627-637.

Bartee, M.Y., Ralle, M., and Lutsenko, S. (2009). The loop connecting metal-binding domains 3 and 4 of ATP7B is a target of a kinase-mediated phosphorylation. Biochemistry *48,* 5573-5581.

Bonifacino, J.S., and Traub, L.M. (2003). Signals for sorting of transmembrane proteins to endosomes and lysosomes. Annu. Rev. Biochem. *72,* 395-447.

Braiterman, L., Nyasae, L., Guo, Y., Bustos, R., Lutsenko, S., and Hubbard, A. (2009). Apical targeting and Golgi retention signals reside within a 9-amino acid sequence in the copper-ATPase, ATP7B. Am. J. Physiol. Gastrointest. Liver Physiol. *296,* G433-44.

Bull, P.C., Thomas, G.R., Rommens, J.M., Forbes, J.R., and Cox, D.W. (1993). The Wilson disease gene is a putative copper transporting P-type ATPase similar to the Menkes gene. Nat. Genet. *5,* 327-337.

Cater, M.A., Forbes, J., La Fontaine, S., Cox, D., and Mercer, J.F. (2004). Intracellular trafficking of the human Wilson protein: the role of the six N-terminal metal-binding sites. Biochem. J. *380,* 805-813.

Cater, M.A., La Fontaine, S., and Mercer, J.F. (2007). Copper binding to the N-terminal metal-binding sites or the CPC motif is not essential for copper-induced trafficking of the human Wilson protein (ATP7B). Biochem. J. *401,* 143-153.

DiDonato, M., Hsu, H.F., Narindrasorasak, S., Que, L.,Jr, and Sarkar, B. (2000). Copper-induced conformational changes in the N-terminal domain of the Wilson disease copper-transporting ATPase. Biochemistry *39,* 1890-1896.

Dmitriev, O., Tsivkovskii, R., Abildgaard, F., Morgan, C.T., Markley, J.L., and Lutsenko, S. (2006). Solution structure of the N-domain of Wilson disease protein: distinct nucleotide-binding environment and effects of disease mutations. Proc. Natl. Acad. Sci. U. S. A. *103,* 5302-5307.

Guo, Y., Nyasae, L., Braiterman, L.T., and Hubbard, A.L. (2005). NH2-terminal signals in ATP7B Cu-ATPase mediate its Cu-dependent anterograde traffic in polarized hepatic cells. Am. J. Physiol. Gastrointest. Liver Physiol. *289,* G904-16.

Gupta, A., Bhattacharjee, A., Dmitriev, O.Y., Nokhrin, S., Braiterman, L., Hubbard, A.L., and Lutsenko, S. (2011). Cellular copper levels determine the phenotype of the Arg875 variant of ATP7B/Wilson disease protein. Proc. Natl. Acad. Sci. U. S. A. *108,* 5390-5395.

Gupta, A., and Lutsenko, S. (2009). Human copper transporters: mechanism, role in human diseases and therapeutic potential. Future Med. Chem. *1,* 1125-1142.

Hinners, I., and Tooze, S.A. (2003). Changing directions: clathrin-mediated transport between the Golgi and endosomes. J. Cell. Sci. *116,* 763-771.

Hung, I.H., Suzuki, M., Yamaguchi, Y., Yuan, D.S., Klausner, R.D., and Gitlin, J.D. (1997). Biochemical characterization of the Wilson disease protein and functional expression in the yeast Saccharomyces cerevisiae. J. Biol. Chem. *272,* 21461-21466.

Huttlin, E.L., Jedrychowski, M.P., Elias, J.E., Goswami, T., Rad, R., Beausoleil, S.A., Villen, J., Haas, W., Sowa, M.E., and Gygi, S.P. (2010). A tissue-specific atlas of mouse protein phosphorylation and expression. Cell *143,* 1174-1189.

La Fontaine, S.L., Firth, S.D., Camakaris, J., Englezou, A., Theophilos, M.B., Petris, M.J., Howie, M., Lockhart, P.J., Greenough, M., Brooks, H., Reddel, R.R., and Mercer, J.F. (1998). Correction of the copper transport defect of Menkes patient fibroblasts by expression of the Menkes and Wilson ATPases. J. Biol. Chem. *273,* 31375-31380.

Lim, C.M., Cater, M.A., Mercer, J.F., and La Fontaine, S. (2006a). Copper-dependent interaction of dynactin subunit p62 with the N terminus of ATP7B but not ATP7A. J. Biol. Chem. *281,* 14006-14014.

Lim, C.M., Cater, M.A., Mercer, J.F., and La Fontaine, S. (2006b). Copper-dependent interaction of glutaredoxin with the N termini of the copper-ATPases (ATP7A and ATP7B) defective in Menkes and Wilson diseases. Biochem. Biophys. Res. Commun. *348,* 428-436.

Lutsenko, S., LeShane, E.S., and Shinde, U. (2007). Biochemical basis of regulation of human copper-transporting ATPases. Arch. Biochem. Biophys. *463,* 134-148.

Lutsenko, S., Petrukhin, K., Cooper, M.J., Gilliam, C.T., and Kaplan, J.H. (1997). N-terminal domains of human copper-transporting adenosine triphosphatases (the Wilson's and Menkes disease proteins) bind copper selectively in vivo and in vitro with stoichiometry of one copper per metal-binding repeat. J. Biol. Chem. *272,* 18939-18944.

Materia, S., Cater, M.A., Klomp, L.W., Mercer, J.F., and La Fontaine, S. (2012). Clusterin and COMMD1 independently regulate degradation of the mammalian copper ATPases ATP7A and ATP7B. J. Biol. Chem. *287,* 2485-2499.

Payne, A.S., Kelly, E.J., and Gitlin, J.D. (1998). Functional expression of the Wilson disease protein reveals mislocalization and impaired copper-dependent trafficking of the common H1069Q mutation. Proc. Natl. Acad. Sci. U. S. A. *95,* 10854-10859.

Pervushin, K., Riek, R., Wider, G., and Wuthrich, K. (1997). Attenuated T2 relaxation by mutual cancellation of dipole-dipole coupling and chemical shift anisotropy indicates an avenue to NMR structures of very large biological macromolecules in solution. Proc. Natl. Acad. Sci. U. S. A. *94,* 12366-12371.

Pilankatta, R., Lewis, D., Adams, C.M., and Inesi, G. (2009). High yield heterologous expression of wild-type and mutant Cu+-ATPase (ATP7B, Wilson disease protein) for functional characterization of catalytic activity and serine residues undergoing copper-dependent phosphorylation. J. Biol. Chem. *284,* 21307-21316.

Pilankatta, R., Lewis, D., and Inesi, G. (2011). Involvement of protein kinase D in expression and trafficking of ATP7B (copper ATPase). J. Biol. Chem. *286,* 7389-7396.

Polishchuk, E.V., Di Pentima, A., Luini, A., and Polishchuk, R.S. (2003). Mechanism of constitutive export from the golgi: bulk flow via the formation, protrusion, and en bloc cleavage of large trans-golgi network tubular domains. Mol. Biol. Cell *14,* 4470-4485.

Roelofsen, H., Wolters, H., Van Luyn, M.J., Miura, N., Kuipers, F., and Vonk, R.J. (2000). Copper-induced apical trafficking of ATP7B in polarized hepatoma cells provides a mechanism for biliary copper excretion. Gastroenterology *119,* 782-793.

Tanzi, R.E., Petrukhin, K., Chernov, I., Pellequer, J.L., Wasco, W., Ross, B., Romano, D.M., Parano, E., Pavone, L., and Brzustowicz, L.M. (1993). The Wilson disease gene is a copper transporting ATPase with homology to the Menkes disease gene. Nat. Genet. *5,* 344-350.

Tao, T.Y., Liu, F., Klomp, L., Wijmenga, C., and Gitlin, J.D. (2003). The copper toxicosis gene product Murr1 directly interacts with the Wilson disease protein. J. Biol. Chem. *278,* 41593-41596.

Tsivkovskii, R., MacArthur, B.C., and Lutsenko, S. (2001). The Lys1010-Lys1325 fragment of the Wilson's disease protein binds nucleotides and interacts with the N-terminal domain of this protein in a copper-dependent manner. J. Biol. Chem. *276,* 2234-2242.

Vanderwerf, S.M., Cooper, M.J., Stetsenko, I.V., and Lutsenko, S. (2001). Copper specifically regulates intracellular phosphorylation of the Wilson's disease protein, a human copper-transporting ATPase. J. Biol. Chem. *276,* 36289-36294.

Voskoboinik, I., Brooks, H., Smith, S., Shen, P., and Camakaris, J. (1998). ATP-dependent copper transport by the Menkes protein in membrane vesicles isolated from cultured Chinese hamster ovary cells. FEBS Lett. *435,* 178-182.

Vulpe, C., Levinson, B., Whitney, S., Packman, S., and Gitschier, J. (1993). Isolation of a candidate gene for Menkes disease and evidence that it encodes a copper-transporting ATPase. Nat. Genet. *3,* 7-13.

III. Novel Regulators of Copper Homeostasis

This research was originally published in Nat Commun, 2014 Feb 13;5:3301., Genome-wide RNAi ionomics screen reveals new genes and regulation of human trace element metabolism, and all text and figures in this chapter have been adapted from it.

Contributing Authors: Malinouski M, Hasan NM, Zhang Y, Seravalli J, Lin J, Avanesov A, Lutsenko S, Gladyshev VN.

Introduction

Copper is essential for normal growth and development; as being a cofactor for a variety of vital metabolic enzymes. However, copper levels must be tightly regulated to avoid oxidative stress and changes in intracellular redox status. Loss of copper homeostasis is associated with heart hypertrophy, liver failure, neuronal de-myelination and other pathologies. ATP7A is a copper ATPase that is involved in maintaining the copper homeostasis. ATP7A is localized to the *trans*-Golgi network (TGN) under basal conditions where it pumps copper to cuproenzymes located in the lumen of the TGN and upon increase of intracellular copper levels it traffics to vesicles and plasma membrane to export excess copper (Gupta and Lutsenko, 2009). Despite its central role, the exact mechanism of ATP7A trafficking between cellular compartments remains only partially characterized.

The regulation of copper-ATPases occurs on multiple levels, some of which have not been characterized well. AIPP1, p97 VCP and glutaredoxin1 have been shown to interact with ATP7A, however their mechanism of action has not been well characterized yet (Lim et al., 2006; Stephenson et al., 2005; Yi et al., 2012). In addition, ATP7A is modified post-translationally by glutathionylation and glycosylation, but little is known about the functional effects of these modifications (Singleton et al., 2010; Yamaguchi et al., 1996). ATP7A also undergoes kinase mediated phosphorylation on multiple serine residues under basal and elevated copper conditions, and the level of phosphorylation is copper-dependent and reversible (Voskoboinik et al., 2003). Therefore, the kinase-mediated phosphorylation of ATP7A might be involved in regulation of trafficking or copper-transport activity. In addition,

copper ATPases traffic in response hormones, such as insulin and estrogen; which again raises the possibility of other regulatory proteins involved (Hardman et al., 2007).

A genome-wide high-throughput siRNA/ionomics screen was performed by our collaborators to determine novel regulators of trace elements homeostasis, yielding eight proteins as potential candidates for regulation of copper homeostasis. Knockdowns of IBTK, CAMK2N2, DNAJC5, DNAJC17, ABCC3, ANKRD9, and SLC6A4 resulted in elevation of intracellular copper levels (Table 3-1) (Malinouski et al., 2014). To uncover the specific roles of these genes in cellular copper balance, we determined the effects of their inactivation on ATP7A, the major copper export protein in HeLa cells. Novel mechanisms controlling the copper ionome through ATP7A were identified. Out of seven tested targets, down-regulation of five had a significant effect on ATP7A. This result emphasizes the primary role of ATPase-mediated copper export in balancing cellular copper.

Results

Characterization of predicted copper regulators reveals new mechanisms controlling the copper ionome through ATP7A

Several candidates not known previously to be involved in the regulation of trace element homeostasis were identified (Table 3-1). Knockdowns of two members of the DNAJ family (DNAJC5 and DNAJC17), two kinase inhibitor genes (CAMK2N2 and IBTK) and two transporters (SLC6A4 and ABCC3) led to increased copper levels (Table 3-1). Following down-regulation of the target genes, we characterized ATP7A expression,

intracellular targeting, and its ability to undergo copper-dependent trafficking from *trans*-Golgi network (TGN) to the plasma membrane (a step required for copper efflux).

Out of seven tested targets, down-regulation of five had a significant effect on ATP7A. This result emphasizes the primary role of ATPase-mediated copper export in balancing cellular copper. Knockdown of DNAJC5 and SLC6A4 did not influence ATP7A protein levels, trafficking or targeting, indicating that these proteins may regulate other components of the copper-handling machinery. In contrast, knockdown of a member of the HSP40 family DNAJC17 produced a significant reduction in ATP7A amount in cells as evidenced by the decreased intensity of ATP7A signal (green) in the TGN compared to the marker TGN46 (red) (Fig. 3-1, Fig. 3-2). The decrease of ATP7A in the TGN was due to lower ATP7A protein levels (rather than the loss of TGN targeting) as evidenced by Western blotting of cellular lysates (Fig. 3-1). The levels of other tested proteins, such as Na,K-ATPase and TGN46, were not affected. Knockdowns of kinase inhibitors IBTK and CAMK2N2 had a dual effect: reduction in the ATP7A levels and a shift in the ATP7A electrophoretic mobility (Fig. 3-1, Fig. 3-2) that suggested changes in posttranslational modification of ATP7A.

A different mode of ATP7A regulation was detected in the case of the ABCC3 knockdown. Downregulation of this gene did not have a significant effect on ATP7A levels (Fig. 3-1) or ATP7A targeting to the TGN (Fig. 3-2a). Instead, in cells with the down-regulated ABCC3 the distribution of ATP7A between the TGN and vesicles was altered, with less ATP7A leaving the TGN in response to copper treatment (Fig. 3-3 b,c).

Perhaps, the most intriguing results were obtained with cells depleted of ANKRD9. Down-regulation of this adaptor protein led to an increased cell size, dispersion of the TGN and a change in ATP7A electrophoretic mobility (Fig. 3-1b, Fig 3-3d). A shift in ATP7A migration on SDS-PAGE gels suggests that the posttranslational modifications of ATP7A, which is a glycosylated protein, are affected. Although the ANKRD9 knockdown affected TGN morphology, it did not disrupt colocalization of ATP7A and TGN46 suggesting that the molecular identity of this compartment was preserved (Fig. 3-2b). We are now facing intriguing mechanistic questions about a link between TGN morphology, ATP7A modification, and cellular copper levels. Taken together, these data show that essentially all effects of the target gene knockdowns with respect to copper elevation can be explained by changes in ATP7A trafficking, modification, and/or expression. Cellular machinery that controls ATP7A mRNA and/or protein stability has not been previously characterized, and the identification of several new regulatory components as a result of the ionomics screen provides exciting opportunities for better understanding of copper metabolism in human cells.

Effect of DNAJC17 downregulation is indirect

Individual siRNA sequences against DNAJC17 were used to confirm the specificity of DNAJC17 knockdown. ATP7A levels were determined by immunoblotting following transfection with siRNAs. ATP7A protein levels were decreased significantly with DNAJC17 #2 siRNA transfection (Fig. 3-4a). ATP7A and DNAJC17 mRNA levels were determined using RT-PCR assays, and although the same level of downregulation of DNAJC17 was achieved with DNAJC17 #2 siRNA and DNAJC17 #1,3,4 siRNAs; only

DNAJC17 #2 siRNA resulted in decreased ATP7A mRNA levels (Fig. 3-4b,c), raising the possibility that the effect of DNAJC17 downregulation is off-target (i.e. not mediated though DNAJC17). In addition, DNAJC17 #2 siRNA transfection resulted in high degree of cell death.

Discussion

In this study, the effect of downregulation of novel regulatory proteins on the copper-exporting ATPase ATP7A was studied. The novel regulatory proteins (IBTK, CAMK2N2, DNAJC5, DNAJC17, ABCC3, ANKRD9, and SLC6A4) were identified through a high-throughput ionomics screen (Malinouski et al., 2014) and their knockdowns resulted in elevation of intracellular copper. Both IBTK (inhibitor of Bruton tyrosine kinase) and CAMK2N2 (calcium/calmodulin-dependent protein kinase II inhibitor 2) are kinase inhibitors, and their down-regulation resulted in a significant decrease in ATP7A protein levels. Kinase-mediated phosphorylation plays a role in the trafficking of ATP7A (Veldhuis et al., 2009; Voskoboinik et al., 2003); however, roles of Bruton tyrosine kinase or CAMK2 in ATP7A phosphorylation have not been previously known or considered. It is interesting that both kinases participate in major signaling pathways involving a nuclear factor-kappaB (NF-κB) (Petro et al., 2000; Scharenberg and Kinet, 1998; Singh et al., 2009). These results suggest a link between the stress-response pathways and a tight regulation of copper homeostasis (Veldhuis et al., 2009; Voskoboinik et al., 2003).

The negative effect of ABCC3 (ATP-binding cassette, subfamily C (CFTR/MRP), member 3) down-regulation on ATP7A trafficking is an equally novel result. ABCC3 is an organic anion and bile acid transporter. Previously, treating hepatocytes (HepG2) with copper resulted in an upregulation of ABCC3 (Song and Freedman, 2005). Together, these results suggest that the bile acid transport and copper metabolism might be linked. The observed increase in copper levels in response to disregulation of lipid metabolism further supports idea of copper and lipid homeostasis being interconnected. The downregulation of ABCC3 may also be affecting the organic anion/bile acid balance in HeLa cells, which might inhibit ATP7A transport activity and copper-responsive trafficking, which are also mutually dependent.

Downregulation of ANKRD9 (ankyrin repeat domain-containing protein 9) produces a complex phenotype, which includes fragmented TGN and apparent changes in ATP7A post-translational modification and protein levels. The function of this protein is not known, but it was suggested to play a role in lipid metabolism (Wang et al., 2009). Other ankyrin proteins are involved in membrane protein trafficking/stabilization (Devarajan et al., 1996; Tamura et al., 2011). Thus, ANKRD9 may bind to ATP7A and stabilize its TGN localization. Furthermore, ANKRD9 induced a decrease in ATP7A protein levels and a shift in ATP7A migration on SDS-PAGE gels, which could be a secondary effect of TGN fragmentation and may alter the ability of ATP7A to efficiently pump excess copper out of the cell.

It is also possible that the identified proteins are affecting other complements of the copper handling machinery within the cells. Further studied will be needed to determine the mechanistic role of the identified proteins in maintaining the copper homeostasis.

Materials and Methods

Cell lines: HeLa cells (obtained from ATCC) were maintained in DMEM supplemented with 10 % FBS and 1 % pen/strep at 37 ºC in a 5% CO_2 incubator.

siRNA transfection, western blotting and immunohistochemistry: Modified version of the Dharmacon's Wet Reverse Transfection Protocol was used for the transfection of HeLa cells. Dharmafect I reagent (0.4 µl/well) was diluted using Optimem media (24.6 µl/well). Stock siRNA (human siGenome pool siRNA, Dharmafect) was mixed with Optimem to a final volume of 10 µl (the final siRNA concentration is 20 nM/well). Both Dharmafect I/Optimem and siRNA/Optimem solutions were mixed and added to each well of an 8-well chamber (Millipore). Chambers were incubated for 30 min at RT. HeLa cells were trypsinized and resuspended in antibiotic free complete medium. 0.3 x 10^5 cells were added to each well in a volume of 170 µl. The chambers were placed at 37 ºC in a 5% CO_2 incubator. 60 h after the transfection 200 µl of in antibiotic free complete medium was added to each well. Cells were fixed 72 h after the transfection using 3% paraformaldehyde at 37ºC for 12 min. Cells were washed with 1X PBS and blocked/permeabilized simultaneously for 12 min using 1% BSA/ 1% saponin in 1X PBS. Cells were washed with 1X PBS and then incubated with appropriate primary and secondary antibodies diluted in 0.5 % BSA in 1X PBS (Primary antibody: mouse anti-

ATP7A antibody 1:250 (Santa Cruz) and sheep anti-TGN46 1:300 (Genetex). Secondary antibody: Alexa Fluor 488 Goat anti mouse antibody 1:500 (Invitrogen) and Alexa Fluor 555 donkey anti sheep 1:500 (Invitrogen). The glass slides were mounted using Fluoromount G w/DAPI (Electron Microscopy Sciences). Images were taken using a Zeiss LSM 510 confocal microscope and a 40x oil immersion objective. For Western blotting, cells were harvested, the pellet was resuspended in 30 µl of Laemmli loading buffer, sonicated for 30 sec and centrifuged for 15 min at 3000 g at 4 ºC. The supernatant was loaded to 8 % SDS gel. Proteins were transferred to a PVDF membrane using CAPS buffer, pH 11.0. The membrane was cut at 130 kDa and probed for Na/K ATPase (1:10000, Millipore) and ATP7A (1:3000, Santa Cruz). Goat anti mouse Igg-HRP (1:10000, Santa Cruz) was used as a secondary antibody and the membranes were developed using a SuperSignal West Pico Substrate (Thermo Scientific).

RNA isolation and quantitative PCR: HeLa cells were transiently transfected with the indicated siRNA or scrRNA control and cells were harvested. RNA was isolated using RNeasy Mini Kit (Qiagen) and cDNA was prepared using *Transcriptor First Strand* cDNA Synthesis Kit (Roche). Real-time PCR was performed using a Power SYBR Green master mix (Applied Biosystems) using the following primer sequences: ATP7A, DNAJC17, GAPDH. GAPDH was used as an internal control for data normalization.

Table 3-1. Ionomic profiles of siRNA gene knockdowns involved in copper metabolism. Knockdown of the listed genes results in increase in copper levels specifically. z-scores, represent the number of standard deviations from the mean value the listed value is (z-score >3 was defined as the threshold) .

Gene	Description	Effect of knockdown (Increase in copper levels	z-score
DNAJC5	DnaJ (Hsp40) homolog, subfamily C, member 5	1.3	3.5
DNAJC17	DnaJ (Hsp40) homolog, subfamily C, member 17	1.3	5.1
IBTK	Inhibitor of Bruton agammaglobulinemia tyrosine kinase	1.4	6.7
ATP7A	ATPase, Cu^{+2} transporting, alpha polypeptide (Menkes syndrome)**	1.6	9.5
SLC6A4	Neurotransmitter transporter, serotonin, member 4	1.4	3.5
ANKRD9	Ankyrin repeat domain 9	1.7	7.2
CAMK2N2	Calcium/calmodulin-dependent protein kinase II inhibitor 2	1.6	6.0
ABCC3	ATP-binding cassette, sub-family C (CFTR/MRP)	1.6	5.6

*Genes previously implicated in regulation of indicated trace elements.

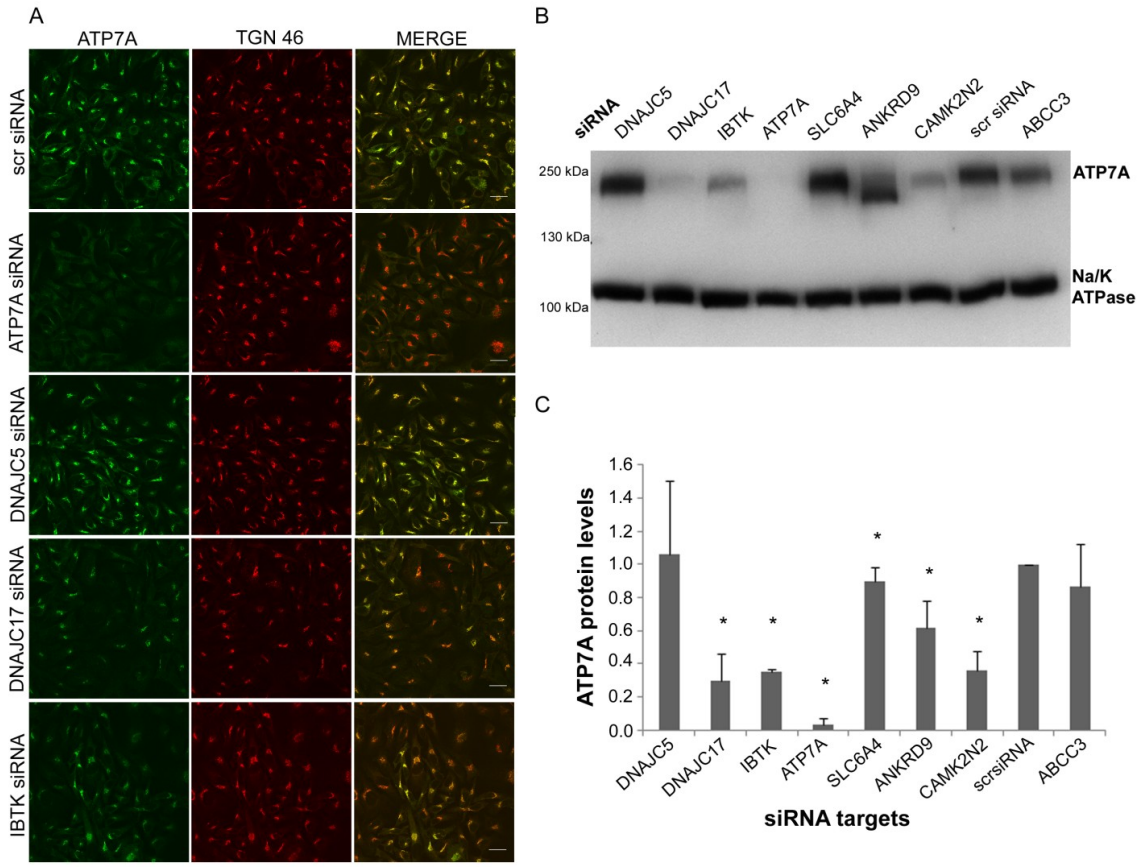

Figure 3-1. Characterization of targets that affect copper levels in HeLa cells. (a) Effect of targets downregulation on ATP7A localization in basal conditions. Following gene-specific siRNA-mediated knockdowns, HeLa cells were fixed, stained with the antibodies against ATP7A (green) and the TGN marker TGN46 (red) and analysed by confocal microscopy. The merged image is shown in the right panel. Scale bar, 25 μm. (b) Effect of target downregulation on ATP7A protein levels and electrophoretic mobility. Following gene knockdowns, HeLa cell lysates were analysed by western blotting. The blot was cut at 130 kDa; the upper part was immunostained for ATP7A and the lower part was immunostained for Na/K-ATPase. A representative blot is shown. (c) Quantification of western blot data by densitometry. The ATP7A protein levels were normalized to Na/K-ATPase protein levels and the values were compared with the intensity of ATP7A in cells transfected with a non-targeting siRNA (scrRNA). The error bars correspond to s.d. values from four independent experiments. Asterisks mark significant changes (the Mann–Whitney U-test, Po0.05; lower panel).

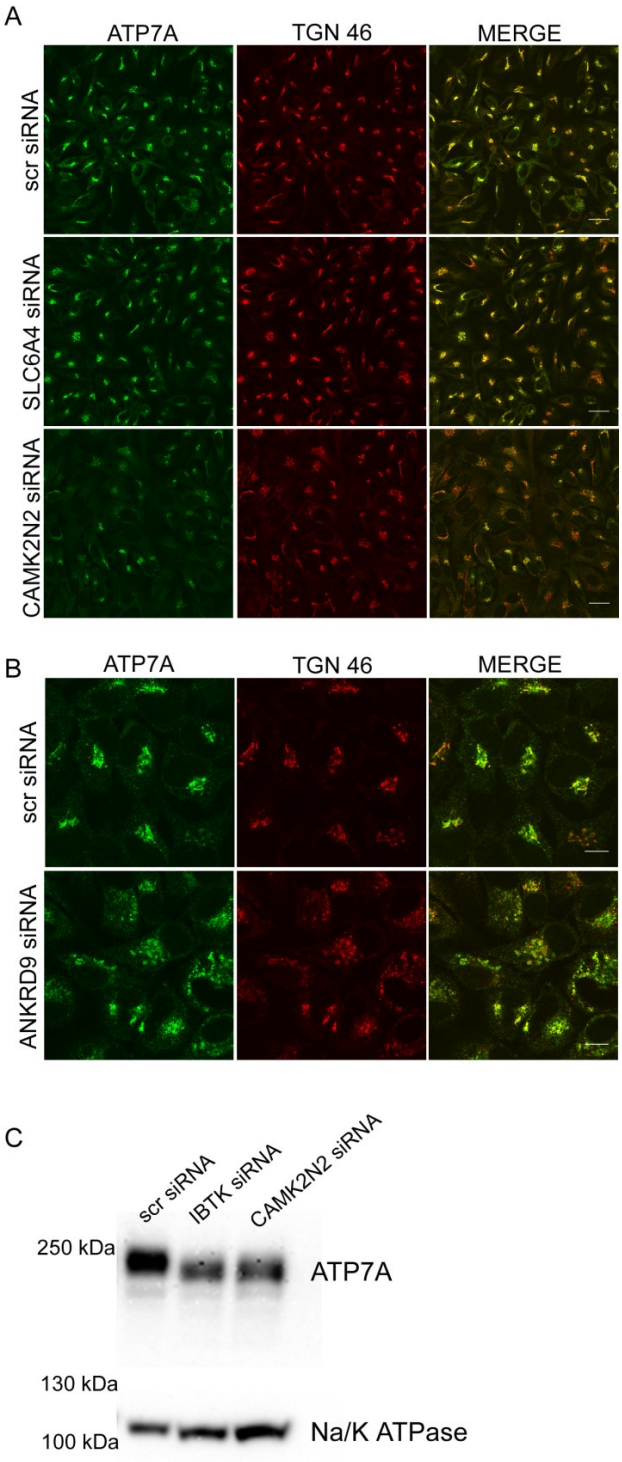

Figure 3-2. Characterization of genes that affect copper levels in HeLa cells. Following gene-specific knockdowns, HeLa cells were fixed and analyzed by confocal microscopy with antibodies against ATP7A (green) and the trans-Golgi network marker TGN46 (red). Scale bar: 25 μm. (b) 100x magnification images. ANKRD9 knockdown results in fragmented TGN and fragmented ATP7A staining pattern. Scale bar: 10 μm. (c) HeLa cells were transiently transfected with siRNAs, and cell lysates were analyzed by western blotting. The blot was cut at 130 kDa and the upper part was immunoblotted for ATP7A and the lower part was immunoblotted for Na/K ATPase. A representative blot is shown.

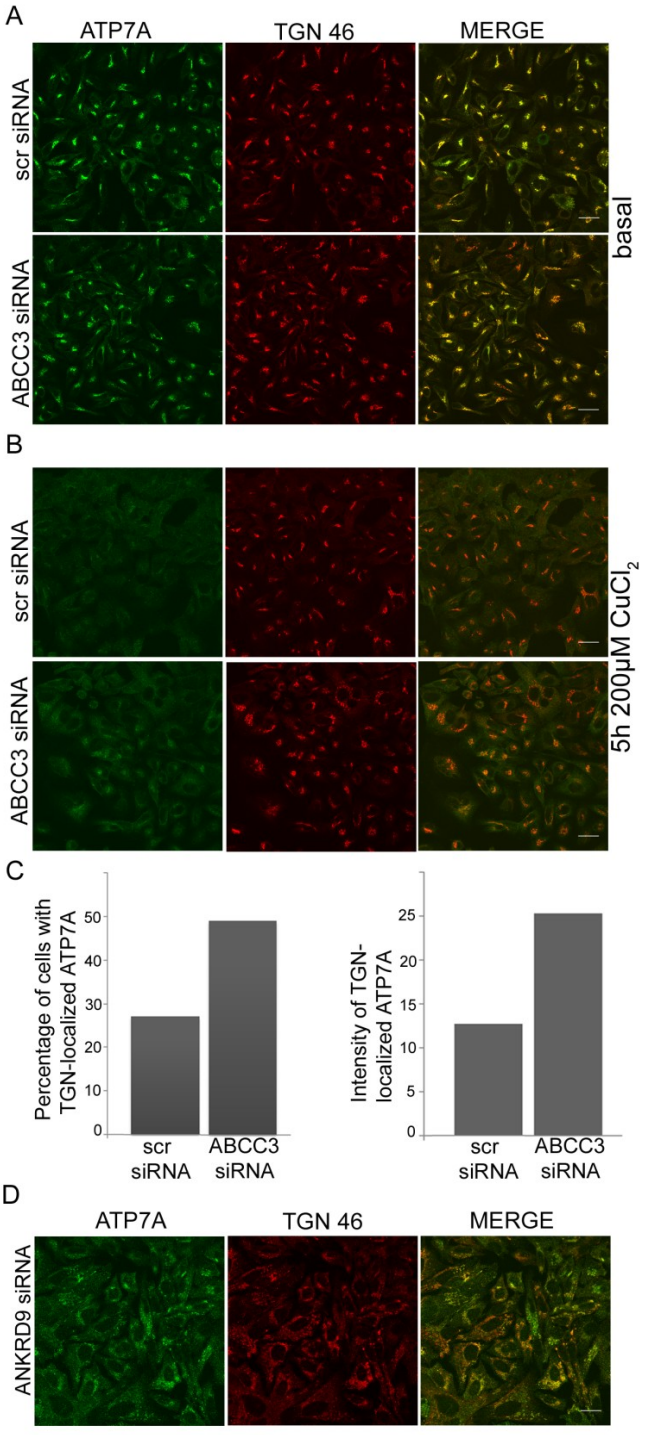

Figure 3-3. ABCC3 and ANKRD9 are new regulators of ATP7A. (a–c) Downregulation of ABCC3 affects ATP7A trafficking. Following siRNA-mediated knockdown, HeLa cells were kept under basal conditions (panel a, scale bar, 25 μm) or treated with 200 μM $CuCl_2$ for 5 h (panel b, scale bar, 25 μm), and then fixed, immmunostained with antibodies against ATP7A (green) and TGN46 (red) and analysed by confocal microscopy. (c) Percentage of cells with ATP7A in the TGN following the copper treatment (left panel). Intensity of ATP7A signal in the TGN was quantified using Image J (right panel). (d) ANKRD9 knockdown results in fragmented TGN and fragmented ATP7A staining pattern. Following siRNA-mediated knockdown, HeLa cells in basal conditions were fixed, stained with antibodies against ATP7A (green) and TGN46 (red) and analysed by confocal microscopy. Scale bar, 25 μm.

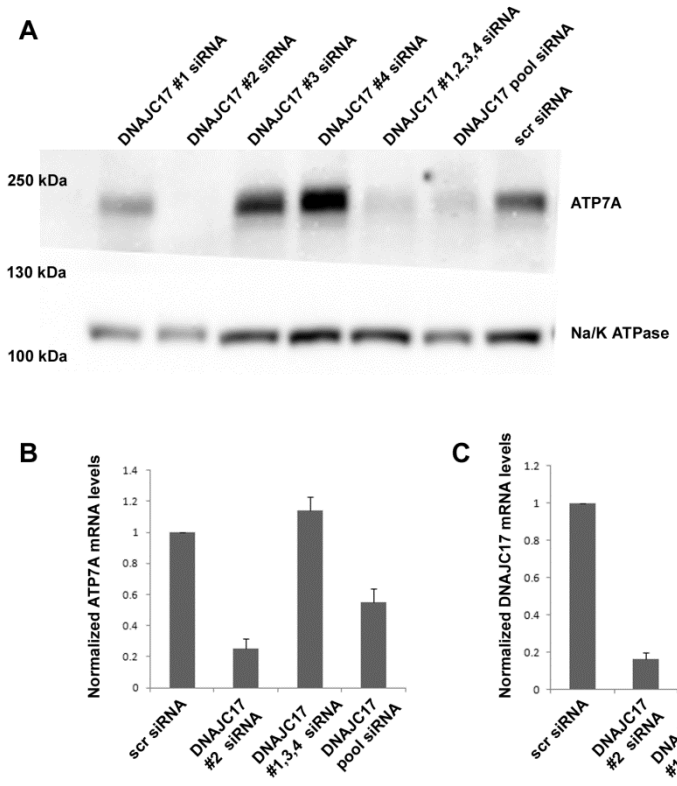

Figure 3-4. Effect of DNAJC17 downregulation is indirect. (a) HeLa cells were transiently transfected with siRNAs, and cell lysates were analyzed by western blotting. The blot was cut at 130 kDa and the upper part was immunoblotted for ATP7A and the lower part was immunoblotted for Na/K ATPase. A representative blot is shown. (b) ATP7A mRNA levels in transiently-transfected cells were analyzed by RT-PCR. (c) DNAJC17 mRNA levels in transiently-transfected cells were analyzed by RT-PCR.

Reference List

Devarajan, P., Stabach, P.R., Mann, A.S., Ardito, T., Kashgarian, M., and Morrow, J.S. (1996). Identification of a small cytoplasmic ankyrin (AnkG119) in the kidney and muscle that binds beta I sigma spectrin and associates with the Golgi apparatus. J. Cell Biol. *133,* 819-830.

Gupta, A., and Lutsenko, S. (2009). Human copper transporters: mechanism, role in human diseases and therapeutic potential. Future Med. Chem. *1,* 1125-1142.

Hardman, B., Michalczyk, A., Greenough, M., Camakaris, J., Mercer, J.F., and Ackland, M.L. (2007). Hormonal regulation of the Menkes and Wilson copper-transporting ATPases in human placental Jeg-3 cells. Biochem. J. *402,* 241-250.

Hasan, N.M., and Lutsenko, S. (2012). Regulation of copper transporters in human cells. Curr. Top. Membr. *69,* 137-161.

Lim, C.M., Cater, M.A., Mercer, J.F., and La Fontaine, S. (2006). Copper-dependent interaction of glutaredoxin with the N termini of the copper-ATPases (ATP7A and ATP7B) defective in Menkes and Wilson diseases. Biochem. Biophys. Res. Commun. *348,* 428-436.

Malinouski, M., Hasan, N.M., Zhang, Y., Seravalli, J., Lin, J., Avanesov, A., Lutsenko, S., and Gladyshev, V.N. (2014). Genome-wide RNAi ionomics screen reveals new genes and regulation of human trace element metabolism. Nat. Commun. *5,* 3301.

Petro, J.B., Rahman, S.M., Ballard, D.W., and Khan, W.N. (2000). Bruton's tyrosine kinase is required for activation of IkappaB kinase and nuclear factor kappaB in response to B cell receptor engagement. J. Exp. Med. *191,* 1745-1754.

Scharenberg, A.M., and Kinet, J.P. (1998). PtdIns-3,4,5-P3: a regulatory nexus between tyrosine kinases and sustained calcium signals. Cell *94,* 5-8.

Singh, M.V., Kapoun, A., Higgins, L., Kutschke, W., Thurman, J.M., Zhang, R., Singh, M., Yang, J., Guan, X., Lowe, J.S.*, et al.* (2009). Ca2+/calmodulin-dependent kinase II triggers cell membrane injury by inducing complement factor B gene expression in the mouse heart. J. Clin. Invest. *119,* 986-996.

Singleton, W.C., McInnes, K.T., Cater, M.A., Winnall, W.R., McKirdy, R., Yu, Y., Taylor, P.E., Ke, B.X., Richardson, D.R., Mercer, J.F., and La Fontaine, S. (2010). Role of glutaredoxin1 and glutathione in regulating the activity of the copper-transporting P-type ATPases, ATP7A and ATP7B. J. Biol. Chem. *285,* 27111-27121.

Song, M.O., and Freedman, J.H. (2005). Expression of copper-responsive genes in HepG2 cells. Mol. Cell. Biochem. *279,* 141-147.

Stephenson, S.E., Dubach, D., Lim, C.M., Mercer, J.F., and La Fontaine, S. (2005). A single PDZ domain protein interacts with the Menkes copper ATPase, ATP7A. A new protein implicated in copper homeostasis. J. Biol. Chem. *280,* 33270-33279.

Tamura, K., Ohbayashi, N., Ishibashi, K., and Fukuda, M. (2011). Structure-function analysis of VPS9-ankyrin-repeat protein (Varp) in the trafficking of tyrosinase-related protein 1 in melanocytes. J. Biol. Chem. *286,* 7507-7521.

Veldhuis, N.A., Valova, V.A., Gaeth, A.P., Palstra, N., Hannan, K.M., Michell, B.J., Kelly, L.E., Jennings, I., Kemp, B.E., Pearson, R.B., Robinson, P.J., and Camakaris, J. (2009). Phosphorylation regulates copper-responsive trafficking of the Menkes copper transporting P-type ATPase. Int. J. Biochem. Cell Biol. *41,* 2403-2412.

Voskoboinik, I., Fernando, R., Veldhuis, N., Hannan, K.M., Marmy-Conus, N., Pearson, R.B., and Camakaris, J. (2003). Protein kinase-dependent phosphorylation of the Menkes copper P-type ATPase. Biochem. Biophys. Res. Commun. *303,* 337-342.

Wang, X., Newkirk, R.F., Carre, W., Ghose, P., Igobudia, B., Townsel, J.G., and Cogburn, L.A. (2009). Regulation of ANKRD9 expression by lipid metabolic perturbations. BMB Rep. *42,* 568-573.

Yamaguchi, Y., Heiny, M.E., Suzuki, M., and Gitlin, J.D. (1996). Biochemical characterization and intracellular localization of the Menkes disease protein. Proc. Natl. Acad. Sci. U. S. A. *93,* 14030-14035.

Yi, L., Donsante, A., Kennerson, M.L., Mercer, J.F., Garbern, J.Y., and Kaler, S.G. (2012). Altered intracellular localization and valosin-containing protein (p97 VCP) interaction underlie ATP7A-related distal motor neuropathy. Hum. Mol. Genet. *21,* 1794-1807.

IV. ANKRD9 is a Novel Regulator of Copper Homeostasis

Introduction

Ankyrins comprise a family of intracellular adaptor proteins that link integral membrane proteins to the intracellular spectrin-actin cytoskeleton. In complexes with their binding partners, ankyrins organize distinct membrane domains. Ankyrins were shown to interact with diverse proteins: ion channels (voltage-gated Na^+ channels, voltage-gated potassium channel subunits KCNQ2 and KCNQ3, KCNG2/3, Rh antigen, IP3 receptor, ryanodine receptor), Na^+/Ca^{2+} exchanger, Na^+/K^+ ATPase, cell adhesion molecules (L1-CAMs, CD44, E-cadherin, dystroglycan), cellular trafficking proteins (tubulin, clathrin)). Ankyrin proteins consist of three domains: membrane protein binding domain containing ankyrin repeats (24 ankyrin repeats in major isoforms), spectrin binding domain, regulatory domain, and so-called "death" domain. Ankyrins and their isoforms are expressed in many tissues including cardiomyocytes, neurons, skeletal muscle cells and epithelial cells. Dysfunction of ankyrins results in defective membrane expression of the ankyrin-binding partners and leads to diseases such as such as haemolytic anaemia, cardiac arrhythmia and neurological disorders (Bennett and Healy, 2009; Cunha and Mohler, 2009).

Ankyrins are involved in trafficking of channels/ion-exchangers/transporting ATPases (Bennett and Healy, 2009). One of the most studied ankyrin proteins, Ankyrin G, binds to a variety of channels/pumps and cell adhesion molecules via its ankyrin repeats and links these membrane proteins to the actin cytoskeleton (Bennett and Healy, 2009). In neuronal cells, Ankyrin G acts as an adaptor and binds KIF5/kinesin-1 to transport Nav channels into axons (Barry et al., 2014). Another ankyrin protein, ankyrin B forms microdomain

complexes with Na^+/K^+ ATPase (α1 and α2 isoforms), Na^+/Ca^{2+} exchanger 1, and InsP3 receptor in cardiomycoytes to regulate cytosolic Ca^{2+} levels (Mohler et al., 2005). Ankyrin B associates with the cardiac K_{ATP} channel via Kir6.2 and downregulation of Ankyrin B decreases the plasma membrane expression of both Kir6.2 and K_{ATP} channel (Li et al., 2010).

In addition to ankyrins, cells express a large spectrum of proteins containing ankyrin (ANK) repeats. ANK repeats are 33 amino acid motifs found in viral, bacterial and archaeal proteins, and most commonly in eukaryotic proteins. Presently, 19,276 ankyrin repeat sequences have been identified in 3608 non-redundant proteins (Letunic et al., 2002; Schultz et al., 1998). ANK repeats are present in a diverse set of proteins involved in transcription, cell cycle regulation, cell signaling, cytoskeleton integrity, endocytosis, inflammatory response, and various transport phenomena. Each ankyrin repeat folds into two antiparallel α-helices that are connected by an exposed loop or a β-hairpin (Mosavi et al., 2004). Exposed loops contain non-conserved residues, which are likely to be involved in the recognition of specific proteins. Ankyrin repeats stack together to form an L-shaped structure known as Ankyrin Repeat Domains (ANKRD). Examples of ANKRD-binding proteins include Cdk4/6 cell cycle regulators, signaling protein Notch, Nf-κB inhibitor IκB, TRP cation channels, megalin (Mosavi et al., 2004). ANKRD proteins mediate specific protein–protein interactions and do not appear to have an enzymatic function. ANKRD can be present as a domain in complex multi-domain proteins or exist Ankyrin repeat domain-containing protein 9 (ANKRD9) was identified as a potential regulator of copper homeostasis through a genome-wide high-throughput

siRNA/ionomics screen (Malinouski et al., 2014). Information about properties and cellular/molecular function of ANKRD9 is very limited. Expression of hepatic ANKRD9 mRNA is increased 30-40 fold in chicken with hepatic accumulation of lipids caused by riboflavin deficiency and fatty acid oxidation. Fasting and thyroid hormone (which reduces hepatic triglyceride content) decrease hepatic mRNA levels of ANKRD9, whereas re-feeding increases its levels (Wang et al., 2009). Unpublished data shows that ANKRD9 knock-out mice ($Ankrd9^{tm1(KOMP)Wtsi}$) have a decreased amount of total body fat, increased lean body mass, and increased bone mineral content (https://www.mousephenotype.org/data/genes/MGI:1921501). These data suggest the role for ANKRD9 in lipid homeostasis

ANKRD9 levels are changed upon cell damage or in apoptosis in chicken, human HepG2 cells, and Hek293 cells (Wang et al., 2009). A microarray analysis revealed that ANKRD9 was downregulated in mouse colonic epithelial cells treated with epithelial-disrupting agent dextransulfate sodium (DSS), which induces tissue damage (Rogier et al., 2014). Another study in zebrafish, determined that ANKRD9 is an estrogen target gene, but the mechanism of estrogen-dependent regulation of ANKRD9 expression is unknown (Hao et al., 2013). Overall, ANKRD9 levels respond to different apparently unrelated stimuli, and the actual function of ANKRD9 remains largely unknown.

In our collaborative study, we found that ANKRD9 downregulation leads to an increase of intracellular copper (Malinouski et al., 2014) and the aim of current study was to understand the role of ANKRD9 in copper homeostasis. We found that ANKRD9

downregulation resulted in fragmentation of Golgi apparatus, raising the possibility that ANKRD9 might be involved in maintaining Golgi integrity. In addition, the proteins that we examined were partially glycosylated in cells with decreased levels of ANKRD9. It has been previously shown that disruption of Golgi structure and defects in glycosylation are linked events, (Petrosyan et al., 2012; Pokrovskaya et al., 2011; Shestakova et al., 2006; Struwe and Reinhold, 2012), however ANKRD9 has not been previously implicated in this process. In addition, we found that ANKRD9 downregulation resulted in sequestration of intracellular copper and significant upregulation of the copper uptake protein Ctr1, presumably as a mechanism to compensate for functional copper deficiency We conclude that ANKRD9 is a multifunctional protein with important role in copper homeostasis.

Results

Initial characterization of recombinant ANKRD9

ANKRD9 consists of 317 amino acids and it is conserved among vertebrates (Fig. 4-1a). It has a predicted size of 34.3 kDa and based on Pymol model predictions it consists of several alpha helices and loops (Fig. 4-1b). The number of ankyrin repeats in ANKRD9 is unclear. Wang et al. predicted that ANKRD9 has three ankyrin repeats at its N-terminus (ANK1:71-100 aa, ANK2: 112-141 aa, ANK3: 158-187 aa) and a poly-Leu motif (Wang et al., 2009). Similarly, three repeats were predicted in ANKRD9 protein in uniprot.org database, whereas InterPro database indicates one ankyrin repeat between the 158th and 190th amino acids (http://www.ebi.ac.uk/interpro/protein/ Q96BM1). We

performed homology modeling using Phyre2; this program revealed a typical ANKRD fold containing 8 repetitive sequences (Fig. 4-1b).

To begin characterization of ANKRD9, we generated a corresponding cDNA by RT-PCR using mRNA isolated from HeLa cells. The sequence encoding Flag-tag was introduced at the 5'-end and the final product was cloned into a pcDNA 3.1 (+) vector. HeLa cells were then transfected with Flag-ANKRD9 and expression and localization of recombinant protein was monitored by immunostaining. Fig. 4-1c illustrates that Flag-ANKRD9 localizes primarily to cytoplasmic vesicles in agreement with the findings of a previous study (Wang et al., 2009). Cell lysates were used for immunoblotting, and Flag-ANKRD9 was detected as two major bands around 35 kDa (Fig. 4-1d). We confirmed that there was a single plasmid species with Flag-ANKRD9/pcDNA 3.1(+) construct, so the double bands might be due to posttranslational modifications. Since ANKRD9 is predicted to be a soluble protein, yet is is observed targeted to vesicles, it is possible that it is palmitoylated at the invariant Cys residue 110.

Down-regulation of ANKRD9 increases intracellular copper levels

The genome-wide siRNA-mediated screen found that down-regulation of ANKRD9 in HeLa cells by transient transfection with a pool of four ANKRD9 siRNAs increases copper levels by 1.7 fold (Fig. 4-1e, f, g). The levels of other elements were not altered significantly (Fig. 4-1e, f, g). We repeated the down-regulation experiments along with the copper content measurements. The efficiency of ANKRD9 was determined using qPCR. In our experiments ANKRD9 mRNA was decreased 50% in cells transfected with

ANKRD9 siRNA compared to cells transfected with non-targetting siRNA (Fig. 4-2b). Atomic absorption spectroscopy of whole cell lysates showed that decrease of ANKRD9 amount is associated with 1.3 fold higher copper compared to control cells transfected with the non-targeting (NT) siRNA (Fig. 4-2a). By comparison, complete knock-down of ATP7A, which is the major copper-exporting ATPase in HeLa cells, resulted in a 1.9 fold increase of intracellular copper levels (Fig. 4-2a).

ANKRD9 is required for normal Golgi structure

To explain elevation of cellular copper in cell with lower ANKRD9 levels, we first examined the effect of ANKRD9 downregulation on ATP7A, the major copper export protein in HeLa cells. Under basal conditions, ATP7A is localized to the *trans*-Golgi network (TGN), where it pumps copper to cuproenzymes located in the lumen. Upon increase of intracellular copper, ATP7A traffics to vesicles and plasma membrane to export excess copper (Gupta and Lutsenko, 2009). Since other ankyrin proteins are known to be involved in membrane protein trafficking/stabilization (Devarajan et al., 1996; Tamura et al., 2011), we tested whether down-regulation of ANKRD9 affects ATP7A or its localization at the TGN.

HeLa cells were transfected with the NT siRNA or ANKRD9 siRNA and immunostained with the markers of Golgi compartments and anti-ATP7A antibodies. Depletion of ANKRD9 resulted in a dispersion of TGN46 (trans Golgi marker) (Fig. 4-2c) and Gpp130 (cis-medial Golgi marker) (Fig. 4-2d). ATP7A, which normally localizes to the TGN (Fig. 4-2c) and partially to cis-medial Golgi (Fig. 4-2d), also showed a fragmented

staining pattern in ANKRD9 depleted cells. ATP7A still retained its Golgi localization, it colocalized with the fragmented TGN (Fig. 4-2c).

We used electron microscopy to determine the effect of ANKRD9 downregulation on the Golgi structure in more detail; we also examined if the structure of other organelles was affected by ANKRD9 down-regulation. Consistent with the immunostaining data, we observed that the Golgi increased in size significantly and was fragmented in the ANKRD9-depleted cells (Fig. 4-3). The fragmented Golgi vesicles were not dispersed throughout the cytoplasm, but were arranged in clusters. No significant changes in the structure of other organelles were observed, which point to the Golgi organelle as the primary (direct or indirect) target of ANKRD9 downregulation. To verify our electron microscopy observations that other organelles were not significantly affected by ANKRD9 depletion, we immunostained siRNA-transfected HeLa cells with antibodies against calreticulin (endoplasmic reticulum (ER) marker) and Lamp1 (lysosomal marker) (Fig. 4-4). No significant difference in the pattern of ER or lysosomes was seen between control and ANKRD9-depleted cells.

ANKRD9 depletion results in partial glycosylation of ATP7A

ATP7A is the major copper exporting protein in HeLa cells. Therefore if ANKRD9 downregulation decreases ATP7A levels, the intracellular copper levels would increase due to inefficient copper export out of the cells. We measured both the mRNA and protein levels of ATP7A in ANKRD9-depleted cells to test this possibility. The effect of ANKRD9 downregulation on the level of ATP7A protein level was determined by immunoblotting after SDS-PAGE separation of cell lysates. Quantification of ATP7A

protein bands using densitometry showed that the amount of ATP7A was decreased by 40% in the ANKRD9-depleted cells; however, that might be due to differences in comparing a single crisp band (control) versus a diffuse band (ANKRD9 knock down) (Fig. 4-5b). In contrast, the qPCR analysis of mRNA levels demonstrated that ATP7A mRNA levels were increased 1.8 fold in ANKRD9-downregulated cells (Fig. 4-5c). Thus, at present we cannot exclude the possibility that the loss of ANKRD9 was associated with enhanced degradation of ATP7A.

Interestingly, we also observed a shift in the electrophoretic mobility of ATP7A in the ANKRD9-depleted cells. ATP7A undergoes N-linked glycosylation (Yamaguchi et al., 1996), so we hypothesized that the glycosylation of ATP7A was affected as a result of ANKRD9 downregulation. Tunicamycin inhibits N-acetylglucosamine transferases disrupting glycosylation of newly synthesized proteins (Heifetz et al., 1979). Fig. 4-5a shows a fully glycosylated band and a lower unglycosylated band of ATP7A in cells treated with tunicamycin. The ATP7A protein band in ANKRD9-downregulated cells was more diffuse suggesting presence of partially glycosylated ATP7A intermediates (Fig. 4-5a).

ANKRD9-dependent loss of Golgi structure does not appear to affect normal protein sorting

Given significant change in Golgi morphology we tested whether this structural change affects the ability of the TGN to retain and/or sort proteins to other compartments. We first examined whether the dispersed structures containing ATP7A in the ANKRD9-

depleted cells were mistargeted and fused to the lysosomes. No significant colocalization was observed between ATP7A in dispersed TGN and lysosomal markers, demonstrating that ATP7A was not mislocalized to the lysosomes (Fig. 4-4b).

We further tested whether the cis-medial Golgi and trans-Golgi compartments mix as a result of the fragmentation caused by ANKRD9 depletion. In control cells, the cis-medial Golgi (Gpp130) and trans-Golgi (TGN 46) colocalized partially (Fig. 4-6). In ANKRD9 depleted cells, two different patterns were observed. In a subset of cells Gpp130 and TGN 46 colocalized in the fragmented structures, whereas in another subset Gpp130 and TGN 46 did not colocalize significantly (Fig. 4-6). In this second subset of cells, the cis-medial Golgi had a more dispersed staining pattern compared to the *trans*-Golgi, suggesting that the dispersion of the cis-medial Golgi may precede the dispersion of the trans Golgi. This observation raised the possibility that the ANKRD9 depletion may primarily affect the cis-medial Golgi sub-compartment resulting in its dispersion followed by the dispersion of the trans Golgi sub-compartment.

Next we examined whether the fragmented Golgi vesicles colocalize with vesicular organelles, which are involved in retrograde/anterograde trafficking and sorting, such as early endosomes, late endosomes, and lysosomes. ANKRD9-depleted cells were immunostained for both TGN 46 and the lysosomal marker Lamp1, to determine if the fragmented Golgi vesicles and lysosomes colocalize. No significant colocalization was observed, suggesting that ANKRD9 downregulation did not cause mislocalization of the TGN proteins to lysosomes (Fig. 4-7a). We also did not observe a significant difference in the pattern of early/late endosomal structures between control and ANKRD9-depleted cells. As seen in Fig. 4-7b and Fig. 4-7c, the TGN46 targeted to fragmented trans Golgi

compartments did not colocalize with the early or late endosomes, confirming that the fragmented Golgi vesicles retained their Golgi identity and were not fused with other organelles.

ATP7A traffics to the plasma membrane in response to copper in ANKRD9-depleted cells

In order to determine whether glycosylation of ATP7A was important for trafficking from the TGN to the plasma membrane, cells were treated with 200 μM $CuCl_2$ for 5 h and then immunostained for ATP7A and TGN 46. As seen in Fig. 4-8, in control cells ATP7A localized to the TGN under basal conditions, and trafficked out of the TGN in response to copper treatment. The same phenomenon was observed in ANKRD9-depleted cells (Fig. 4-8). In high confluency areas, the plasma membrane staining of ATP7A in both control cells and ANKRD9-depleted cells was detected (Fig. 4-8c). Thus, partially glycosylated ATP7A could traffic to its correct localization (plasma membrane) in response to copper treatment in ANKRD9-depleted cells with fragmented Golgi. Surface biotinylation was used to confirm that the partially glycosylated ATP7A was localized to the plasma membrane under high copper conditions (data not shown).

Effect of ANKRD9 depletion on localization and glycosylation of Na/K ATPase β1-subunit, Lamp1 and TGN 46

We wanted to determine whether ANKRD9 depletion affected the localization of other membrane glycoproteins known to be targeted to different cellular compartments and whether their glycosylation status was altered. We focused on the plasma membrane localized Na/K ATPase β1-subunit, lysosomal membrane localized Lamp1, and Golgi-

localized TGN 46 proteins. As seen in Fig. 4-9a, depletion of ANKRD9 resulted in a shift of Na/K ATPase β1-subunit from a mature form to a high mannose glycosylated form (which is the predominant form found in the ER (Tokhtaeva et al., 2009)). Thus, ANKRD9 depletion presumably affects glycosylation of proteins after they exit the ER. Tunicamycin treatment of cells resulted in a shift towards the unglycosylated form of the protein (Fig. 4-9a). The plasma membrane localization of Na/K ATPase β1-subunit was not altered significantly as observed by immunostaining (Fig. 4-9b) or surface biotinylation studies (Fig. 4-17). The Na/K-ATPase consists of one α and one β subunits (Kaplan, 2002). To confirm the plasma membrane localization of the fully assembled complex at the plasma membrane, cells were immunostained against the Na/K ATPase α1-subunit and as expected it was localized to the plasma membrane (Fig. 4-9c). Thus, ANKRD9 depletion did not alter the localization of Na/K ATPase to the plasma membrane.

Lamp1 is a transmembrane protein that localizes to lysosomes and undergoes N-linked glycosylation (Andrejewski et al., 1999). ANKRD9-downregulation and tunicamycin treatment altered the glycosylation pattern of Lamp1, as evidenced by changes in its electrophoretic mobility (Fig. 4-10). Lamp 1-immunostained lysosomal structures were not altered in ANKRD9-downregulated cells (Fig. 4-4b, Fig. 4-7a). Similar loss of glycosylation but targeting fidelity to the compartment was observed for TGN 46, which is a glycosylated protein (Prescott et al., 1997). ANKRD9 downregulation or tunicamycin treatment both resulted in a shift from the 100 kDa band towards 70 kDa band. Thus, ANKRD9 downregulation has a global effect on the glycosylation of proteins located at

different regions within the cell and does not appear to alter their targeting/localization significantly.

Individual ANKRD9 siRNAs #2 and #3 affect the Golgi structure and protein glycosylation similarly to the siRNA pool

Multiple effects of ANKRD9 depletion (changes in Golgi morphology, loss of complex glycosylation and increase of copper levels) suggested that ANKRD9 had either multiple roles or more than one protein was affected by siRNA pool directed against ANKRD9 (off-target effect). In order to determine specificity of siRNA-mediated down-regulation, we used individual siRNAs to knock down ANKRD9 in HeLa cells. The degree of ANKRD9 depletion and phenotypic consequences were evaluated. The siRNA sequences were targeted against different regions of ANKRD9 and had varying effects. ANKRD9 siRNA #1 and ANKRD9 siRNA #4 had no apparent effect on Golgi structure (Fig. 4-11). By contrast, ANKRD9 siRNA #2 and ANKRD9 siRNA #3 resulted in Golgi fragmentation as evidenced by the TGN 46 and ATP7A staining patterns. Cells transfected with ANKRD9 siRNA #2 had more fragmented pattern of Golgi, whereas cells transfected with ANKRD9 siRNA #3 had more dispersed pattern of the Golgi. ATP7A localized to the TGN under basal conditions (Fig. 4-11) and it trafficked out of the TGN in response to copper (Fig. 4-12) in cells transfected with the individual ANKRD9 siRNA sequences.

We then used lysates of ANKRD9 siRNA transfected cells to determine the effect of the individual ANKRD9 siRNAs on protein glycosylation (ATP7A, Lamp1 and Na/K ATPAse β1-subunit). ANKRD9 siRNA #1 and ANKRD9 siRNA #4 had no significant

effect on ATP7A glycosylation supporting the idea that structure of Golgi and complex glycosylation could be linked. In contrast, we observed partially glycosylated intermediates of ATP7A with ANKRD9 siRNA #2 and ANKRD9 siRNA #3. ANKRD9 siRNA #2 resulted in several partially glycosylated intermediates of ATP7A, whereas ANKRD9 siRNA #3 yielded one major partially glycosylated intermediate (Fig. 4-13a). Similarly, partial glycosylation was observed for Lamp1 and Na/K ATPAse β1-subunit with ANKRD9 siRNA #2 and ANKRD9 siRNA #3 (Fig. 4-13b).

To determine whether different effects of individual mRNA correlated with the degree of ANKRD9 down-regulation we quantified ANKRD9 mRNA by qPCR after treatment with individual siRNAs. Treatment with ANKRD9 siRNA #2, ANKRD9 siRNA #3 and ANKRD9 siRNA #4 resulted in a similar 46-56% decrease of ANKRD9 mRNA levels (Fig. 4-16a, b). The fact that ANKRD9 siRNA #4 did not affect Golgi structure and glycosylation with levels of ANKRD9 depletion comparable to ANKRD9 siRNA #2 and #3 suggests the possibility of downregulation of different isoforms of ANKRD9 or off-target effects. ANKRD9 siRNA #1 did not decrease the ANKRD9 levels significantly, and as evidenced from the previous experiments did not have a significant effect on Golgi structure and glycosylation.

ANKRD9 is shown to have five protein coding splice variants (Fig. 4-14). Multiple sequence alignment was performed to compare the sequence similarity between the five variants. Only three of the splice variants result in a full length ANKRD9 protein. Only two of the siRNA sequences (ANKRD9 siRNA#1 and ANKRD9 siRNA#3) targeted the mRNA sequences encoding all five variants. The primer set used for qPCR detected all

five ANKRD9 transcripts (Appendix, Fig. 6-2). Further information regarding the ANKRD9 sequences, exons and siRNA target sequences can be found on Fig. 4-14 and Appendix, Fig. 6-2. We are currently not sure whether the difference in phenotypes observed by different siRNA sequences is due the presence of different isoforms and differences in the downregulation efficiency of each isoform.

ANKRD9 depletion results in a significant increase of the copper uptake protein Ctr1 to compensate for the "copper-deficient" state of the cells

The above experiments revealed an interesting link between Golgi structure and protein glycosylation, and the possibility that ANKRD9 might be critically involved in these processes. Although ATP7A localized to the TGN and trafficked to its correct location in ANKRD9-depleted cells, intracellular copper was elevated in these cells. It is possible that the partially glycosylated ATP7A might have lower copper transport activity compared to fully glycosylated ATP7A, which would lead to inefficient copper export out of the cells. In this part of our study, we focused on the effect of ANKRD9 downregulation on the copper homeostasis and tried to understand the mechanism through which the copper levels are elevated in ANKRD9-depleted cells.

First, we determined the mRNA levels of proteins known to be involved in copper homeostasis in cells transfected with ANKRD9 pool siRNA. We focused on the primary high affinity copper uptake protein Ctr1, low affinity copper uptake protein Ctr2, copper exporting ATPase ATP7A, and a copper chaperone CCS. A significant 6.5 fold increase in the mRNA level of Ctr1 was observed in ANKRD9-depleted cells (Fig. 4-15). The increase in the protein level of Ctr1 was confirmed using individual ANKRD9 siRNA

sequences (Fig. 4-17). The mRNA level of Ctr2 was increased 2.2 fold and the mRNA level of the copper-exporting ATPase ATP7A was increased 1.8 fold in ANKRD9-depleted cells (Fig. 4-15). These results demonstrate that the major effect of ANKRD9 downregulation was on the level of the main copper uptake protein Ctr1.

Previous studies have demonstrated that Ctr1 mRNA levels are sensitive to treatment with high copper or copper chelation. Treating cells with a high copper resulted in a 30-60% decrease of Ctr1 mRNA levels, whereas copper chelation using BCS resulted in a two fold increase of Ctr1 mRNA levels (Song et al., 2008). Additionally, copper-independent conditions such as hypoxia and inflammation have been shown to trigger an increase in Ctr1 levels (White et al., 2009a; White et al., 2009b; Zheng et al., 2010). Therefore the observation that ANKRD9 depletion increases Ctr1 levels by 6.5 fold was very interesting.

It was especially intriguing that the Ctr1 levels were increased when the cells already have excess of copper. We hypothesized that the intracellular copper might be sequestered and inaccessible, therefore the cells might respond by increasing the level of Ctr1. The copper chaperone for superoxide dismutase (CCS) can serve as a marker of cellular copper status. Under high copper conditions CCS protein levels are decreased, and in response to copper chelation CCS protein levels are increased in cells (Dong et al., 2014). Similarly, CCS protein levels were increased in rats fed on a copper deficient diet (Bertinato et al., 2003; Prohaska et al., 2003). Previous studies found no effect of cellular copper status on the mRNA levels of CCS, suggesting that CCS levels in response to copper are regulated post-translationally. In order to determine if the ANKRD-depleted cells were deprived of available/exchangeable copper despite increase of total copper

content, we measured the mRNA level of CCS and we observed 1.8 fold increase in its levels (Fig. 4-15). Based on our results, we think that ANKRD9 depletion triggers changes within the cells, which result in intracellular sequestration and accumulation of copper. The accumulated copper is inaccessible and cells are in a 'pseudo-copper-deficient' state triggering the upregulation of the copper uptake protein Ctr1 as a compensatory effect.

ANKRD9 depletion using ANKRD9 siRNA #2, ANKRD9 siRNA #3 or ANKRD9 siRNA #4 results in increased Ctr1 levels

We have observed that the individual ANKRD9 siRNA sequences have varying effects on Golgi structure and glycosylation of proteins. Therefore, we examined whether the mRNA levels of ANKRD9, Ctr1, Ctr2, CCS, and ATP7A are different in response to each individual ANKRD9 siRNA (Fig. 4-16).

Three of the tested siRNA sequences, ANKRD9 siRNA #2, #3 and #4, yielded consistent results. All three resulted in significant decrease of ANKRD9 mRNA levels, increase of Ctr1 mRNA/protein levels, and increase in CCS mRNA levels (Fig. 4-16). Interestingly, ANKRD9 siRNA #4 resulted in decrease of ANKRD9 mRNA levels comparable to levels with ANKRD9 siRNA #2 and ANKRD9 siRNA #3, however the increase in Ctr1 mRNA levels was less significant (2.6 fold increase with ANKRD9 siRNA #4 versus 4 fold increase with ANKRD9 siRNA #2 and 8 fold increase with ANKRD9 siRNA #3). The increase in Ctr1 mRNA and CCS mRNA levels was only observed in cases in which the ANKRD9 depletion was significant. It would be interesting to determine whether the increase of Ctr1 mRNA/protein levels correlates with the increase of intracellular copper

levels and changes in Golgi structure. The levels Ctr2 mRNA were altered depending on the siRNA sequence; they increased with ANKRD9 siRNAs #2 and #3 and decreased with ANKRD9 siRNA #4. ANKRD9 siRNA #1 did not decrease ANKRD9 mRNA levels significantly, and consequently it did not have a significant effect on Ctr1 and CCS mRNA levels; however the Ctr2 mRNA levels were decreased by 50%. We confirmed that ANKRD9 downregulation also affected the protein levels of Ctr1. As seen in Fig. 4-17, Ctr1 levels were increased in cells transfected with ANKRD9 siRNA #2 (lane 2) and ANKRD9 siRNA #3 (lane 4), compared to control cells (lane 1). Similar to the qPCR results, ANKRD9 siRNA #3 had more pronounced effect on Ctr1 protein levels. In addition, ANKRD9 depletion resulted in partially glycosylated intermediates of Ctr1. The ANKRD9 siRNA #3 had a more pronounced effect on glycosylation than ANKRD9 siRNA #2. The glycosylation of Ctr1 is normally in a mature form (lane 1), but ANKRD9 siRNA #3 caused nearly all glycosylation to be a high mannose form (lane 4), as demonstrated via EndoH deglycosylation treatment (lane 12). Surface biotinylation was used to confirm that Ctr1 was able to traffic to the plasma membrane regardless of its immature glycosylation (lanes 6, 8). Similar results were obtained for Na/K ATPase β subunit. Both ANKRD9 siRNA #2 and ANKRD9 siRNA #3 resulted in defects in glycosylation of the Na/K ATPase β subunit (Fig. 4-17, lanes 2,4), which was able to traffic to the plasma membrane regardless of its glycosylation status (Fig. 4-17, lanes 6,8). Based on these results both Ctr1 and Na/K ATPase β subunit were able to traffic to the plasma membrane regardless of their glycosylation status.

Discussion

ANKRD9 was identified as a novel regulator of copper homeostasis thorough a high throughput ionomics study and its depletion resulted in increase of intracellular copper levels (Malinouski et al., 2014). We characterized the involvement of ANKRD9 in copper homeostasis by focusing primarily on the high affinity copper uptake protein Ctr1 and copper-exporting ATPase ATP7A that are involved in determining copper levels in cells. We found that ANKRD9 depletion resulted in significant increase in the levels of Ctr1 mRNA and protein, whereas the effect on ATP7A was less significant. Based on previous studies, the Ctr1 levels increased in mice fed on copper deficient diet (Nose et al., 2010). Therefore, it was intriguing that in ANKRD9-depleted cells the Ctr1 levels were increased despite an increase of intracellular copper. One possible explanation of this phenomenon was sequestration of copper in some intracellular "storage" vesicles that would render cytosol copper deficient and induce upregulation of Ctr1 to maintain the intracellular copper levels. The levels of the copper chaperone CCS can be used to determine the copper content of cells, since CCS protein expression increases in copper deficiency (Bertinato et al., 2003). We measured the level of CCS in ANKRD9-depleted cells and observed an increase of the CCS mRNA. This result strongly suggests that the cells were in a 'copper-deficient' state, which explains the increase of Ctr1 mRNA and protein levels. This observation also suggests that copper is sequestered within vesicles in the ANKRD9-depleted cells. Given the vesicular localization of ANKRD9 (at least for the recombinant protein) it is possible that ANKRD9 is involved in the release of copper from "copper storage" vesicles.

Another interesting finding was that ANKRD9 depletion led to dilation/fragmentation of the Golgi cisternae and defects in protein glycosylation. ANKRD9 depletion primarily disrupted the Golgi structure with no detectable effect on the structure of other organelles. We observed dispersed patterns of the cis-medial Golgi and trans-Golgi compartments in ANKRD9-depleted cells. The fragmented Golgi compartment appeared to retain its Golgi identity as it did not mix with the ER, lysosomes, early endosomes or late endosomes. In addition, the glycosylation of proteins such as Ctr1, ATP7A, Na+/K+ ATPase, Lamp1 and TGN 46 was impaired, with no significant effect on their localization except for the dispersed pattern of TGN 46.

ATP7A, the major copper-exporting ATPase in HeLa cells was localized to the fragmented Golgi compartments. ATP7A was partially glycosylated and it trafficked in response to copper, so the partial glycosylation of ATP7A did not influence its ability to traffic from TGN to the plasma membrane in high copper. The effect of partial glycosylation on copper export has not been studied yet; therefore no conclusions can be made regarding the copper transport activity of ATP7A. The proposed glycosylation motifs of ATP7A are N^{686}MS and N^{975}RS, localized within the lumenal loops between transmembrane segments 1 and 2 and segments 5 and 6, respectively (Liu et al., 2010). The partial glycosylation might interfere with the copper transfer from ATP7A to the acceptor proteins within the Golgi lumen; copper sequestering vesicles or extracellular copper binding proteins. The lumenal loop M672-P707 was previously shown to be involved in transferring copper to an acceptor protein, peptidylglycine monooxygenase (Lutsenko et al., 2007; Otoikhian et al., 2012); therefore it is plausible that the partial glycosylation might influence the folding of the loops and result in less efficient copper

transfer to acceptor proteins. Future studies can use glycosylation-impaired ATP7A and measure its copper transport activity to more firmly determine the effect glycosylation on ATP7A-mediated copper transport from cells. A second possibility is that glycosylation of ATP7A might protect it from degradation, therefore the partially glycosylated ATP7A might have a shorter half life compared to its fully glycosylated version.

In addition, the glycosylation of the high affinity copper uptake protein Ctr1 was impaired by ANKRD9 depletion. Ctr1 undergoes both N-linked and O-linked glycosylation (Maryon et al., 2007). The N-linked glycosylation occurs at its N-terminus at the Asn15 residue; however impairing N-linked glycosylation has no obvious effect on the half life of Ctr1, or cell surface targeting of Ctr1. However, the $Asn^{15}Gln$ Ctr1 mutant, which lacks N-linked glycosylation, has a lower copper transport activity (decreased by 25%) in comparison to the wild-type Ctr1 protein (Eisses and Kaplan, 2002; Klomp et al., 2002; Klomp et al., 2003; Maryon et al., 2007). O-linked glycosylation occurs at Thr 27, and it protects Ctr1 from proteolytic degradation. Inhibiting O-linked glycosylation of Ctr1 results in a removal of 30 amino acids from its N-terminus producing a cleaved form of Ctr1, which has lower copper uptake efficiency (about 50%) compared to the full length Ctr1 protein (Maryon et al., 2007). It appears that both the N-linked and O-linked glycosylation are required for efficient copper transport by Ctr1. Our data suggests that defects in N-linked glycosylation are responsible for the partially glycosylated Ctr1 protein. Since the copper transport activity of Ctr1 lacking N-linked glycosylation was decreased, it is possible that the partially glycosylated Ctr1 can transport copper less efficiently to meet the cellular needs, which might explain the upregulation of Ctr1 levels. Further studies will focus on copper uptake

and export out of the cells using radioactive Cu^{64} to determine which step is affected due to ANKRD9 downregulation.

We cloned ANKRD9 and observed it to be localized to cytoplasmic vesicles. Ctr1 is endocytosed in response to high copper, therefore we would like to compare the localization of Ctr1 and ANKRD9 and determine whether under high copper conditions they are localized to the same vesicular compartments. Additionally, we observed that Flag-ANKRD9 is a monomeric protein with two major bands, which raises the possibility that it might be modified post-translationally, such as palmitoylation which might recruit ANKRD9 to the vesicular membranes.

In order to determine the specificity of ANKRD9 downregulation, individual ANKRD9 siRNAs were used. ANKRD9 siRNA #2 and ANKRD9 siRNA #3 had an effect on Golgi structure and protein glycosylation, whereas ANKRD9 siRNA #4 had no effect although it has similar downregulation efficiency. ANKRD9 #2, ANKRD9 #3 and ANKRD9 #4 resulted in an increase of Ctr1 levels. Copper levels in cells transfected with ANKRD9 siRNAs #2, #3 and #4 will be measured to determine whether the increase of Ctr1 mRNA/protein levels correlates with the increase of intracellular copper levels and changes in Golgi structure. Further studies will focus on understanding the mechanisms through which the copper uptake is increased in ANKRD9-depleted cells. Specificity of the phenotype will be further confirmed by transfecting ANKRD9-depleted cells with siRNA resistant ANKRD9 constructs.

ANKRD9 depletion resulted in Golgi fragmentation and specific elevation of copper. We wanted to determine whether Golgi fragmentation and elevation of copper levels are linked events. Based on several studies which have identified proteins important for maintaining the Golgi integrity, and comparing the copper levels obtained from our high throughput ionomics screen in response to downregulation of these proteins, we observed that the Golgi fragmentation not always was associated with increase in copper levels (details are listed below).

Golgi is a complex organelle consisting of stacks of cisternae. It is important for the anterograde (and sometimes retrograde) trafficking and sorting of proteins. Glycosylation of proteins and lipids in mammalian cells occurs in the Golgi and it is a highly ordered process. Therefore the Golgi structure is arranged in cisternae with a particular set of glycosyltransferase enzymes residing in each of them, ensuring the sequential processing of glycans. The conserved oligomeric Golgi complex (COG complex) is a tethering complex, which plays an important role in Golgi glycosylation. It is a hetero-oligomer consisting of eight subunits, COG1–COG8. Disruption to the COG complex results in mislocalization of the glycosyltransferase enzymes and interferes with normal protein glycosylation in the medial and/or trans-Golgi (Pokrovskaya et al., 2011).

Cells transiently transfected with COG3 siRNA have fragmented Golgi, and defective protein glycosylation. The partially glycosylated proteins Lamp2 and CD44 were localized to their correct compartments following COG3 knockdown, demonstrating that it does not affect anterograde trafficking and protein sorting. In these cells medial-Golgi enzymes were severely mislocalized (Shestakova et al., 2006). ICP-MS data shows that COG3 knockdown resulted in increase of copper levels (Cu-fold change: 1.369, Cu-z

score: 4.328). In contrast, knockdown of the other COG subunits has no effect on copper levels. For example, COG7 knockdown results in Golgi fragmentation, mislocalization of several glycosyltransferases and defective protein glycosylation of LAMP2 and CD44 (Shestakova et al., 2006), with no significant effect on the copper levels (Cu-fold change: 0.996, Cu-z score: -0.078). Other proteins shown to cause Golgi fragmentation are the centromere/kinetochore protein ZW10 and a RAD50-interacting protein RINT-1 (Sun et al., 2007). The copper levels in HeLa cells with downregulation of either proteins was as follows: ZW10 siRNA (Cu-fold change: 1.000, Cu-z score: -0.051), RINT-1 siRNA (Cu-fold change: 0.848, Cu-z score: -2.717). The siRNA transfections need to be repeated to confirm that they result in Golgi fragmentation in HeLa cells with no increase in copper levels; however it appears that the Golgi fragmentation and increase of copper levels are independent events (i.e. Golgi fragmentation can occur without copper increase and vice versa).

The target binding proteins of ANKRD9 and its intracellular localization have not been identified; therefore currently we are not sure about the sequence of events causing the increase in intracellular copper levels observed by ANKRD9 downregulation: Golgi fragmentation, defects in glycosylation of proteins, copper sequestration, and possible increase of copper uptake or possible decrease of copper export. The possibilities are that copper misbalance induces Golgi fragmentation and defects in glycosylation or vice versa. Copper misbalance can be induced if ANKRD9 is involved in targeting and trafficking of Ctr1 or ATP7A in cells either directly or indirectly which would result in copper accumulation triggering Golgi fragmentation and defects in glycosylation. Another possibility is that ANKRD9 is involved in maintaining Golgi structure either

directly by being localized to the Golgi membranes or indirectly by the influencing the targeting of another Golgi resident structural protein. The third possibility is that ANKRD9 is involved in the targeting of a channel, pump, or glycosyltransferases to the Golgi. Further studies will focus on understanding the mechanisms through which the copper uptake is increased in ANKRD9-depleted cells.

Materials and Methods

Cell lines: HeLa cells (obtained from ATCC) were maintained in DMEM supplemented with 10 % FBS and 1 % pen/strep at 37 ºC in a 5% CO_2 incubator.

siRNA transfection: Dharmacon's Wet Reverse Transfection Protocol was used for the transfection of HeLa cells. ANKRD9 siRNA was used at final concentration of 5 nM or 20 nM for individual siRNA sequences or 20 nM for the pool (human siGenome ANKRD9 siRNA, M-015551-01, Dharmacon). Dharmafect I was used as a transfection reagent. 72 h after transfection cells were harvested or fixed for immunostaining.

Treatments with tunicamycin, excess copper and copper chelation: Cells were treated with 10 µg/ml Tunicamycin overnight. Copper treatment was done with 200 µM $CuCl_2$ for 5 h and copper chelation was done using 100 µM bathocuproine disulfonate (BCS) for 3 h.

Immunohistochemistry with organellar markers: For the TGN46, Lamp1, Calreticulin, Gpp130 and ATP7A immunostaining the following protocol was used. Cells were fixed using 3% paraformaldehyde at 37ºC for 12 min. Cells were washed with 1X PBS and blocked/permeabilized simultaneously for 12 min using 1% BSA/ 1% saponin in 1X

PBS. Cells were washed with 1X PBS and then incubated with appropriate primary and secondary antibodies diluted in 0.5 % BSA in 1X PBS. (Primary antibodies: mouse anti-ATP7A antibody 1:250 (Santa Cruz), rabbit anti-ATP7A antibody 1:300 (Hycult Biotech), sheep anti-TGN46 1:300 (Genetex), mouse anti-Lamp1 1:500 (Developmental Studies Hybridoma Bank), rabbit anti-Gpp130 1:500 (Covance), rabbit anti-calreticulin 1:300 (Stressgen) . Secondary antibodies: Alexa Fluor 488 Goat anti mouse antibody 1:500 (Invitrogen), Alexa Fluor 555 donkey anti sheep 1:500 (Invitrogen), Alexa Fluor 555 donkey anti mouse 1:500 (Invitrogen), Alexa Fluor 488 donkey anti rabbit 1:500 (Invitrogen), Alexa Fluor 555 Goat anti rabbit antibody 1:500 (Invitrogen). The glass slides were mounted using Fluoromount G w/DAPI (Electron Microscopy Sciences). Images were taken using a Zeiss LSM 510 confocal microscope and a 40x oil or 100x oil immersion objective.

Immunohistochemistry with Na/K ATPase antibodies: Cells were washed with 1X PBS and fixed/permeabilized using cold (-20°C) acetone for 30 sec. Cells were washed with 1X PBS and blocked overnight with blocking solution (1% BSA, 2% goat serum in PBS). Cells were washed with 1X PBS and then incubated with the appropriate primary and secondary antibodies. The primary antibodies were diluted in 1% BSA, 0.2% saponin in 1X PBS and cells were immunoprobed for 3 h. The secondary antibodies were diluted in blocking solution and cells were immunoprobed for 1h at 37 °C (Primary antibodies: mouse anti-Na/K ATPase β subunit 1:1000 (Affinity Bioreagents), mouse anti-Na/K ATPase α1 subunit 1:1000 (Millipore), and sheep anti-TGN46 1:300 (Genetex); Secondary antibodies: Alexa Fluor 488 Goat anti mouse antibody 1:500 (Invitrogen) and Alexa Fluor 555 donkey anti sheep 1:500 (Invitrogen)). The glass slides were mounted

using Fluoromount G w/DAPI (Electron Microscopy Sciences). Images were taken using a Zeiss LSM 510 confocal microscope and a 40x oil or 100x oil immersion objective.

Immunohistochemistry with endosomal markers: Cells were washed with 1X cold PBS, followed by 2 min incubation on ice with 0.025% saponin in PHEM buffer. Cells were incubated twice for 2 min with 0.025% saponin/8% sucrose in PHEM buffer, and fixed for 30 min at room temperature with 4% paraformaldehyde in 1X PBS (PHEM buffer: 60 mM PIPES, 25 mM HEPES, 10 mM EGTA, 2 mM $MgCl_2$). Cells were washed with 1X PBS and blocked using blocking buffer (1% BSA, 0.025% saponin in 1X PBS) for 1 h. Cells were washed with 1X PBS and then incubated with the appropriate primary and secondary antibodies diluted in blocking buffer. (Primary antibodies: sheep anti-TGN46 1:300 (Genetex), mouse anti EEA1 1:300 (BD Biosciences) and mouse LBPA 1:100 (Echelon Biosciences). Secondary antibodies: Alexa Fluor 555 donkey anti mouse antibody 1:500 (Invitrogen) and Alexa Fluor 488 donkey anti sheep 1:500 (Invitrogen)). The glass slides were mounted using Fluoromount G w/DAPI (Electron Microscopy Sciences). Images were taken using a Zeiss LSM 510 confocal microscope and a 40x oil or 100x oil immersion objective.

Western blotting: Cells were harvested, the pellet was resuspended in Laemmli loading buffer, sonicated for 30 sec and centrifuged for 15 min at 3000 g at 4 ºC. The supernatant was loaded to 8 % or 12% SDS gel. Proteins were transferred to a PVDF membrane using CAPS buffer, pH 11.0. The membrane was cut at 130 kDa and probed using mouse anti-Na/K ATPase α1 subunit (1:10000, Millipore), mouse anti-ATP7A (1:3000, Santa Cruz), mouse anti-Na/K ATPase β subunit (1:10000, Affinity Bioreagents), sheep anti-TGN 46 (1:3000, Genetex), or mouse anti-Lamp1 (1:5000, Developmental Studies

Hybridoma Bank). Goat anti mouse Igg-HRP (1:10000, Santa Cruz) or donkey anti sheep Igg-HRP (1:10000, Santa Cruz) was used as a secondary antibody and the membranes were developed using a SuperSignal West Pico Substrate (Thermo Scientific).

Electron microscopy sample preparation: Cells were rinsed using warm 1X PBS, and fixed using 2% glutaraldehyde (2% paraformaldehyde, 0.1 M NaCacodylate, 3 mM $CaCl_2$ pH 7.2-7.4) for 1 hr at RT. Cells were washed three times for 10 min each using a solution containing 0.1 M Na Cacodylate, 3% sucrose, and 3mM $CaCl_2$. Cells were incubated on ice for 1 h in dark in a solution containing 1% OsO4, 0.8% $KFeCn_6$, 0.1M NaCacodylate, and 3mM $CaCl_2$. Cells were rinsed twice for 5 min using water. Cells were incubated for 1 hr in dark in 2% uranyl acetate. Cells were washed for 5 min using 30% ethanol, 50% ethanol, 70% ethanol, and 90% ethanol, followed by three washes for 5 min with 100% ethanol. Cells were incubated overnight with 100% embedding resin (Epon (1:1 A:B)) (Electron Microscopy Sciences). Next day the resin was changed three times with Epon (1:1 A:B) containing 1.5% DMP-30 catalyst and a 15 psi vacuum step for 2 h was included during each incubation. The resin was dried 3 days at 37°C oven for three days, followed by and overnight incubation at 60°C. Ultra thin sections were cut, placed on grids and imaged using Hitachi 7600 transmission electron microscope.

Cloning of Flag tagged ANKRD9: ANKRD9 was amplified from cDNA obtained from HeLa cells using the following primers: Nhe I restriction site/Flag tag containing Fwd primer (CGGCTAGCATGGATTACAAGGATGACGACGATAAGATGCCGTGGG ACG) and Hind III restriction site containing Rev primer (AAAAGCTTCTAG CCTTTGCCAGTGAGG). The amplified fragment was digested using Nhe I and Hind III

restriction enzymes and ligated into an expression vector pcDNA 3.1(+) (Invitrogen) digested with the same enzymes. The vector was sequenced and mutations were not detected.

Transient transfection of HeLa cells with Flag-ANKRD9: HeLa cells were grown on coverslips and transfected with 2 µg of Flag-ANKRD9 using Lipofectamine-2000 (Invitrogen) according to manufacturer's instructions. 16 h after transfection cells were either harvested for western blotting or fixed for immunostaining. Cells were rinsed with 1X PBS and fixed in cold acetone-methanol mixture (1:1) for 30 sec. The cells were blocked in blocking buffer (1 % gelatin, 1 % BSA in PBS) and then incubated with appropriate primary and secondary antibodies diluted in blocking buffer. (Primary antibody: mouse anti-Flag antibody 1:300 (Sigma) and rabbit anti-Gpp130 1:500 (Covance). Secondary antibody: Alexa Fluor 488 Goat anti mouse antibody 1:500 (Invitrogen) and Alexa Fluor 555 goat anti rabbit 1:500 (Invitrogen)). The glass slides were mounted using Fluoromount G w/DAPI (Electron Microscopy Sciences). Images were taken using a Zeiss LSM 510 confocal microscope and a 100x oil immersion objective. For Western blotting, cells were harvested, the pellet was resuspended in 30 µl of Laemmli loading buffer, sonicated for 30 sec and centrifuged for 15 min at 3000 g at 4 ºC. The supernatant was loaded to 8 % SDS gel. Proteins were transferred to a PVDF membrane using CAPS buffer, pH 11.0. The membrane was probed for Flag-ANKRD9 using Flag antibody (1:5000, Sigma). Goat anti mouse Igg-HRP (1:10000, Santa Cruz) was used as a secondary antibody and the membranes were developed using a SuperSignal West Pico Substrate (Thermo Scientific).

Measurement of copper levels using atomic absorption spectroscopy: Cells transfected with siRNAs were counted and $1x10^6$ cells were pelleted in an Eppendorf tube. 100 µl of concentrated HNO_3 was added to the pellet and the tubes were incubated at 50°C for 30 min. 25 µl of the solution was mixed with 115 µl water and copper content was measured using SHIMADZU AA - 6650 Atomic Absorption Spectrophotometer.

Biotinylation of Surface CTR1. All biotinylation procedures were carried out at 4ºC or on ice. Cell surface proteins in siRNA-transfected cells were labeled with cell-impermeable Sulfo-NHS-SS-biotin (Pierce) reagent. Plates were placed on ice and cells were washed with cold 1X PBS. EZ-Link Sulfo-NHS-biotin was diluted in biotinylation buffer (10 mM trithanolamine, pH 7.5, 2 mM $CaCl_2$, and 150 mM NaCl) at a final concentration of 0.5 mg/ml and added to the cells. Cells were incubated on ice for 30 min with a slow rocking motion. Cells were rinsed twice with quench buffer (100 mM glycine in 1X PBS) for 20 min. The buffer was aspirated, cells were harvested and incubated in lysis buffer (1% Triton-X-100, 150 mM NaCl, 5 mM EDTA, and 50 mM Tris-HCl, pH 7.5) for 1h. Cells were centrifuged at 10000g for 10 min, and an aliquot was taken. The remaining supernatant was incubated with streptavidin-agarose beads (Pierce) in a centrifuge spin-column (Pierce) overnight at 4ºC. The column was centrifuged at 500g for 3 min at 4ºC to remove the buffer. The beads were washed three times with lysis buffer, twice with salt wash buffer (500 mM EDTA, 0.1% Triton-X-100 and 50 mM Tris, pH 7.5) followed by a single wash with 10 mM Tris, pH 7.5 solution. The column was centrifuged at 10000g for 10 min at 4ºC. The protein elution was done by adding 100 µL of 2X-SDS PAGE sample buffer containing 150 mM dithiothreitol and incubating the column overnight. The sample was centrifuged at 3000g for 5 min to elute the biotinylated

protein from the beads. Samples were separated by SDS-PAGE, and Ctr1 and Na/ K ATPase β 1 subunit was detected using Western blot analysis.

RNA isolation and quantitative PCR: HeLa cells were transiently transfected with the indicated siRNA or NT RNA control and cells were harvested. RNA was isolated using RNeasy Mini Kit (Qiagen) and cDNA was prepared using Transcriptor First Strand cDNA Synthesis Kit (Roche). RNA or cDNA was used as a template and real-time PCR was performed using Power SYBR Green master mix (Applied Biosystems). The following primer sequences were used: Ctr1-Fwd (GACCAAATGGAACCATCCTT), Ctr1-Rev (ATGACCACCTGGATGATGTG), Ctr2-Fwd (TCAGATTCATTCCCTGT TGG), Ctr2-Rev (GCATGATGAAGTAGCCGATG), ANKRD9-Fwd (ACATCCC CGG AACTAGGTGA), ANKRD9-Rev (GTAGAAGGCGAACGACGACT), GAPDH-Fwd (CATCAATGGAAATCCCATCA), GAPDH-Rev (GACTCCACGACGTACTCAGC), ATP7A-Fwd (TGGTTCAAATTGATGCCAGT), ATP7A-Rev (CCGGTTACCAATGA GGACTT), CCS-Fwd (CAACAGCTGTGGGAATCACT), CCS-Rev (AGCTGCTCA TCCTCCATTCT). GAPDH was used as an internal control for data normalization.

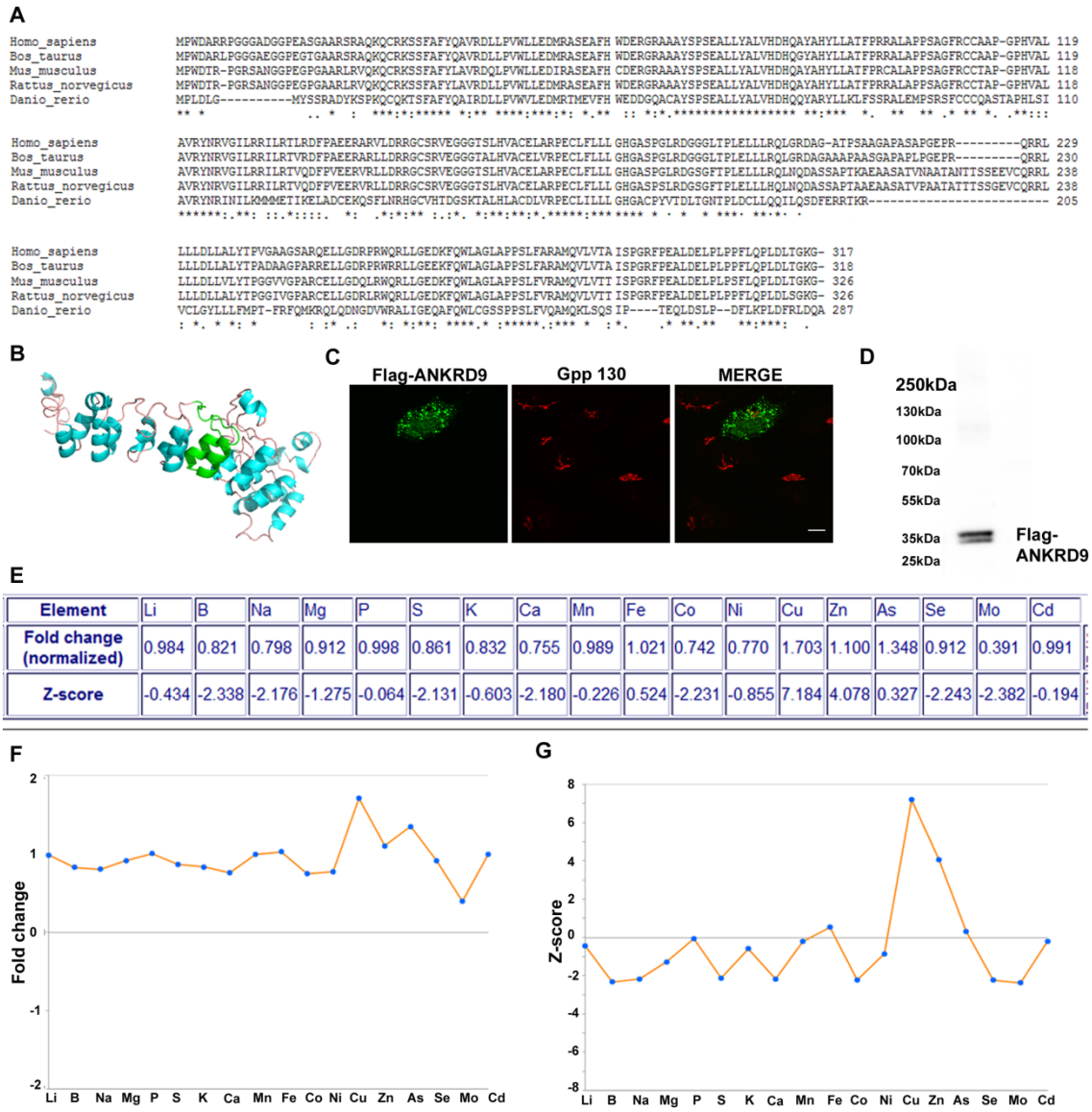

Element	Li	B	Na	Mg	P	S	K	Ca	Mn	Fe	Co	Ni	Cu	Zn	As	Se	Mo	Cd
Fold change (normalized)	0.984	0.821	0.798	0.912	0.998	0.861	0.832	0.755	0.989	1.021	0.742	0.770	1.703	1.100	1.348	0.912	0.391	0.991
Z-score	-0.434	-2.338	-2.176	-1.275	-0.064	-2.131	-0.603	-2.180	-0.226	0.524	-2.231	-0.855	7.184	4.078	0.327	-2.243	-2.382	-0.194

Figure 4-1. Flag-ANKRD9 localizes mainly to cytoplasmic vesicles and ANKRD9 knockdown results in increased copper levels. (a) Multiple sequence alignment of ANKRD9 protein sequences. (b) Pymol model of ANKRD9. ANKRD9 consists of several alpha helices and loops. Alpha helices are shown in blue color and loops are shown in pink color. A single ankyrin repeat sequence (amino acids 158-190) is shown in green color. (c) HeLa cells were transiently transfected with Flag-ANKRD9. Fixed cells were immunostained using antibodies against Flag-ANKRD9 and cis- medial Golgi (Gpp130) (Scale bar:10µm) (d) Cells lysates from transfected cells were used for immunoblotting against Flag-ANKRD9 using Flag antibody. Two major bands around 35kDa were detected corresponding to the monomeric size of ANKRD9. (e) Following gene-specific knockdowns, metal contents were measured using ICP-MS (Inductively coupled plasma mass spectrometry). Shown is the effect of ANKRD9 downregulation on intracellular metal content of cells. (f) Fold change of different metals in ANKRD9 downregulated cells. (g) Z-score of different metals in ANKRD9 downregulated cells.

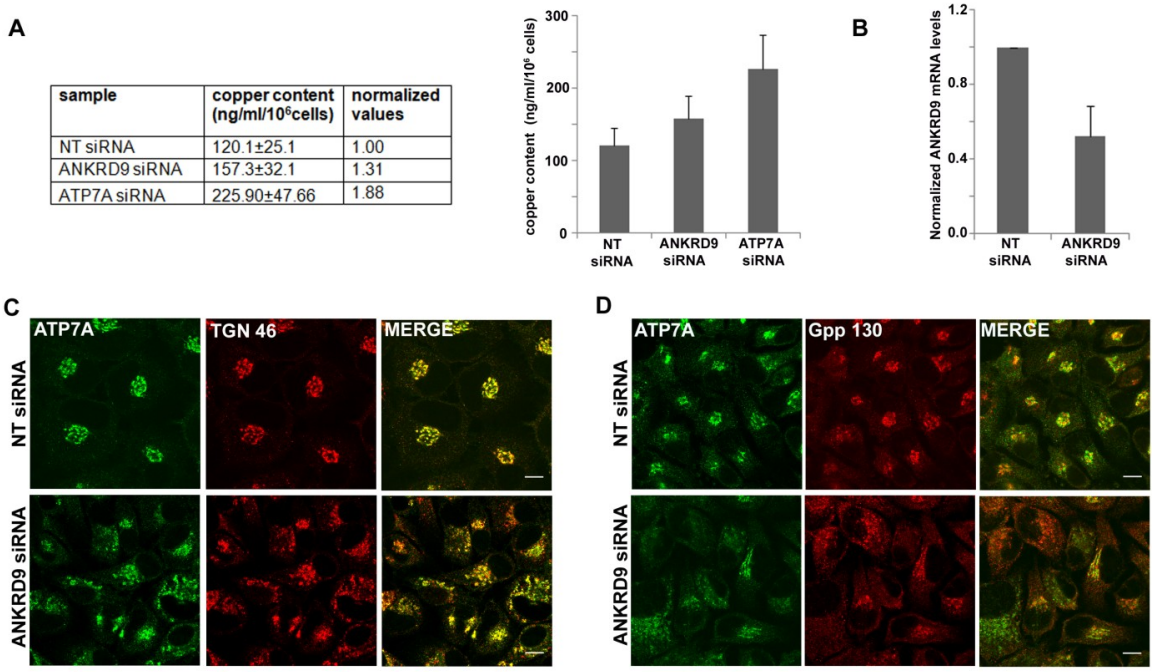

Figure 4-2. ANKRD9 knockdown results in increased copper levels and changes in Golgi structure and ATP7A localization. HeLa cells were transfected with 20 nM NT (non-targeting), ANKRD9 pool siRNA or ATP7A pool siRNA, and harvested for copper content measurement/qPCR or fixed for immunostaining. (a) Copper levels in ANKRD9-siRNA and ATP7A-siRNA transfected cells are increased, as measured using AAS (atomic absorption spectrophotometer). (b) ANKRD9 mRNA levels are decreased in ANKRD9-siRNA transfected cells as determined by qPCR. (c) ANKRD9 downregulation causes dispersion of trans-Golgi network (TGN 46) (red, middle panel) and ATP7A (green, left panel) (Scale bar: 10µm). (d) ANKRD9 downregulation causes dispersion of Gpp130 cis-medial Golgi (Gpp130) (red, middle panel) and ATP7A (green, left panel) (Scale bar: 10µm).

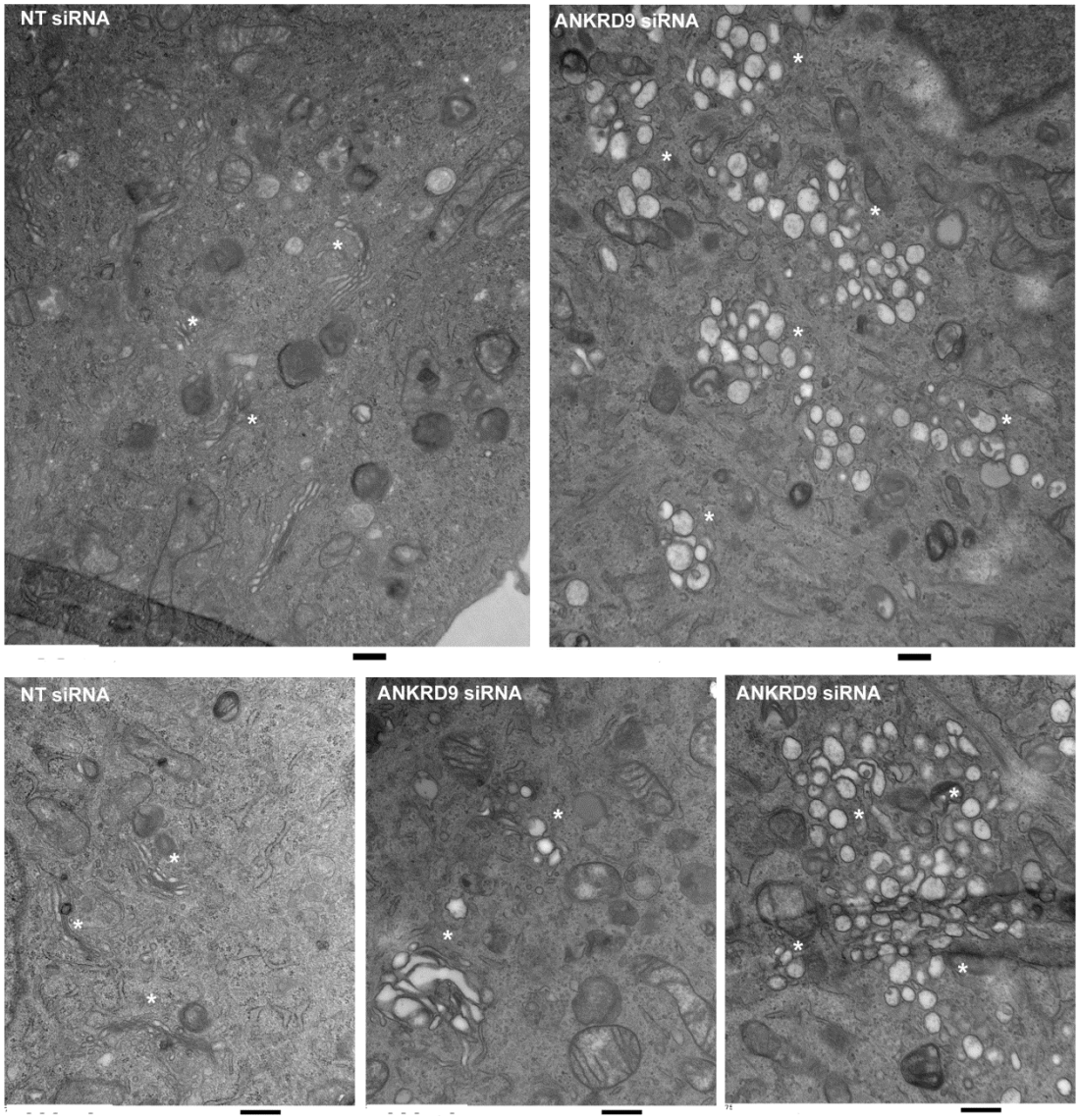

Figure 4-3. ANKRD9 downregulation results in Golgi dilation and fragmentation. Electron microscopy analysis of HeLa cells transiently transfected with non-targeting (NT) siRNA or ANKRD9 pool siRNA. Different magnifications are shown. Asterics mark the Golgi region. In NT siRNA-transfected cells Golgi structure is characterized by ribbons (left panels), whereas in ANKRD9-downregulated cells (middle and right panels) Golgi is fragmented and enlarged (phenotype depends on downregulation efficiency). No significant changes in the structure of other organelles were observed (Scale bar: 500 nm).

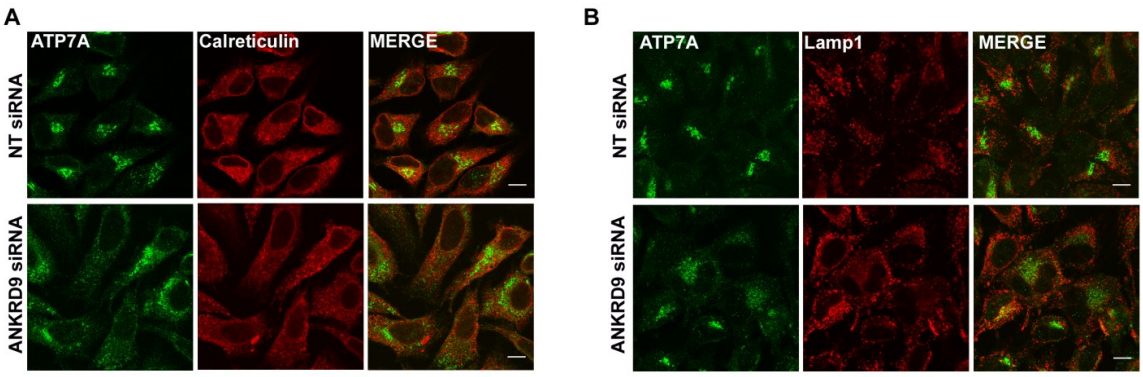

Figure 4-4. ANKRD9 depletion does not affect the structure of endoplasmic reticulum (ER) and lysosomes, and dispersed ATP7A does not mis-localize to lysosomes. Following siRNA transfection with non-targeting (NT) siRNA or ANKRD9 pool siRNA cells were fixed, immunostained and analyzed by confocal microscopy. (a) ATP7A and ER (calreticulin) immunostaining or (b) ATP7A and lysosomes (Lamp1) immunostaining in transiently transfected HeLa cells (Scale bar: 10μm).

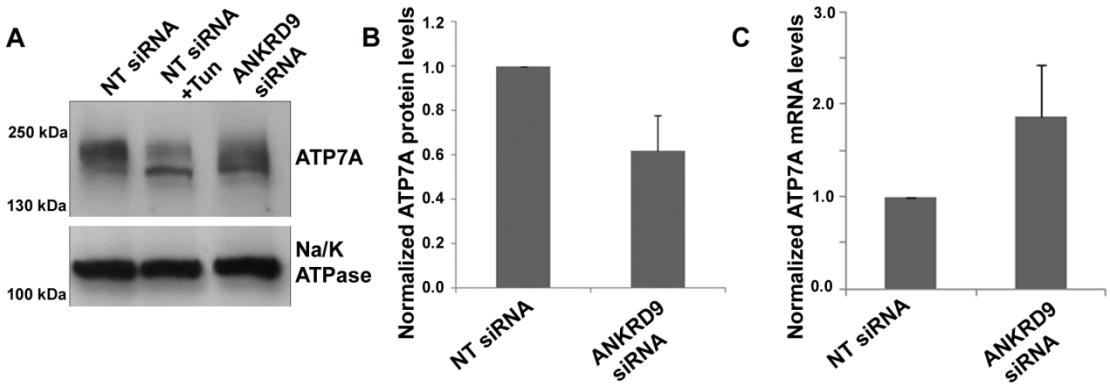

Figure 4-5. ANKRD9 downregulation results in changes in electrophoretic mobility of ATP7A, decreased ATP7A protein and increased ATP7A mRNA levels. HeLa cells were transfected with NT (non-targeting) or ANKRD9 pool siRNA. Cells lysates were used for immunoblotting against ATP7A and Na/K ATPase. (a) ATP7A glycosylation was affected as a result of ANKRD9 downregulation. A representative blot is shown. Tunicamycin treatment was used to inhibit N-linked glycosylation resulting in a lower molecular weight band which is the unglycosylated ATP7A. (b) Quantification of western blot data by densitometry. The ATP7A protein levels were normalized to Na/K-ATPase protein levels and the values were compared with the intensity of ATP7A in cells transfected with a non-targeting siRNA (NT siRNA). The error bars correspond to s.d. values from four independent experiments. (c) ATP7A mRNA levels in NT (non-targeting) or ANKRD9 pool siRNA-transfected HeLa cells. GAPDH mRNA levels were used as internal control. The error bars correspond to s.d. values from four independent experiments.

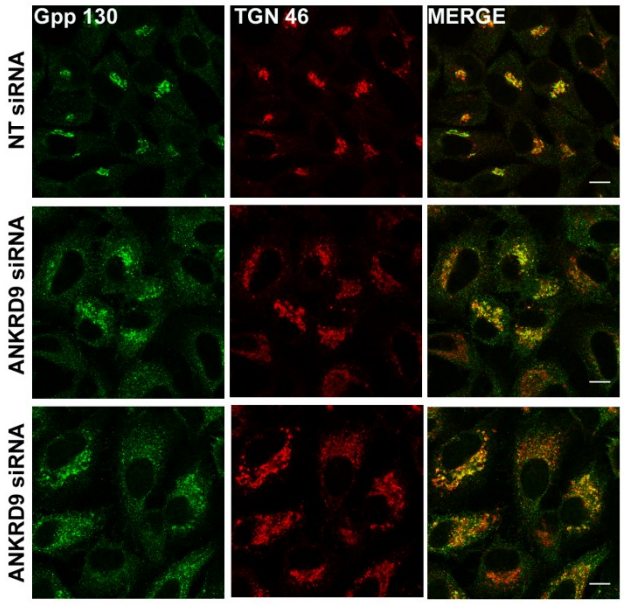

Figure 4-6. ANKRD9 depletion results in partial overlap or no overlap between cis-medial Golgi and trans-Golgi compartments. HeLa cells transiently transfected with non-targeting (NT) siRNA or ANKRD9 pool siRNA were immunostained using antibodies against cis-medial Golgi (Gpp130) (left panel, green) and trans-Golgi (TGN46) (middle panel, red). Partial overlap is observed in control cells transfected with NT siRNA and some cells transfected with ANKRD9 siRNA. In some cases no significant overlap is observed between the two compartments in ANKRD9 siRNA-transfected cells (Scale bar: 10μm).

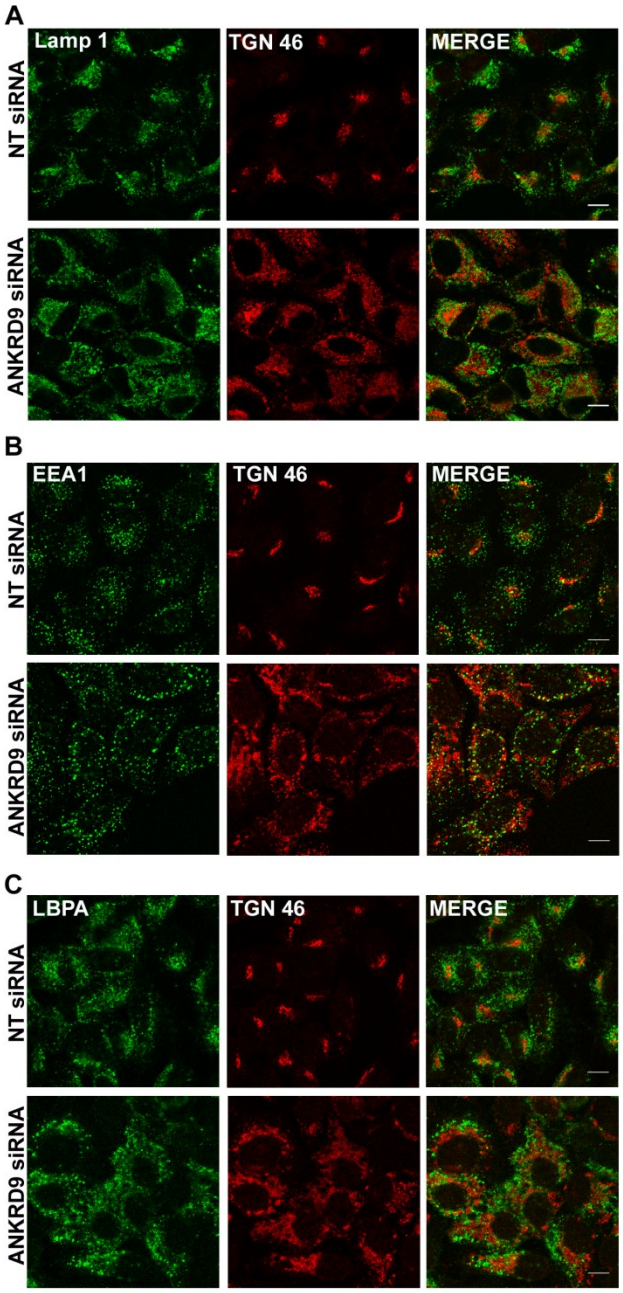

Figure 4-7. Trans-Golgi organelles do not localize to lysosomes, early endosomes or late endosomes in ANKRD9-depleted cells. HeLa cells were transiently transfected with non-targeting (NT) siRNA or ANKRD9 pool siRNA and immunostained using antibodies against Trans-Golgi network (TGN 46) and (a) lysosomes-Lamp1, (b) early endosomes-EEA1 (c) and late endosomes-LBPA and analyzed by confocal microscopy (Scale bar:10µm).(Intensity of red signal in ANKRD9-depleted cells was increased to match the intensity signal in control cells).

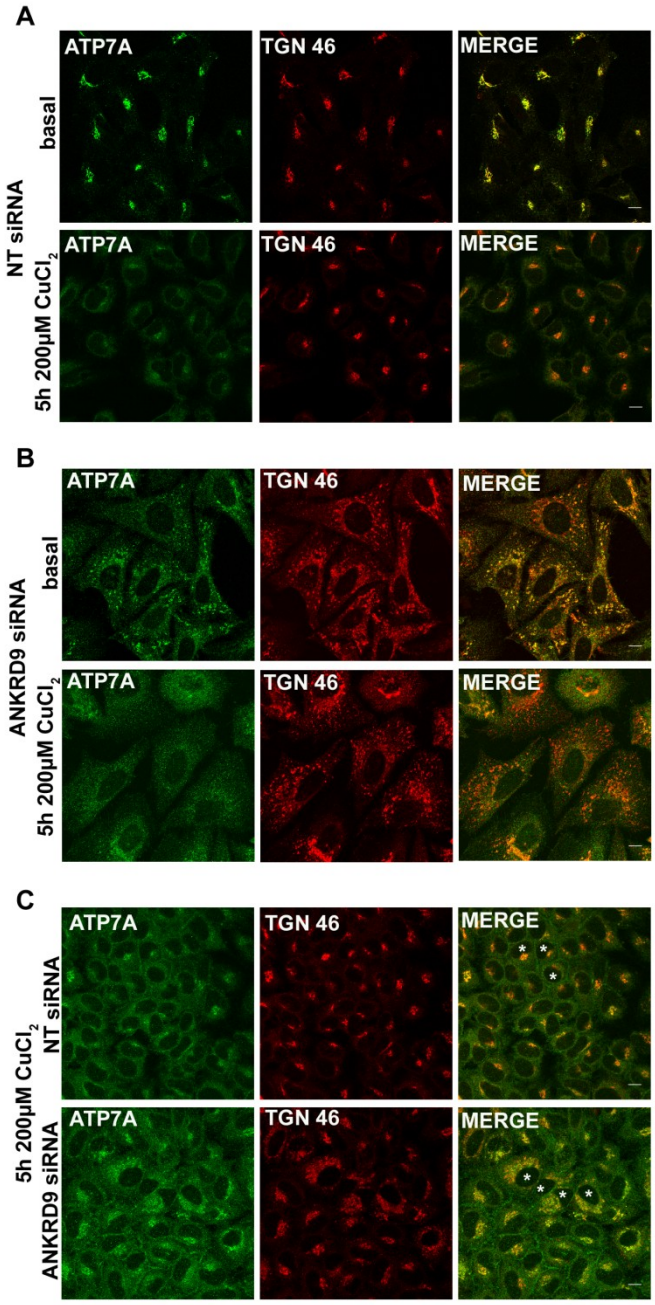

Figure 4-8. ATP7A traffics out of the Golgi and to the plasma membrane in response to copper in ANKRD9-donwregulated cells. Following siRNA-mediated knockdown with non-targeting (NT) siRNA or ANKRD9 pool siRNA, HeLa cells were kept under basal conditions or treated with 200 μM $CuCl_2$ for 5 h, and immmunostained with antibodies for ATP7A (green) and TGN46 (red) (Scale bar:10μm). ATP7A traffics out of the TGN in response to copper in both NT siRNA (panel a) and ANKRD9 siRNA (panel b) transfected cells. ATP7A also localizes to the plasma membrane in copper treated cells (panel c, asterisk mark the cells with plasma membrane staining of ATP7A, intensity of green signal was increased to show plasma membrane staining).

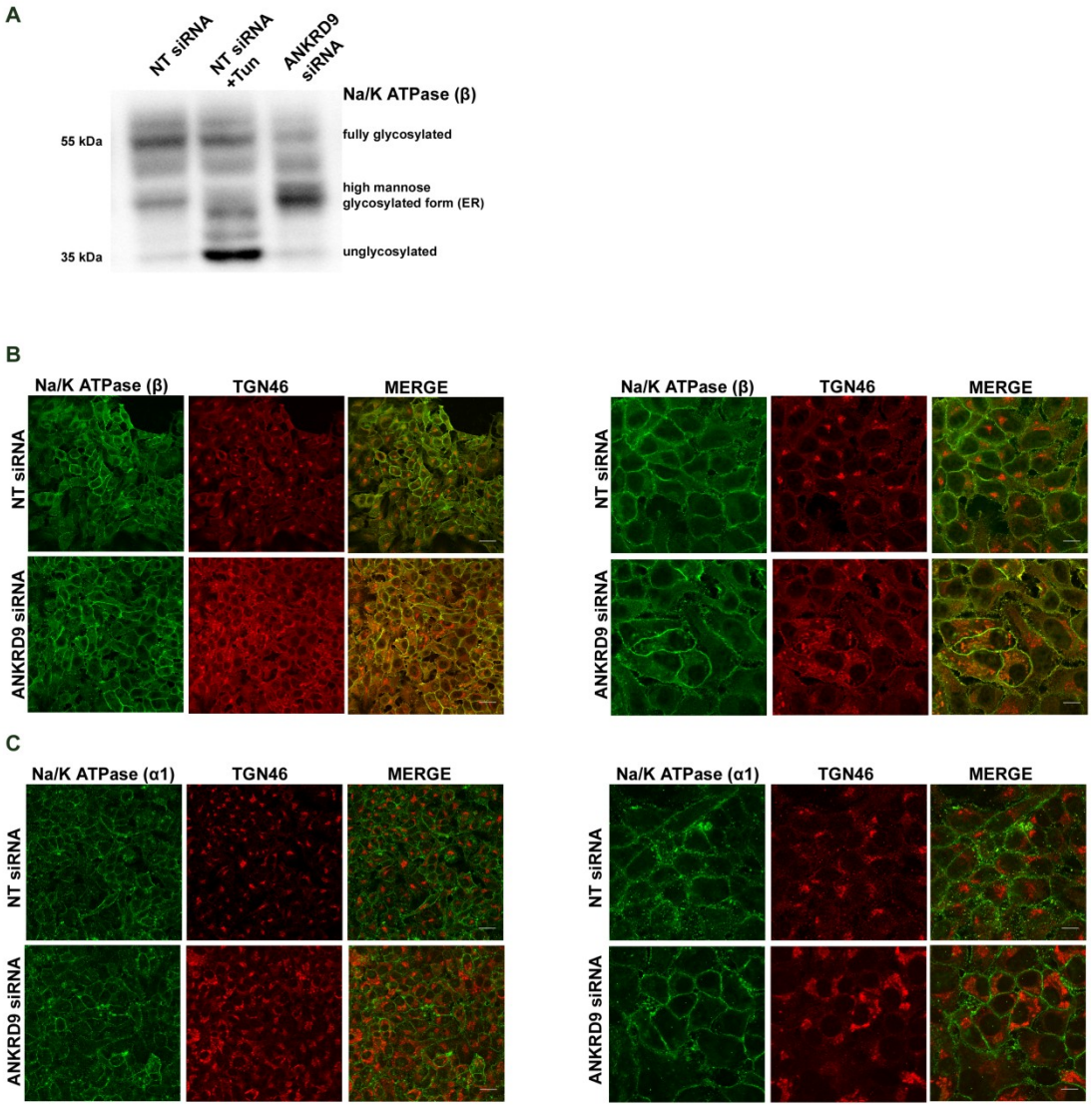

Figure 4-9. ANKRD9 downregulation influences glycosylation of Na/K ATPase (β subunit), but its plasma membrane localization is not altered significantly. (a) Following siRNA-mediated knockdown with non-targeting (NT) siRNA or ANKRD9 pool siRNA, HeLa cell lysates were used for immunoblotting against Na/K ATPase (β subunit). Glycosylation of Na/K ATPase (β subunit) was affected as a result of ANKRD9 downregulation resulting in a high mannose glycosylated form. Tunicamycin treatment was used to inhibit N-linked glycosylation resulting in a proportion of unglycosylated Na/K ATPase (β subunit). A representative blot is shown. (b) Cells were fixed, immmunostained with antibodies against Na/K ATPase (β and α1 subunits) (green) and TGN46 (red) and analyzed by confocal microscopy (left panels (40x images)-scale bar:25μm, right panels (100x images)-scale bar:10μm). Na/K ATPase localized to the plasma membrane, and its localization was not altered significantly as a result of ANKRD9 downregulation.

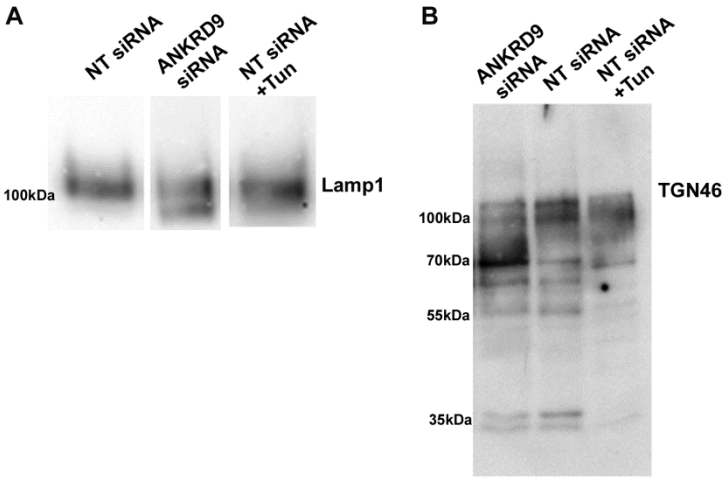

Figure 4-10. ANKRD9 depletion influences glycosylation of Lamp1 and TGN46. Following siRNA-mediated knockdown with non-targeting (NT) siRNA or ANKRD9 pool siRNA, and treatment with tunicamycin, HeLa cell lysates were used for immunoblotting against Lamp1 (a) or TGN 46 (b). Representative blots are shown. (a) ANKRD9 downregulation results in changes in glycosylation pattern of Lamp1, resulting in 2 bands. (b) ANKRD9 downregulation results in changes in glycosylation pattern of TGN 46, resulting in a shift of TGN 46 protein bands from 100 kDa towards 70 kDa. Tunicamyin treatment results in a shift of the 100kDa bands and the 70 kDa band.

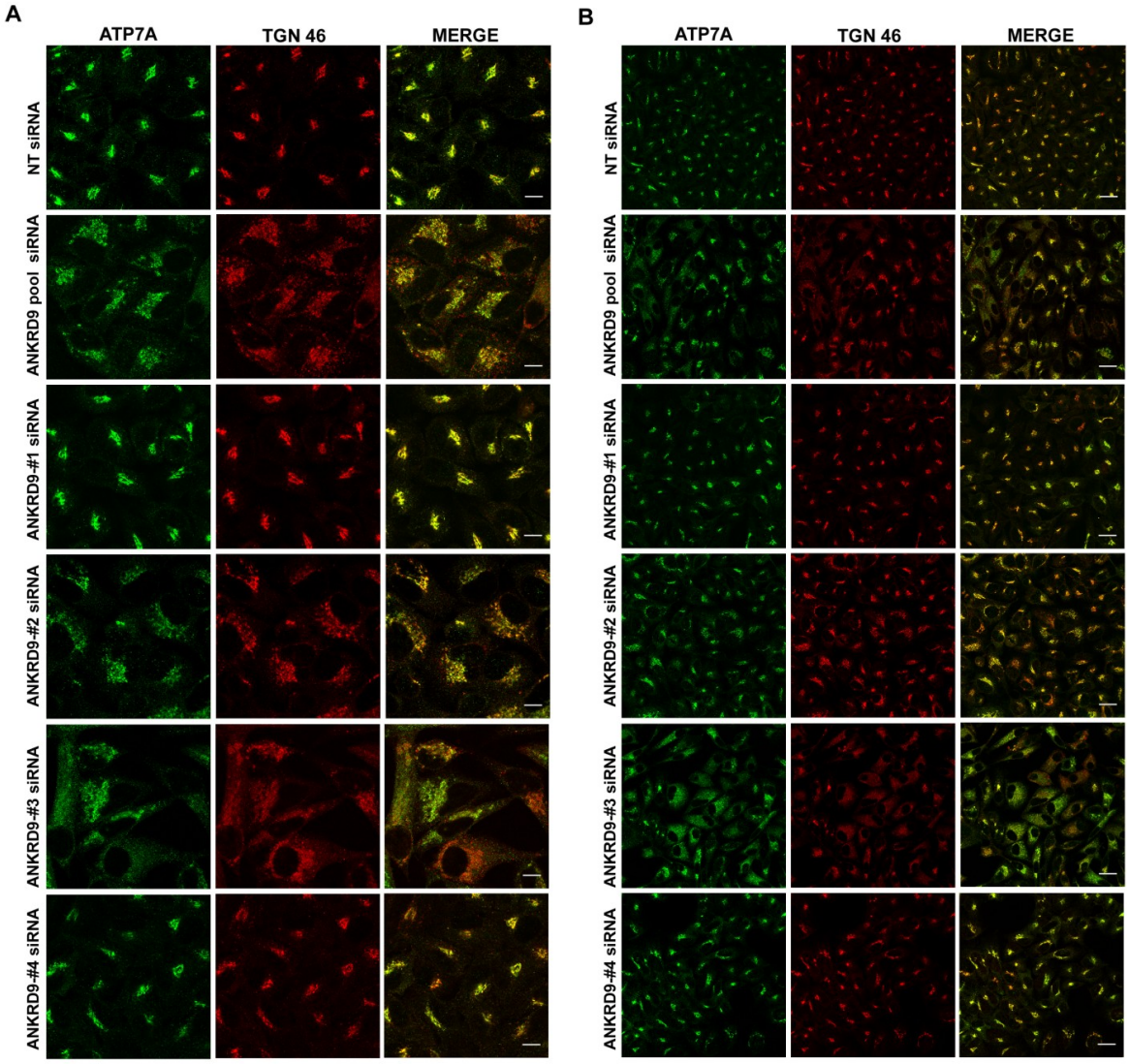

Figure 4-11. ANKRD9 siRNAs #2 and #3 affect ATP7A localization and Golgi structure, whereas ANKRD9 siRNAs #1 and #4 have no significant effect on ATP7A localization and Golgi structure. HeLa cells were transfected with 5 nM NT (non-targeting), individual ANKRD9 siRNAs (numbered 1-4) or 20 nM ANKRD9 pool siRNA. Cells were immunostained using antibodies against ATP7A (green, left panel) and trans-Golgi network (TGN 46) (red, middle panel). Shown are 100x images, (Scale bar: 10µm) (a) and 40x images (Scale bar: 25µm) (b). ANKRD9 downregulation using ANKRD9 siRNA #2, ANKRD9 siRNA #3 and ANKRD9 pool siRNA causes dispersion of TGN 46 and ATP7A. ANKRD9 siRNAs #1 and #4 have no significant effect on ATP7A localization and Golgi structure.

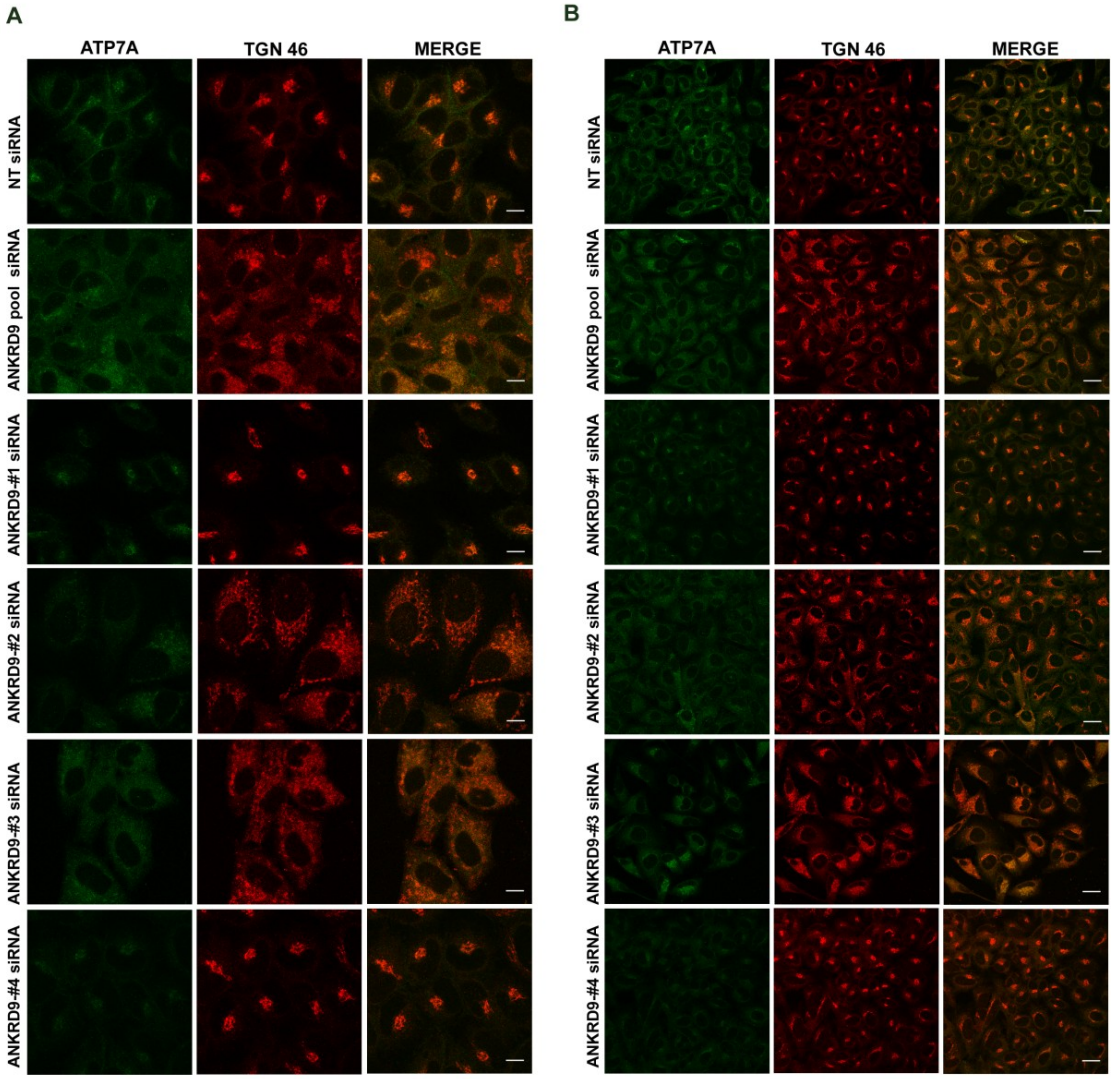

Figure 4-12. ATP7A traffics out of the Golgi in response to copper in ANKRD9-depleted cells. HeLa cells were transfected with 5 nM NT (non-targeting), individual ANKRD9 siRNAs (numbered 1-4) or 20 nM ANKRD9 pool siRNA. 72 h after transfection cells were treated with 200 μM $CuCl_2$ for 5 h and fixed for immunostaining. Cells were immunostained using antibodies against ATP7A (green, left panel) and trans-Golgi network (TGN 46) (red, middle panel). Shown are 100x images (Scale bar:10μm) (a) and 40x images (Scale bar:25μm) (b).

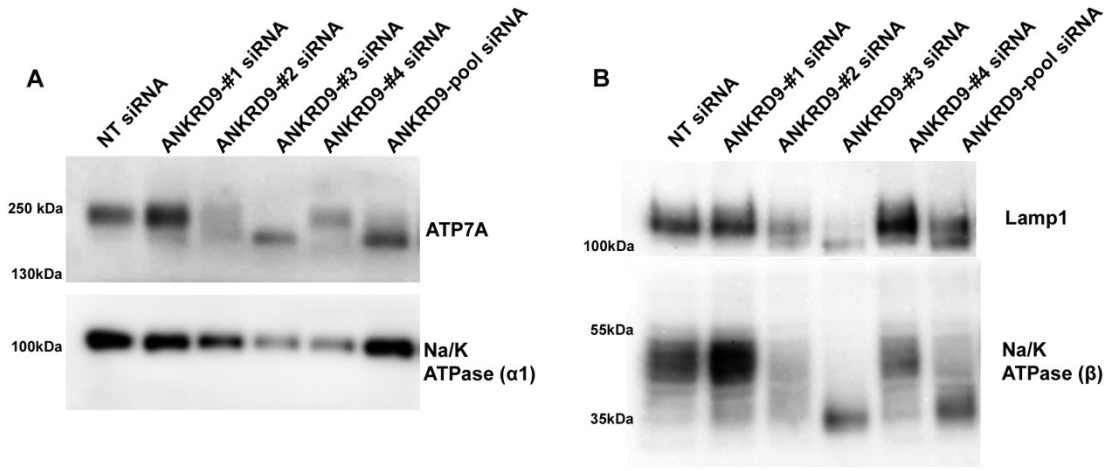

Figure 4-13. Depletion of ANKRD9 using individual ANKRD9 siRNA sequences results in shifts of electrophoretic mobility of ATP7A, Lamp1 and Na/K ATPase (β subunit). Following siRNA-mediated knockdown with 20nM of non-targeting (NT) siRNA, ANKRD9 individual siRNAs or ANKRD9 pool siRNA, HeLa cell lysates were used for immunoblotting for ATP7A, Na/K ATPase (α1 subunit), Lamp1 and Na/K ATPase (β subunit). A representative blot is shown. (a) ANKRD9 siRNA #2 and ANKRD9 siRNA #3 result in changes of glycosylation of ATP7A, and ANKRD9 siRNA #1 and ANKRD9 siRNA #4 have no effect. (b) ANKRD9 siRNA #2 and ANKRD9 siRNA #3 result in changes of glycosylation of Lamp1 (upper panel) and Na/K ATPase (β subunit) (lower panel), and ANKRD9 siRNA #1 and ANKRD9 siRNA #4 have no effect.

A

	Length (bp)	Length (aa)	Biotype	transcript ID	protein ID
ANKRD9-transcript 1	1645	317	protein-coding	ENST00000286918	ENSP00000286918
ANKRD9-transcript 2	1444	317	protein-coding	ENST00000560748	ENSP00000453650
ANKRD9-transcript 3	1413	317	protein-coding	ENST00000559651	ENSP00000454100
ANKRD9-transcript 4	1502	260	protein-coding	ENST00000559404	ENSP00000453417
ANKRD9-transcript 5	620	105	protein-coding	ENST00000557902	ENSP00000454080

B

C

	siRNA sequence	transcript1	transcript2	transcript3	transcript4	transcript5
ANKRD9 siRNA #1	GCAAGTCGTCGTTCGCCTT	yes	yes	yes	yes	yes
ANKRD9 siRNA #2	CGTTGGACCTCACTGGCAA	yes	yes	yes	no	no
ANKRD9 siRNA #3	ACCAAGCGTACGCGCATTA	yes	yes	yes	yes	yes
ANKRD9 siRNA #4	GCTACAACCGCGTGGGCAT	yes	yes	yes	yes	no

Figure 4-14. Information about ANKRD9 transcripts and siRNA targeting regions. (a)ANKRD9 has five protein coding splice variants (transcripts). (b) Clustal W multiple sequence alignment of the ANKRD9 splice variants and targeting sites of the ANKRD9 siRNA sequences. (c) ANKRD9 siRNA sequences and targeting of the ANKRD9 transcripts.

A

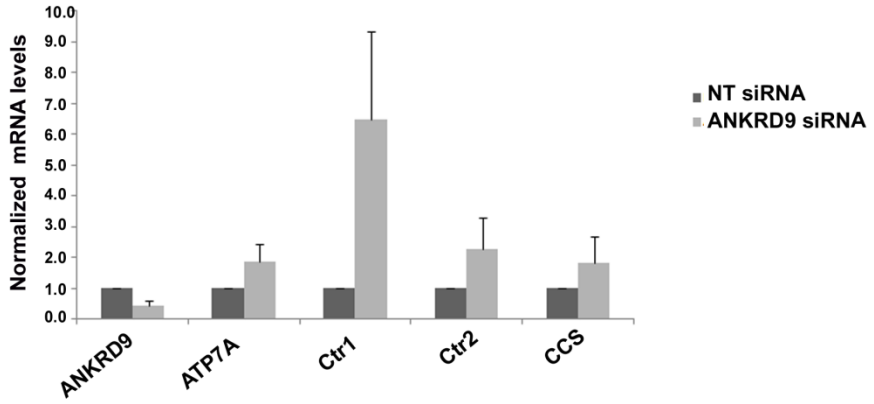

B

	ANKRD9	ATP7A	CTR1	CTR2	CCS
NT siRNA	1.000±0.000	1.000±0.000	1.000±0.000	1.000±0.000	1.000±0.000
ANKRD9-pool siRNA	0.451±0.133	1.868±0.559	6.477±2.858	2.275±1.008	1.826±0.871

Figure 4-15. Depletion of ANKRD9 affects copper homeostasis genes. Following siRNA-mediated knockdown with 20nM of non-targeting (NT) siRNA, or ANKRD9 pool siRNA, HeLa cell lysates were used for RNA isolation. mRNA levels of ANKRD9, ATP7A, Ctr1, Ctr2 and CCS were determined using qPCR. GAPDH mRNA levels were used as internal control. (a) Bar graph demonstrating mRNA levels in ANKRD9 downregulated cells. ANKRD9 downregulation results in increase of ATP7A, Ctr1, Ctr2 and CCS mRNA levels. The error bars correspond to s.d. values from three independent experiments. (b) Table summarizing the relative mRNA ΔΔCt data.

A

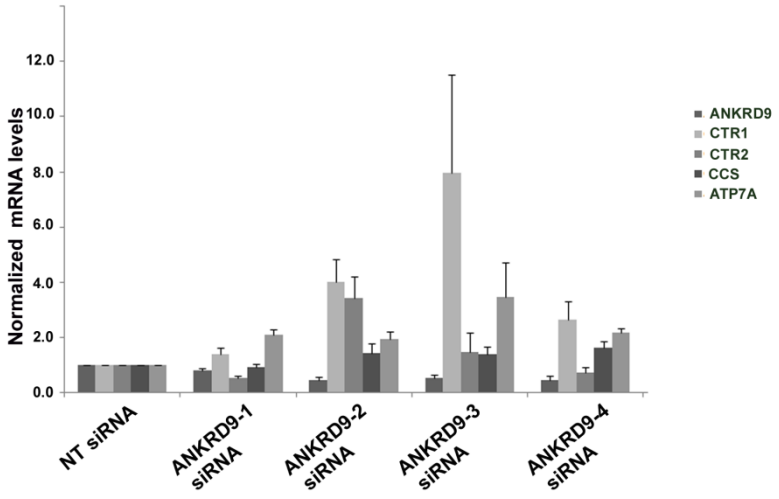

B

	ANKRD9	CTR1	CTR2	CCS	ATP7A
NT siRNA	1.000±0.000	1.000±0.000	1.000±0.000	1.000±0.000	1.000±0.000
ANKRD9-1 siRNA	0.795±0.082	1.397±0.223	0.507±0.085	0.924±0.120	2.071±0.207
ANKRD9-2 siRNA	0.444±0.136	3.993±0.839	3.424±0.796	1.413±0.371	1.937±0.264
ANKRD9-3 siRNA	0.535±0.122	7.968±3.572	1.450±0.710	1.401±0.253	3.443±1.261
ANKRD9-4 siRNA	0.462±0.154	2.644±0.671	0.716±0.191	1.615±0.251	2.186±0.136

Figure 4-16. Effect of individual ANKRD9 siRNA sequences on copper homeostasis. Following siRNA-mediated knockdown with 20nM of non-targeting (NT) siRNA, or ANKRD9 individual siRNAs (labeled 1-4), HeLa cell lysates were used for RNA isolation. mRNA levels of ANKRD9, ATP7A, Ctr1, Ctr2 and CCS were determined using qPCR. GAPDH mRNA levels were used as internal control. (a) Bar graph demonstrating mRNA levels in ANKRD9 downregulated cells. The error bars correspond to s.d. values from two independent experiments. (b) Table summarizing the relative mRNA ΔΔCt data.

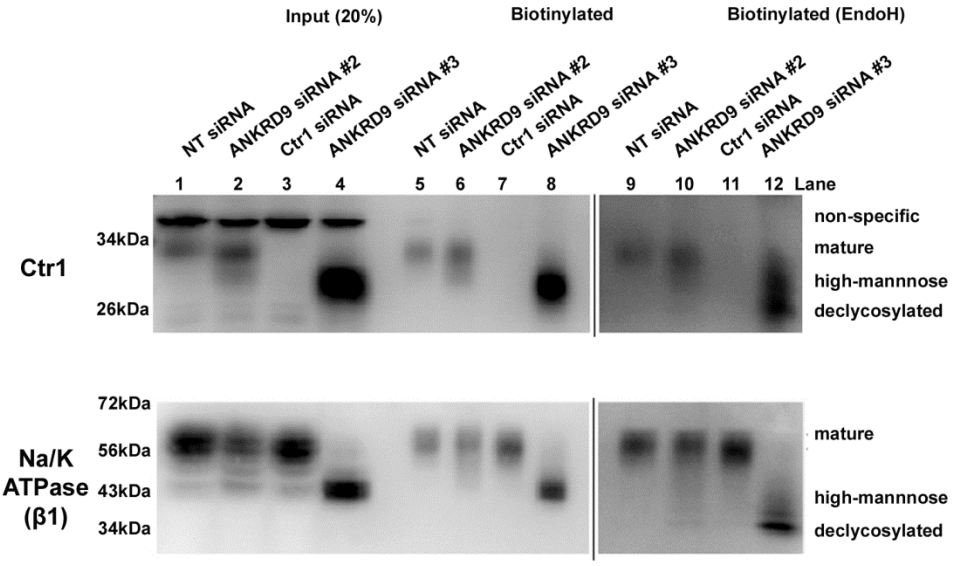

Figure 4-17. ANKRD9 depletion results in increased protein amount of high mannose Ctr1 that can traffic to the plasma membrane regardless of its immature glycosylation. Following siRNA-mediated knockdown with 5nM of non-targeting (NT) siRNA, Ctr1 siRNA, ANKRD9 siRNA #2 or ANKRD9 siRNA #3, cell surface proteins were biotinylated, cells were lysed and biotinylated cell surface proteins were isolated. Endoglycosidase H (EndoH) was used to remove high mannose N-glycans. Shown is a western blot of total cell lysate (input) or eluted cell surface protein samples (biotinylated) probed with an antibody to Ctr1 or Na/K ATPase (β1 subunit). Ctr1 siRNA was used as a control to verify Ctr1 bands in the western blots.

Reference List

Andrejewski, N., Punnonen, E.L., Guhde, G., Tanaka, Y., Lullmann-Rauch, R., Hartmann, D., von Figura, K., and Saftig, P. (1999). Normal lysosomal morphology and function in LAMP-1-deficient mice. J. Biol. Chem. 274, 12692-12701.

Barry, J., Gu, Y., Jukkola, P., O'Neill, B., Gu, H., Mohler, P.J., Rajamani, K.T., and Gu, C. (2014). Ankyrin-G directly binds to kinesin-1 to transport voltage-gated Na+ channels into axons. Dev. Cell. 28, 117-131.

Bennett, V., and Healy, J. (2009). Membrane domains based on ankyrin and spectrin associated with cell-cell interactions. Cold Spring Harb Perspect. Biol. 1, a003012.

Bertinato, J., Iskandar, M., and L'Abbe, M.R. (2003). Copper deficiency induces the upregulation of the copper chaperone for Cu/Zn superoxide dismutase in weanling male rats. J. Nutr. 133, 28-31.

Cunha, S.R., and Mohler, P.J. (2009). Ankyrin protein networks in membrane formation and stabilization. J. Cell. Mol. Med. 13, 4364-4376.

Devarajan, P., Stabach, P.R., Mann, A.S., Ardito, T., Kashgarian, M., and Morrow, J.S. (1996). Identification of a small cytoplasmic ankyrin (AnkG119) in the kidney and muscle that binds beta I sigma spectrin and associates with the Golgi apparatus. J. Cell Biol. 133, 819-830.

Dong, D., Xu, X., Yin, W., and Kang, Y.J. (2014). Changes in copper concentrations affect the protein levels but not the mRNA levels of copper chaperones in human umbilical vein endothelial cells. Metallomics 6, 554-559.

Eisses, J.F., and Kaplan, J.H. (2002). Molecular characterization of hCTR1, the human copper uptake protein. J. Biol. Chem. 277, 29162-29171.

Gupta, A., and Lutsenko, S. (2009). Human copper transporters: mechanism, role in human diseases and therapeutic potential. Future Med. Chem. 1, 1125-1142.

Hao, R., Bondesson, M., Singh, A.V., Riu, A., McCollum, C.W., Knudsen, T.B., Gorelick, D.A., and Gustafsson, J.A. (2013). Identification of estrogen target genes during zebrafish embryonic development through transcriptomic analysis. PLoS One 8, e79020.

Heifetz, A., Keenan, R.W., and Elbein, A.D. (1979). Mechanism of action of tunicamycin on the UDP-GlcNAc:dolichyl-phosphate Glc-NAc-1-phosphate transferase. Biochemistry 18, 2186-2192.

Kaplan, J.H. (2002). Biochemistry of Na,K-ATPase. Annu. Rev. Biochem. 71, 511-535.

Kellokumpu, S., Sormunen, R., and Kellokumpu, I. (2002). Abnormal glycosylation and altered Golgi structure in colorectal cancer: dependence on intra-Golgi pH. FEBS Lett. 516, 217-224.

Klomp, A.E., Juijn, J.A., van der Gun, L.T., van den Berg, I.E., Berger, R., and Klomp, L.W. (2003). The N-terminus of the human copper transporter 1 (hCTR1) is localized extracellularly, and interacts with itself. Biochem. J. 370, 881-889.

Klomp, A.E., Tops, B.B., Van Denberg, I.E., Berger, R., and Klomp, L.W. (2002). Biochemical characterization and subcellular localization of human copper transporter 1 (hCTR1). Biochem. J. 364, 497-505.

Letunic, I., Goodstadt, L., Dickens, N.J., Doerks, T., Schultz, J., Mott, R., Ciccarelli, F., Copley, R.R., Ponting, C.P., and Bork, P. (2002). Recent improvements to the SMART domain-based sequence annotation resource. Nucleic Acids Res. 30, 242-244.

Li, J., Kline, C.F., Hund, T.J., Anderson, M.E., and Mohler, P.J. (2010). Ankyrin-B regulates Kir6.2 membrane expression and function in heart. J. Biol. Chem. 285, 28723-28730.

Liu, Y., Pilankatta, R., Hatori, Y., Lewis, D., and Inesi, G. (2010). Comparative features of copper ATPases ATP7A and ATP7B heterologously expressed in COS-1 cells. Biochemistry 49, 10006-10012.

Lutsenko, S., LeShane, E.S., and Shinde, U. (2007). Biochemical basis of regulation of human copper-transporting ATPases. Arch. Biochem. Biophys. 463, 134-148.

Malinouski, M., Hasan, N.M., Zhang, Y., Seravalli, J., Lin, J., Avanesov, A., Lutsenko, S., and Gladyshev, V.N. (2014). Genome-wide RNAi ionomics screen reveals new genes and regulation of human trace element metabolism. Nat. Commun. 5, 3301.

Maryon, E.B., Molloy, S.A., and Kaplan, J.H. (2007). O-linked glycosylation at threonine 27 protects the copper transporter hCTR1 from proteolytic cleavage in mammalian cells. J. Biol. Chem. 282, 20376-20387.

Mohler, P.J., Davis, J.Q., and Bennett, V. (2005). Ankyrin-B coordinates the Na/K ATPase, Na/Ca exchanger, and InsP3 receptor in a cardiac T-tubule/SR microdomain. PLoS Biol. 3, e423.

Mosavi, L.K., Cammett, T.J., Desrosiers, D.C., and Peng, Z.Y. (2004). The ankyrin repeat as molecular architecture for protein recognition. Protein Sci. 13, 1435-1448.

Nose, Y., Wood, L.K., Kim, B.E., Prohaska, J.R., Fry, R.S., Spears, J.W., and Thiele, D.J. (2010). Ctr1 is an apical copper transporter in mammalian intestinal epithelial cells in vivo that is controlled at the level of protein stability. J. Biol. Chem. 285, 32385-32392.

Otoikhian, A., Barry, A.N., Mayfield, M., Nilges, M., Huang, Y., Lutsenko, S., and Blackburn, N.J. (2012). Lumenal loop M672-P707 of the Menkes protein (ATP7A)

transfers copper to peptidylglycine monooxygenase. J. Am. Chem. Soc. 134, 10458-10468.

Petrosyan, A., Ali, M.F., and Cheng, P.W. (2012). Glycosyltransferase-specific Golgi-targeting mechanisms. J. Biol. Chem. 287, 37621-37627.

Pokrovskaya, I.D., Willett, R., Smith, R.D., Morelle, W., Kudlyk, T., and Lupashin, V.V. (2011). Conserved oligomeric Golgi complex specifically regulates the maintenance of Golgi glycosylation machinery. Glycobiology 21, 1554-1569.

Prescott, A.R., Lucocq, J.M., James, J., Lister, J.M., and Ponnambalam, S. (1997). Distinct compartmentalization of TGN46 and beta 1,4-galactosyltransferase in HeLa cells. Eur. J. Cell Biol. 72, 238-246.

Prohaska, J.R., Geissler, J., Brokate, B., and Broderius, M. (2003). Copper, zinc-superoxide dismutase protein but not mRNA is lower in copper-deficient mice and mice lacking the copper chaperone for superoxide dismutase. Exp. Biol. Med. (Maywood) 228, 959-966.

Rogier, E.W., Frantz, A.L., Bruno, M.E., Wedlund, L., Cohen, D.A., Stromberg, A.J., and Kaetzel, C.S. (2014). Secretory antibodies in breast milk promote long-term intestinal homeostasis by regulating the gut microbiota and host gene expression. Proc. Natl. Acad. Sci. U. S. A. 111, 3074-3079.

Schultz, J., Milpetz, F., Bork, P., and Ponting, C.P. (1998). SMART, a simple modular architecture research tool: identification of signaling domains. Proc. Natl. Acad. Sci. U. S. A. 95, 5857-5864.

Shestakova, A., Zolov, S., and Lupashin, V. (2006). COG complex-mediated recycling of Golgi glycosyltransferases is essential for normal protein glycosylation. Traffic 7, 191-204.

Song, I.S., Chen, H.H., Aiba, I., Hossain, A., Liang, Z.D., Klomp, L.W., and Kuo, M.T. (2008). Transcription factor Sp1 plays an important role in the regulation of copper homeostasis in mammalian cells. Mol. Pharmacol. 74, 705-713.

Struwe, W.B., and Reinhold, V.N. (2012). The conserved oligomeric Golgi complex is required for fucosylation of N-glycans in Caenorhabditis elegans. Glycobiology 22, 863-875.

Sun, Y., Shestakova, A., Hunt, L., Sehgal, S., Lupashin, V., and Storrie, B. (2007). Rab6 regulates both ZW10/RINT-1 and conserved oligomeric Golgi complex-dependent Golgi trafficking and homeostasis. Mol. Biol. Cell 18, 4129-4142.

Tamura, K., Ohbayashi, N., Ishibashi, K., and Fukuda, M. (2011). Structure-function analysis of VPS9-ankyrin-repeat protein (Varp) in the trafficking of tyrosinase-related protein 1 in melanocytes. J. Biol. Chem. 286, 7507-7521.

Tokhtaeva, E., Sachs, G., and Vagin, O. (2009). Assembly with the Na,K-ATPase alpha(1) subunit is required for export of beta(1) and beta(2) subunits from the endoplasmic reticulum. Biochemistry 48, 11421-11431.

Wang, X., Newkirk, R.F., Carre, W., Ghose, P., Igobudia, B., Townsel, J.G., and Cogburn, L.A. (2009). Regulation of ANKRD9 expression by lipid metabolic perturbations. BMB Rep. 42, 568-573.

White, C., Kambe, T., Fulcher, Y.G., Sachdev, S.W., Bush, A.I., Fritsche, K., Lee, J., Quinn, T.P., and Petris, M.J. (2009a). Copper transport into the secretory pathway is regulated by oxygen in macrophages. J. Cell. Sci. 122, 1315-1321.

White, C., Lee, J., Kambe, T., Fritsche, K., and Petris, M.J. (2009b). A role for the ATP7A copper-transporting ATPase in macrophage bactericidal activity. J. Biol. Chem. 284, 33949-33956.

Yamaguchi, Y., Heiny, M.E., Suzuki, M., and Gitlin, J.D. (1996). Biochemical characterization and intracellular localization of the Menkes disease protein. Proc. Natl. Acad. Sci. U. S. A. 93, 14030-14035.

Zheng, Z., White, C., Lee, J., Peterson, T.S., Bush, A.I., Sun, G.Y., Weisman, G.A., and Petris, M.J. (2010). Altered microglial copper homeostasis in a mouse model of Alzheimer's disease. J. Neurochem. 114, 1630-1638.

V. Conclusions

The studies described in this thesis were focused on understanding different modes of regulation of copper homeostasis in human cells. Our experiments determined the role of a kinase mediated phosphorylation in trafficking of the copper-transporting ATPase ATP7B (Chapter 2), identified and provided initial characterization of novel regulators of copper homeostasis (Chapter 3), and investigated the cellular function of the adaptor protein ANKRD9, especially its role in copper homeostasis (Chapter 4).

Prior to this work, it was known that kinase mediated phosphorylation and trafficking of the copper exporting ATPases ATP7A and ATP7B to vesicles might be linked events (Vanderwerf et al., 2001), however the exact role of kinase mediated phosphorylation in trafficking had not been determined. We characterized the role of the predicted phosphorylation sites Ser340 and Ser341 residues in the kinase-mediated phosphorylation, subcellular localization, structure and activity of ATP7B. We determined that Ser340 and Ser341 are involved in the exit of ATP7B from the trans-Golgi network (TGN) and identified the mechanism through which this event occurs. Both serine residues are important for copper-dependent kinase-mediated phosphorylation and modification of these residues minimizes interactions between the N-terminal domain and the nucleotide binding domain. We conclude that the role of a kinase-mediated phosphorylation is to maintain an "open" conformation of ATP7B and that stabilization of this state is the key trigger of ATP7B trafficking to vesicles. We propose that trafficking of ATP7B in response to elevated copper is initiated by structural changes, induced by copper binding to the regulatory N-terminal domain. These structural changes disrupt interdomain contacts allowing access to a kinase and phosphorylation of residues 340/341. Phosphorylation at these (and possibly other)

residues stabilizes and maintains the "trafficking-compatible" state in which ATP7B is sorted to exit sites for further relocation to vesicles.

Information about proteins regulating trafficking of Cu-ATPases is very limited. The role of AP1 protein complex and CD42 kinase in trafficking of ATP7A has been directly demonstrated (Holloway et al., 2013) and ATP7A was found among proteins associated with WASH trafficking complex (Ryder et al., 2013). The studies on ATP7B point to the role of glutaredoxin, protein kinase D is trafficking of this Cu-ATPases. Our data from the ionomic screen suggest that copper homeostasis is maintained mostly by trafficking and post-translational modifications. Knockdown of IBTK, CAMK2N2, DNAJC5, DNAJC17, ABCC3, ANKRD9, and SLC6A4 resulted in elevation of intracellular copper levels. Our initial studies revealed that out of seven tested targets, down-regulation of five had a significant effect on ATP7A. This result emphasizes that ATP7A is primarily responsible for maintaining cellular copper balance in HeLa cells. Novel regulators of ATP7A, which alter its post-translational modification status (phosphorylation and glycosylation), were characterized. The depletion of the kinase inhibitors IBTK (inhibitor of Bruton tyrosine kinase) and CAMK2N2 (calcium/calmodulin-dependent protein kinase II inhibitor 2) resulted in a significant decrease in ATP7A protein levels. The involvement of these kinase inhibitors in phosphorylation of ATP7A have not been previously known or considered, and controlling the ATP7A levels through kinase mediated phosphorylation is a novel possible mechanism of maintaining copper homeostasis. Further studies will be needed to determine whether the effect of the above mentioned proteins is direct or indirect.

Finally, we found that in HeLa cells ANKRD9 (ankyrin repeat domain-containing protein 9) plays a role in maintenance of Golgi flat stacks and/or proper glycosylation of proteins, and contributes to cellular copper homeostasis. ANKRD9 depletion resulted in partial glycosylation of ATP7A and decreased protein levels; raising the possibility that proper glycosylation is needed for the stability of ATP7A. Since ATP7A trafficked in response to copper (i.e. copper export was normal) but total levels of copper in a cell were nevertheless increased we examined other copper homeostasis related proteins in ANKRD9-depleted cells. Unexpectedly, ANKRD9 depletion led to a significant increase in the levels of the copper uptake protein, Ctr1 and the copper chaperone CCS mRNA levels. Both these proteins are known to be regulated by copper deficiency suggesting that the cells were in 'copper-deficient' state, and that excess copper was sequestered (possibly in vesicles) and not available. Given the vesicular localization of recombinant ANKRD9 it is possible that ANKRD9 is involved in the release of copper from "copper storage" vesicles and that upon its depletion copper is trapped and unavailable.

It is also possible that the effect of ANKRD9 on copper transport is indirect. The glycosylation of Ctr1 is affected by ANKRD9 depletion The loss of complex glycosylation may decrease the transport rate decreasing copper uptake, which might explain the upregulation of Ctr1 levels. Another important aspect is that Ctr1 is involved in the uptake of the anticancer-drug cisplatin (Ishida et al., 2002), therefore increasing Ctr1 levels through ANKRD9 depletion might lead to an increased uptake of cisplatin to cancer cells. Further studies will be done to better understand the mechanism through which ANKRD9 regutlates CTR1 and to measure cisplatin uptake in ANKRD9-depleted cells

The results in chapter three, demonstrating the negative effect of ABCC3 (ATP-binding cassette, subfamily C (CFTR/MRP), member 3) down-regulation on ATP7A trafficking are equally novel ABCC3 is an organic anion and bile acid transporter. Previously, treating hepatocytes (HepG2) with copper resulted in upregulation of ABCC3 (Song and Freedman, 2005). In the liver, excess copper is excreted from hepatocytes into the bile, therefore bile acid transport and copper metabolism might be linked events. This hypothesis awaits further experimental testing.

Taken together our studies have pointed to the existence of novel regulatory pathways in copper homeostasis. We have determined that structural changes initiate the exit of ATP7B from the Golgi in response to copper, and kinase mediated phosphorylation might be needed to keep the domains apart. The initial characterization of novel proteins involved in maintaining copper homeostasis was done, and yielded interesting results linking kinase inhibitors, and an anion transporter in regulation of copper levels through ATP7A. The role of the anion transporter ABCC3 in regulating copper-responsive trafficking of ATP7A is a novel regulatory pathway, and further studies will be needed to characterize its mechanism. It was a very intriguing finding that ANKRD9 depletion led to 'copper-deficient' state of cells and upregulation of the copper uptake protein, Ctr1. So far, no other protein has been linked to increasing Ctr1 levels and we are still working on identifying the role of ANKRD9 in copper homeostasis.

Reference List

Holloway, Z.G., Velayos-Baeza, A., Howell, G.J., Levecque, C., Ponnambalam, S., Sztul, E., and Monaco, A.P. (2013). Trafficking of the Menkes copper transporter ATP7A is regulated by clathrin-, AP-2-, AP-1-, and Rab22-dependent steps. Mol. Biol. Cell *24,* 1735-48, S1-8.

Ishida, S., Lee, J., Thiele, D.J., and Herskowitz, I. (2002). Uptake of the anticancer drug cisplatin mediated by the copper transporter Ctr1 in yeast and mammals. Proc. Natl. Acad. Sci. U. S. A. *99,* 14298-14302.

Ryder, P.V., Vistein, R., Gokhale, A., Seaman, M.N., Puthenveedu, M.A., and Faundez, V. (2013). The WASH complex, an endosomal Arp2/3 activator, interacts with the Hermansky-Pudlak syndrome complex BLOC-1 and its cargo phosphatidylinositol-4-kinase type IIalpha. Mol. Biol. Cell *24,* 2269-2284.

Song, M.O., and Freedman, J.H. (2005). Expression of copper-responsive genes in HepG2 cells. Mol. Cell. Biochem. *279,* 141-147.

Vanderwerf, S.M., Cooper, M.J., Stetsenko, I.V., and Lutsenko, S. (2001). Copper specifically regulates intracellular phosphorylation of the Wilson's disease protein, a human copper-transporting ATPase. J. Biol. Chem. *276,* 36289-36294.

VI. Appendix 1: ANKRD9 is a Novel Regulator of Copper Homeostasis

Results

Glycosylation is not required for ATP7A trafficking to the plasma membrane in tunicamycin-treated cells

The ability of partially glycosylated ATP7A to traffic to the plasma membrane in response to copper, suggested that complex sugars were not required for trafficking (Fig 4-8, Fig 4-12). Consequently, we were interested whether complete removal of sugars would disrupt ATP7A trafficking. Cells were treated with tunicamycin to inhibit the glycosylation of newly synthesized proteins and ATP7A localization was determined in basal and high copper conditions. The loss of glycosylation of ATP7A was verified using Western blotting.

As seen in Fig 6-1, ATP7A localized to the TGN under basal conditions in both control and tunicamycin-treated cells. In cells treated with excess copper, ATP7A trafficked out of the TGN and upon removal of excess copper and treatment with the copper chelator BCS, ATP7A returned to the TGN. Surface biotinylation experiments confirmed that the unglycosylated ATP7A could traffic to the plasma membrane in response to copper (data not shown). Altogether our results indicate that N-linked glycosylation of ATP7A was not important for its trafficking in response to copper overload or copper chelation. Future studies will include measuring the copper content of tunicamycin-treated cells, to determine whether glycosylation influences the copper export activity of ATP7A.

Effect of downregulation of other ankyrin proteins and glycosyltransferases on copper levels

ANKRD9 is a member of a large family of structurally similar proteins. We were interested whether down-regulation of other ANKRD proteins would alter the cellular copper levels or the effects of ANKRD9 were unique. In order to determine the specificity of ANKRD9, we compared the effect of downregulation of other ankyrin repeat or ankyrin proteins using the data generated by siRNA ionomic screen (Malinouski et al., 2014). The analyzed proteins are listed in Table 6-1. Most of the listed ankyrin/ankyrin repeat proteins have no significant effect on copper levels as evidenced by the low z-scores (z-score<2) (Table 6-1). Several downregulated proteins have a high z-score (ranging from 4 to 7), which coincides with significant changes in copper levels. These proteins included an adaptor protein AGAP2 that was shown to be involved in the retrograde trafficking from endosome to the TGN (Wu et al., 2013), protein ANKS3 that is a polymeric scaffolding protein (Leettola et al., 2014), and ASB13 the function of which is currently unknown. These proteins are interesting potential regulator of copper metabolism and their role in regulation of copper uptake or export should be investigated further.

In our analysis of ANKRD9 we found that loss of this protein is associated with decreased complex glycosylation and increased levels of CTR1; there was also a reciprocal relationship between these two phenomena. Consequently, we were interested whether downregulation of glycosyltransferases has an effect on the copper levels. We hypothesized that a missing glycosyltransferases would result in defects in glycosylation,

and possible changes in copper contents of cells. Majority of known glycosylation enzymes had no significant effect on copper levels (z-score<2) (Table 6-2). In Table 6-3, the glycosyltransferases enzymes which have an effect on copper levels are listed (z-score>2), however their effect was not specific for copper levels.

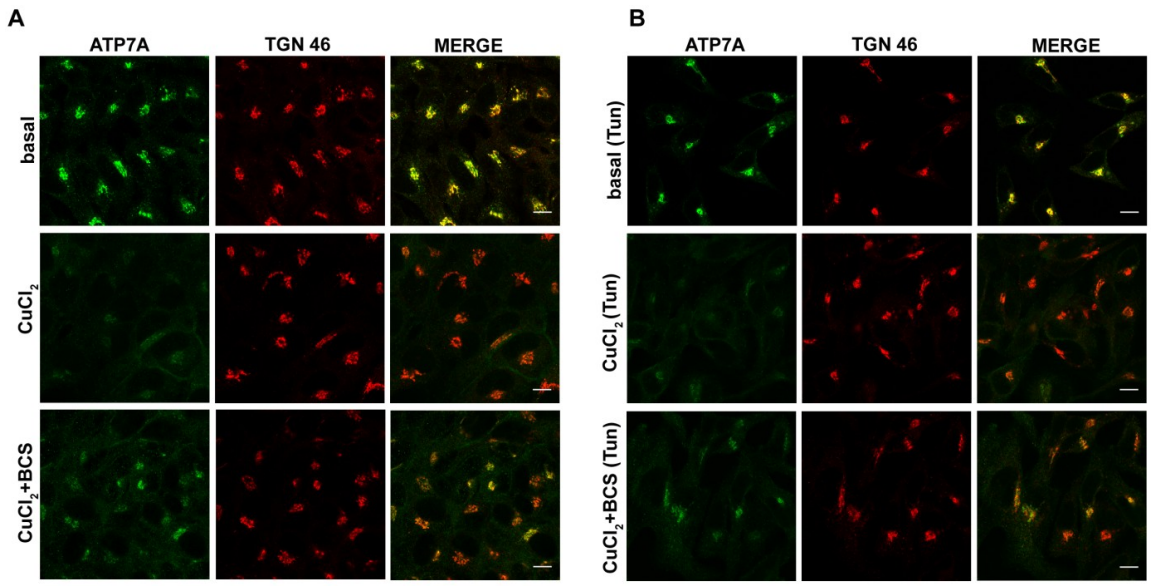

Figure 6-1. ATP7A traffics in response to copper treatment and copper chelation in tunicamycin-treated cells. In response to excess copper ATP7A traffics out of the TGN, and removal of excess copper using BCS triggers the trafficking of ATP7A to TGN. No significant difference was observed in the trafficking pattern of ATP7A control (a) and in tunicamycin-treated (b) cells which have a mixture of both glycosylated and unglycosylated proteins. (Scale bar:10μm).

ANKRD9 splice variants and siRNA targeting regions

```
ANKRD9-transcript4      ------------------------------------------------------------
ANKRD9-transcript5      ------------------------------------------------------------
ANKRD9-transcript2      CGGCGGCGGACGGTCCCGCTGTCCTGCCTGGCCGGGGCCGCACTGCGCCGCCCGCCGCCC 60
ANKRD9-transcript1      --------GACGGTCCCGCTGTCCTGCCTGGCCGGGGCCGCACTGCGCCGCCCGCCGCCC 52
ANKRD9-transcript3      ------------------------------------------------------------

ANKRD9-transcript4      ------------------------------------------------------------
ANKRD9-transcript5      ------------------------------------------------------------
ANKRD9-transcript2      GCCGCCCGCCGCCCGCCGCCGGCGACGGCACCGCCGCCCTGCGATCCGGCCGCGGCGGCT 120
ANKRD9-transcript1      GCCGCCCGCCGCCCGCCGCCGGCGACGGCACCGCCGCCCTGCGATCCGGCCGCGGCGGCT 112
ANKRD9-transcript3      ------------------------------------------------------------

ANKRD9-transcript4      ------------------------------------------------------------
ANKRD9-transcript5      ------------------------------------------------------------
ANKRD9-transcript2      CAGAGCGCGGCTGCGGCGGGCGCGGGCGGCGGTGGCTCCCTCCCGTGCGTCCGTCGTGGG 180
ANKRD9-transcript1      CAGAGCGCGGCTGCGGCGGGCGCGGGCGGCGGTGGCTCCCTCCCGTGCGTCCGTCGTGGG 172
ANKRD9-transcript3      ------------------------------------------------------------

ANKRD9-transcript4      ------------------------------------------------------------
ANKRD9-transcript5      ------------------------------------------------------------
ANKRD9-transcript2      ACCTTTGCCCGCTCGCCCGCGGGGGACAGCGCGCGCTCCGGTCCGCGGCAGGGGCGGGGA 240
ANKRD9-transcript1      ACCTTTGCCCGCTCGCCCGCGGGGGACAGCGCGCGCTCCGGTCCGCGGCAGGGGCGGGGA 232
ANKRD9-transcript3      ------------------------------------------------------------

ANKRD9-transcript4      ------------------------------------------------------------
ANKRD9-transcript5      ------------------------------------------------------------
ANKRD9-transcript2      CGCCCGGCCTGTGGCCCCCGCGCCCCCCATGGTGAGTCCCCGTCCCCCGCGCCGCGCCCG 300
ANKRD9-transcript1      CGCCCGGCCTGTGGCCCCCGCGCCCCCCATGGTGAGTCCCCGTCCCCCGCGCCGCGCCCG 292
ANKRD9-transcript3      ------------------------------------------------------------

ANKRD9-transcript4      ------------------------------------------------------------
ANKRD9-transcript5      ------------------------------------------------------------
ANKRD9-transcript2      CGGCCGCCGCCCCCTCCTCCTCCGGCACACGCGCACGCAGGTGCAGCCCTCGCTGCGCCG 360
ANKRD9-transcript1      CGGCCGCCGCCCCCTCCTCCTCCGGCACACGCGCACGCAGGTGCAGCCCTCGCTGCGCCG 352
ANKRD9-transcript3      ------------------------------------------------------------

ANKRD9-transcript4      ------------------------------------------------------------
ANKRD9-transcript5      ------------------------------------------------------------
ANKRD9-transcript2      GCCACCTGCGCGCGGACGCCCCGCTCGGCCCCGCGACCCTCCGCCGCCCGACGTCTGGCC 420
ANKRD9-transcript1      GCCACCTGCGCGCGGACGCCCCGCTCGGCCCCGCGACCCTCCGCCGCCCGACGTCTGGCC 412
ANKRD9-transcript3      ------------------------------------------------------------

ANKRD9-transcript4      ------------------------------------------------------------
ANKRD9-transcript5      ------------------------------------------------------------
ANKRD9-transcript2      GTGCAGGCCGGGAGGGGACGGGTAGGAGGTGGCGGGTGGCCCCGGGCGCGGCGCTGCCTT 480
ANKRD9-transcript1      GTGCAGGCCGGGAGGGGACGGGTAGGAGGTGGCGGGTGGCCCCGGGCGCGGCGCTGCCTT 472
ANKRD9-transcript3      ------------------------------------------------------------

ANKRD9-transcript4      ------------------------------------------------------------
ANKRD9-transcript5      ------------------------------------------------------------
ANKRD9-transcript2      CGATGGCCCAACCCCCTTATTCACGAGCCGCGGCCGTGACTCTGCCCGGTGACGTGGGGA 540
ANKRD9-transcript1      CGATGGCCCAACCCCCTTATTCACGAGCCGCGGCCGTGACTCTGCCCGGTGACGTGGGGA 532
ANKRD9-transcript3      ------------------------------------------------------------

ANKRD9-transcript4      ------------------------GGCGCCCCACGCGTGCCGGCACAGGGCATATCTGGG 36
ANKRD9-transcript5      ------------------------------------------------------------
ANKRD9-transcript2      GGCCGAACTTTACGTAACCCGCCCGGCGCCCCACGCGTGCCGGCACAGGGCATATCTGGG 600
ANKRD9-transcript1      GGCCGAACTTTACGTAACCCGCCCGGCGCCCCACGCGTGCCGGCACAGGGCATATCTGGG 592
ANKRD9-transcript3      ------------------------------------------------------------

ANKRD9-transcript4      GCCCGGAGGCCCAGGCTTGGGGAAGGGGCTCCAGTCACGGTGTTGCCCACGGGCCACAGC 96
ANKRD9-transcript5      ------------------------------------------------------------
ANKRD9-transcript2      GCCCGGAGGCCCAGGCTTGGGGAAGGGGCTCCAGTCACGGTGTTGCCCACGGGCCACAGC 660
ANKRD9-transcript1      GCCCGGAGGCCCAGGCTTGGGGAAGGGGCTCCAGTCACGGTGTTGCCCACGGGCCACAGC 652
ANKRD9-transcript3      ------------------------------------------------------------
```

```
ANKRD9-transcript4      CTACCCGCACCGCGCCGCTCTCTTTAACTCAGTTACTGCCAGTGATAGTGACCCAGTCAG 156
ANKRD9-transcript5      ------------------------------------------------------------
ANKRD9-transcript2      CTACCCGCACCGCGCCGCTCTCTTTAACTCAGTTACTGCCAGTGATAGTGACCCAGTCAG 720
ANKRD9-transcript1      CTACCCGCACCGCGCCGCTCTCTTTAACTCAGTTACTGCCAGTGATAGTGACCCAGTCAG 712
ANKRD9-transcript3      ------------------------------------------------------------

ANKRD9-transcript4      TGTGTGTGGACGCGGCCTGCCTTCTGTCCCAGGCCCCTTGTGACCAAGGGCTTACCCTTG 216
ANKRD9-transcript5      ------------------------------------------------------------
ANKRD9-transcript2      TGTGTGTGGACGCGGCCTGCCTTCTGTCCCAGGCCCCTTGTGACCAAGGGCTTACCCTTG 780
ANKRD9-transcript1      TGTGTGTGGACGCGGCCTGCCTTCTGTCCCAGGCCCCTTGTGACCAAGGGCTTACCCTTG 772
ANKRD9-transcript3      ------------------------------------------------------------

ANKRD9-transcript4      AAAGAAGGCAGTAGGGAGGTTGGGACGGAGCCAGAGGTCAGACGCCTAGGCTCAGGTCGG 276
ANKRD9-transcript5      ------------------------------------------------------------
ANKRD9-transcript2      AAAGAAGGCAGTAGGGAGGTTGGGACGGAGCCAGAGGTCAGACGCCTAGGCTCAGGTCGG 840
ANKRD9-transcript1      AAAGAAGGCAGTAGGGAGGTTGGGACGGAGCCAGAGGTCAGACGCCTAGGCTCAGGTCGG 832
ANKRD9-transcript3      ------------------------------------------------------------

ANKRD9-transcript4      GGCTGGGGACTCAGAGGGCAGGGTCAGGGCCTAAGCTCGATTGCCTGTGGGTTGGGGGTC 336
ANKRD9-transcript5      ------------------------------------------------GGGTTGGGGGTC  12
ANKRD9-transcript2      GGCTGGGGACTCAGAGGGCAGGGTCAGGGCCTAAGCTCGATTGCCTGTGGGTTGGGGGTC 900
ANKRD9-transcript1      GGCTGGGGACTCAGAGGGCAGGGTCAGGGCCTAAGCTCGATTGCCTGTGGGTTGGGGGTC 892
ANKRD9-transcript3      ------------------------------------------------------------

ANKRD9-transcript4      CCCACCAATTCTGGAATGAGCCCAAACTGAGACGCAGGGGACCTGAGTTCTAGGCCTGGC 396
ANKRD9-transcript5      CCCACCAATTCTGGAATGAGCCCAAACTGAGACGCAGGGGACCTGAGTTCTAGGCCTGGC  72
ANKRD9-transcript2      CCCACCAATTCTGGAATGAGCCCAAACTGAGACGCAGGGGACCTGAGTTCTAGGCCTGGC 960
ANKRD9-transcript1      CCCACCAATTCTGGAATGAGCCCAAACTGAGACGCAGGGGACCTGAGTTCTAGGCCTGGC 952
ANKRD9-transcript3      ------------------------------------------------------------

ANKRD9-transcript4      TCTGCCGTGGCTTGCTGACCTTGGAGAATTGGAGAAGCTTGTGCCCTGCTGGAAAGTGGG 456
ANKRD9-transcript5      TCTGCCGTGGCTTGCTGACCTTGGAGAATTGGAGAAGCTTGTGCCCTGCTGGAAAGTGGG 132
ANKRD9-transcript2      TCTGCCGTGGCTTGCTGACCTTGGAGAATTGGAGAAGCTTGTGCCCTGCTGGAAAGTGGG 1020
ANKRD9-transcript1      TCTGCCGTGGCTTGCTGACCTTGGAGAATTGGAGAAGCTTGTGCCCTGCTGGAAAGTGGG 1012
ANKRD9-transcript3      ----------------------GGAGAATTGGAGAAGCTTGTGCCCTGCTGGAAAGTGGG  38
                                               ************************************

ANKRD9-transcript4      ATGGCAGTACCCGCTTCATCTAGTAGTCGGGGAGATCAAGAGAGGTATGGGACCTGAAGA 516
ANKRD9-transcript5      ATGGCAGTACCCGCTTCATCTAGTAGTCGGGGAGATCAAGAGAGGTATGGGACCTGAAGA 192
ANKRD9-transcript2      ATGGCAGTACCCGCTTCATCTAGTAGTCGGGGAGATCAAGAGAGGTATGGGACCTGAAGA 1080
ANKRD9-transcript1      ATGGCAGTACCCGCTTCATCTAGTAGTCGGGGAGATCAAGAGAGGTATGGGACCTGAAGA 1072
ANKRD9-transcript3      ATGGCAGTACCCGCTTCATCTAGTAGTCGGGGAGATCAAGAGAGGTATGGGACCTGAAGA 98
                        ************************************************************

ANKRD9-transcript4      GGATGGCAGACTGTGCAGTGCGGTGCACACCGGTCTCCAGGTTGTTTTCACCCTCCTATC 576
ANKRD9-transcript5      GGATGGCAGACTGTGCAGTGCGGTGCACACCGGTCTCCAGGTTGTTTTCACCCTCCTATC 252
ANKRD9-transcript2      GGATGGCAGACTGTGCAGTGCGGTGCACACCGGTCTCCAGGTTGTTTTCACCCTCCTATC 1140
ANKRD9-transcript1      GGATGGCAGACTGTGCAGTGCGGTGCACACCGGTCTCCAGGTTGTTTTCACCCTCCTATC 1132
ANKRD9-transcript3      GGATGGCAGACTGTGCAGTGCGGTGCACACCGGTCTCCAGGTTGTTTTCACCCTCCTATC 158
                        ************************************************************

ANKRD9-transcript4      TCCTCCCAGGAGCTAACGTGTAAGCAAACATGTTTGGATAGAGGGCTGGTGCCACGCCCC 636
ANKRD9-transcript5      TCCTCCCAGGAGCTAACGTGTAAGCAAACATGTTTGGATAGAGGGCTGGTGCCACGCCCC 312
ANKRD9-transcript2      TCCTCCCAGGAGCTAACGTGTAAGCAAACATGTTTGGATAGAGGGCTGGTGCCACGCCCC 1200
ANKRD9-transcript1      TCCTCCCAGGAGCTAACGTGTAAGCAAACATGTTTGGATAGAGGGCTGGTGCCACGCCCC 1192
ANKRD9-transcript3      TCCTCCCAGGAGCTAACGTGTAAGCAAACATGTTTGGATAGAGGGCTGGTGCCACGCCCC 218
                        ************************************************************

ANKRD9-transcript4      AGGCTCACCCCGCCCGCACAGCCGTCGTCCACCCCTCCCCTTTCTTACAGATAAAGCTGA 696
ANKRD9-transcript5      AGGCTCACCCCGCCCGCACAGCCGTCGTCCACCCCTCCCCTTTCTTACAGATAAAGCTGA 372
ANKRD9-transcript2      AGGCTCACCCCGCCCGCACAGCCGTCGTCCACCCCTCCCCTTTCTTACAGATAAAGCTGA 1260
ANKRD9-transcript1      AGGCTCACCCCGCCCGCACAGCCGTCGTCCACCCCTCCCCTTTCTTACAGATAAAGCTGA 1252
ANKRD9-transcript3      AGGCTCACCCCGCCCGCACAGCCGTCGTCCACCCCTCCCCTTTCTTACAGATAAAGCTGA 278
                        ************************************************************

ANKRD9-transcript4      GGCTCGGCCAGGGACTGTGATATACCCACATCCCCGGAACTAGGTGATCGCGGTGCAGGA 756
ANKRD9-transcript5      GGCTCGGCCAGGGACTGTGATATACCCACATCCCCGGAACTAGGTGATCGCGGTGCAGGA 432
ANKRD9-transcript2      GGCTCGGCCAGGGACTGTGATATACCCACATCCCCGGAACTAGGTGATCGCGGTGCAGGA 1320
ANKRD9-transcript1      GGCTCGGCCAGGGACTGTGATATACCCACATCCCCGGAACTAGGTGATCGCGGTGCAGGA 1312
ANKRD9-transcript3      GGCTCGGCCAGGGACTGTGATATACCCACATCCCCGGAACTAGGTGATCGCGGTGCAGGA 338
                        ************************************************************

ANKRD9-transcript4      ACCAGGTAGGTCTGAGTCTGGATCATGCCTCTGAACAGCCCAGGAAGAGGCTCCAGGGGC 816
ANKRD9-transcript5      ACCAGGTAGGTCTGAGTCTGGATCATGCCTCTGAACAGCCCAGGAAGAGGCTCCAGGGGC 492
ANKRD9-transcript2      ACCAGGTAGGTCTGAGTCTGGATCATGCCTCTGAACAGCCCAGGAAGAGGCTCCAGGGGC 1380
ANKRD9-transcript1      ACCAGGTAGGTCTGAGTCTGGATCATGCCTCTGAACAGCCCAGGAAGAGGCTCCAGGGGC 1372
ANKRD9-transcript3      ACCAGGTAGGTCTGAGTCTGGATCATGCCTCTGAACAGCCCAGGAAGAGGCTCCAGGGGC 398
```

```
                             ************************************************************

ANKRD9-transcript4           CTCCAAGTGGTCTGGGGTCGGAGATCAGGGTCAGGGTTGCGCTTGGGCTGGAGAGTGGAT 876
ANKRD9-transcript5           CTCCAAGTGGTCTGGGGTCGGAGATCAGGGTCAGGGTTGCGCTTGGGCTGGAGAGTGGAT 552
ANKRD9-transcript2           CTCCAAGTGGTCTGGGGTCGGAGATCAGGGTCAGGGTTGCGCTTGGGCTGGAGAGTGGAT 1440
ANKRD9-transcript1           CTCCAAGTGGTCTGGGGTCGGAGATCAGGGTCAGGGTTGCGCTTGGGCTGGAGAGTGGAT 1432
ANKRD9-transcript3           CTCCAAGTGGTCTGGGGTCGGAGATCAGGGTCAGGGTTGCGCTTGGGCTGGAGAGTGGAT 458
                             ************************************************************

ANKRD9-transcript4           TTGCCTCAGCTTGAGATGTGGGCCCAAGCTTTCTCATCCCCTCCCTGGCCTTTTCTTTAT 936
ANKRD9-transcript5           TTGCCTCAGCTTGAGATGTGGGCCCAAGCTTTCTCATCCCCTCCCTGGCCTTTTCTTTAT 612
ANKRD9-transcript2           TTGCCTCAGCTTGAGATGTGGGCCCAAGCTTTCTCATCCCCTCCCTGGCCTTTTCTTTAT 1500
ANKRD9-transcript1           TTGCCTCAGCTTGAGATGTGGGCCCAAGCTTTCTCATCCCCTCCCTGGCCTTTTCTTTAT 1492
ANKRD9-transcript3           TTGCCTCAGCTTGAGATGTGGGCCCAAGCTTTCTCATCCCCTCCCTGGCCTTTTCTTTAT 518
                             ************************************************************

ANKRD9-transcript4           TTGGGGTCGTATGAACCTGGCTTAGGTGGGAACAGAAGCTCTTCCAGTGGGTCCCTGGGT 996
ANKRD9-transcript5           TTGGGGTCGTATGAACCTGGCTTAGGTGGGAACAGAAGCTCTTCCAGTGGGTCCCTGGGT 672
ANKRD9-transcript2           TTGGGGTCGTATGAACCTGGCTTAGGTGGGAACAGAAGCTCTTCCAGTGGGTCCCTGGGT 1560
ANKRD9-transcript1           TTGGGGTCGTATGAACCTGGCTTAGGTGGGAACAGAAGCTCTTCCAGTGGGTCCCTGGGT 1552
ANKRD9-transcript3           TTGGGGTCGTATGAACCTGGCTTAGGTGGGAACAGAAGCTCTTCCAGTGGGTCCCTGGGT 578
                             ************************************************************

ANKRD9-transcript4           TGGAGAGGGGAGGGGAGATTTGAGGGCATGGGCAGCAAGGGCATTTCCAGCAGAGGTGCC 1056
ANKRD9-transcript5           TGGAGAGGGGAGGGGAGATTTGAGGGCATGGGCAGCAAGGGCATTTCCAGCAGAGGTGCC 732
ANKRD9-transcript2           TGGAGAGGGGAGGGGAGATTTGAGGGCATGGGCAGCAAGGGCATTTCCAGCAGAGGTGCC 1620
ANKRD9-transcript1           TGGAGAGGGGAGGGGAGATTTGAGGGCATGGGCAGCAAGGGCATTTCCAGCAGAGGTGCC 1612
ANKRD9-transcript3           TGGAGAGGGGAGGGGAGATTTGAGGGCATGGGCAGCAAGGGCATTTCCAGCAGAGGTGCC 638
                             ************************************************************

ANKRD9-transcript4           AGAGAGCAAGTCAGTTTCAAGGAGGGAGAACAGGTACAGCTAGATCAAGGATGGAGGCGG 1116
ANKRD9-transcript5           AGAGAGCAAGTCAGTTTCAAGGAGGGAGAACAGGTACAGCTAGATCAAGGATGGAGGCGG 792
ANKRD9-transcript2           AGAGAGCAAGTCAGTTTCAAGGAGGGAGAACAGGTACAGCTAGATCAAGGATGGAGGCGG 1680
ANKRD9-transcript1           AGAGAGCAAGTCAGTTTCAAGGAGGGAGAACAGGTACAGCTAGATCAAGGATGGAGGCGG 1672
ANKRD9-transcript3           AGAGAGCAAGTCAGTTTCAAGGAGGGAGAACAGGTACAGCTAGATCAAGGATGGAGGCGG 698
                             ************************************************************

ANKRD9-transcript4           TGGTTCTGGGCGTCGGAGAGATGGAGCTGTAGGGTGACTGGAAGGGCCTGGCCGAGGCTG 1176
ANKRD9-transcript5           TGGTTCTGGGCGTCGGAGAGATGGAGCTGTAGGGTGACTGGAAGGGCCTGGCCGAGGCTG 852
ANKRD9-transcript2           TGGTTCTGGGCGTCGGAGAGATGGAGCTGTAGGGTGACTGGAAGGGCCTGGCCGAGGCTG 1740
ANKRD9-transcript1           TGGTTCTGGGCGTCGGAGAGATGGAGCTGTAGGGTGACTGGAAGGGCCTGGCCGAGGCTG 1732
ANKRD9-transcript3           TGGTTCTGGGCGTCGGAGAGATGGAGCTGTAGGGTGACTGGAAGGGCCTGGCCGAGGCTG 758
                             ************************************************************

ANKRD9-transcript4           GAGGTAGGTACAGGCCTGGTGGGCCAGGACCGGAGGGGCTGTGTGAGGGGCAGAGGGGAG 1236
ANKRD9-transcript5           GAGGTAGGTACAGGCCTGGTGGGCCAGGACCGGAGGGGCTGTGTGAGGGGCAGAGGGGAG 912
ANKRD9-transcript2           GAGGTAGGTACAGGCCTGGTGGGCCAGGACCGGAGGGGCTGTGTGAGGGGCAGAGGGGAG 1800
ANKRD9-transcript1           GAGGTAGGTACAGGCCTGGTGGGCCAGGACCGGAGGGGCTGTGTGAGGGGCAGAGGGGAG 1792
ANKRD9-transcript3           GAGGTAGGTACAGGCCTGGTGGGCCAGGACCGGAGGGGCTGTGTGAGGGGCAGAGGGGAG 818
                             ************************************************************

ANKRD9-transcript4           TCCCCGGGCCTCCCCAGTTTCCCCGCGCCTCACCGTGGCCTCTTCCTTTCCCCGCAGGTG 1296
ANKRD9-transcript5           TCCCCGGGCCTCCCCAGTTTCCCCGCGCCTCACCGTGGCCTCTTCCTTTCCCCGCAGGTG 972
ANKRD9-transcript2           TCCCCGGGCCTCCCCAGTTTCCCCGCGCCTCACCGTGGCCTCTTCCTTTCCCCGCAGGTG 1860
ANKRD9-transcript1           TCCCCGGGCCTCCCCAGTTTCCCCGCGCCTCACCGTGGCCTCTTCCTTTCCCCGCAGGTG 1852
ANKRD9-transcript3           TCCCCGGGCCTCCCCAGTTTCCCCGCGCCTCACCGTGGCCTCTTCCTTTCCCCGCAGGTG 878
                             ************************************************************

ANKRD9-transcript4           TGCCTTCGCGGGATCCATGCCTTGAGGCCCAGGAACGCCCCGCCGCCAGCATGCCGTGGG 1356
ANKRD9-transcript5           TGCCTTCGCGGGATCCATGCCTTGAGGCCCAGGAACGCCCCGCCGCCAGCATGCCGTGGG 1032
ANKRD9-transcript2           TGCCTTCGCGGGATCCATGCCTTGAGGCCCAGGAACGCCCCGCCGCCAGCATGCCGTGGG 1920
ANKRD9-transcript1           TGCCTTCGCGGGATCCATGCCTTGAGGCCCAGGAACGCCCCGCCGCCAGCATGCCGTGGG 1912
ANKRD9-transcript3           TGCCTTCGCGGGATCCATGCCTTGAGGCCCAGGAACGCCCCGCCGCCAGCATGCCGTGGG 938
                             ************************************************************

ANKRD9-transcript4           ACGCGCGGCGGCCTGGGGGTGGCGCGGACGGCGGGCCCGAGGCCTCGGGCGCGGCGCGCT 1416
ANKRD9-transcript5           ACGCGCGGCGGCCTGGGGGTGGCGCGGACGGCGGGCCCGAGGCCTCGGGCGCGGCGCGCT 1092
ANKRD9-transcript2           ACGCGCGGCGGCCTGGGGGTGGCGCGGACGGCGGGCCCGAGGCCTCGGGCGCGGCGCGCT 1980
ANKRD9-transcript1           ACGCGCGGCGGCCTGGGGGTGGCGCGGACGGCGGGCCCGAGGCCTCGGGCGCGGCGCGCT 1972
ANKRD9-transcript3           ACGCGCGGCGGCCTGGGGGTGGCGCGGACGGCGGGCCCGAGGCCTCGGGCGCGGCGCGCT 998
                             ************************************************************

ANKRD9-transcript4           CGCGAGCGCAGAAGCAGTGCCGCAAGTCGTCGTTCGCCTTCTACCAGGCGGTGCGCGACC 1476
ANKRD9-transcript5           CGCGAGCGCAGAAGCAGTGCCGCAAGTCGTCGTTCGCCTTCTACCAGGCGGTGCGCGACC 1152
ANKRD9-transcript2           CGCGAGCGCAGAAGCAGTGCCGCAAGTCGTCGTTCGCCTTCTACCAGGCGGTGCGCGACC 2040
ANKRD9-transcript1           CGCGAGCGCAGAAGCAGTGCCGCAAGTCGTCGTTCGCCTTCTACCAGGCGGTGCGCGACC 2032
ANKRD9-transcript3           CGCGAGCGCAGAAGCAGTGCCGCAAGTCGTCGTTCGCCTTCTACCAGGCGGTGCGCGACC 1058
                             ************************************************************
```

```
ANKRD9-transcript4      TGCTACCCGTGTGGCTGCTGGAGGATATGCGCGCCAGCGAGGCCTTCCACTGGGACGAGC 1536
ANKRD9-transcript5      TGCTACCCGTGTGGCTGCTGGAGGATATGCGCGCCAGCGAGGCCTTCCACTGGGACGAGC 1212
ANKRD9-transcript2      TGCTACCCGTGTGGCTGCTGGAGGATATGCGCGCCAGCGAGGCCTTCCACTGGGACGAGC 2100
ANKRD9-transcript1      TGCTACCCGTGTGGCTGCTGGAGGATATGCGCGCCAGCGAGGCCTTCCACTGGGACGAGC 2092
ANKRD9-transcript3      TGCTACCCGTGTGGCTGCTGGAGGATATGCGCGCCAGCGAGGCCTTCCACTGGGACGAGC 1118
                        ************************************************************

ANKRD9-transcript4      GCGGGCGCGCCGCCGCCTACTCGCCCTCTGAGGCGCTGCTCTACGCGCTCGTGCACGACC 1596
ANKRD9-transcript5      GCGGGCGCGCCGCCGCCTACTCGCCCTCTGAGGCGCTGCTCTACGCGCTCGTGCACGACC 1272
ANKRD9-transcript2      GCGGGCGCGCCGCCGCCTACTCGCCCTCTGAGGCGCTGCTCTACGCGCTCGTGCACGACC 2160
ANKRD9-transcript1      GCGGGCGCGCCGCCGCCTACTCGCCCTCTGAGGCGCTGCTCTACGCGCTCGTGCACGACC 2152
ANKRD9-transcript3      GCGGGCGCGCCGCCGCCTACTCGCCCTCTGAGGCGCTGCTCTACGCGCTCGTGCACGACC 1178
                        ************************************************************

ANKRD9-transcript4      ACCAAGCGTACGCGCATTACCTGCTGGCCACGTTCCCGCGGCGCGCGCTCGCACCGCCCA 1656
ANKRD9-transcript5      ACCAAGCGTACGCGCATTACCTGCTGGCCACGTTCCCGCGGCGCGCGCTCGCACCGCCCA 1332
ANKRD9-transcript2      ACCAAGCGTACGCGCATTACCTGCTGGCCACGTTCCCGCGGCGCGCGCTCGCACCGCCCA 2220
ANKRD9-transcript1      ACCAAGCGTACGCGCATTACCTGCTGGCCACGTTCCCGCGGCGCGCGCTCGCACCGCCCA 2212
ANKRD9-transcript3      ACCAAGCGTACGCGCATTACCTGCTGGCCACGTTCCCGCGGCGCGCGCTCGCACCGCCCA 1238
                        ************************************************************

ANKRD9-transcript4      GTGCCGGCTTCCGCTGCTGCGCGGCTCCCGGGCCGCACGTGGCGCTGGCAGTGCGCTACA 1716
ANKRD9-transcript5      GTGCCG------------------------------------------------------ 1338
ANKRD9-transcript2      GTGCCGGCTTCCGCTGCTGCGCGGCTCCCGGGCCGCACGTGGCGCTGGCAGTGCGCTACA 2280
ANKRD9-transcript1      GTGCCGGCTTCCGCTGCTGCGCGGCTCCCGGGCCGCACGTGGCGCTGGCAGTGCGCTACA 2272
ANKRD9-transcript3      GTGCCGGCTTCCGCTGCTGCGCGGCTCCCGGGCCGCACGTGGCGCTGGCAGTGCGCTACA 1298
                        ******

ANKRD9-transcript4      ACCGCGTGGGCATTCTGCGCCGCATCCTGCGCACCTTGCGCGACTTCCCGGCCGAGGAGC 1776
ANKRD9-transcript5      ------------------------------------------------------------
ANKRD9-transcript2      ACCGCGTGGGCATTCTGCGCCGCATCCTGCGCACCTTGCGCGACTTCCCGGCCGAGGAGC 2340
ANKRD9-transcript1      ACCGCGTGGGCATTCTGCGCCGCATCCTGCGCACCTTGCGCGACTTCCCGGCCGAGGAGC 2332
ANKRD9-transcript3      ACCGCGTGGGCATTCTGCGCCGCATCCTGCGCACCTTGCGCGACTTCCCGGCCGAGGAGC 1358

ANKRD9-transcript4      GGGCGCGCGTGCTGGACCGGCGTGGCTGCAGCCGCGTGGAGGGCGGTGGCACGTCGCTGC 1836
ANKRD9-transcript5      ------------------------------------------------------------
ANKRD9-transcript2      GGGCGCGCGTGCTGGACCGGCGTGGCTGCAGCCGCGTGGAGGGCGGTGGCACGTCGCTGC 2400
ANKRD9-transcript1      GGGCGCGCGTGCTGGACCGGCGTGGCTGCAGCCGCGTGGAGGGCGGTGGCACGTCGCTGC 2392
ANKRD9-transcript3      GGGCGCGCGTGCTGGACCGGCGTGGCTGCAGCCGCGTGGAGGGCGGTGGCACGTCGCTGC 1418


ANKRD9-transcript4      ACGTGGCCTGTGAGCTGGCGCGCCCCGAGTGCCTCTTCCTGCTGCTGGGCCACGGCGCCT 1896
ANKRD9-transcript5      ------------------------------------------------------------
ANKRD9-transcript2      ACGTGGCCTGTGAGCTGGCGCGCCCCGAGTGCCTCTTCCTGCTGCTGGGCCACGGCGCCT 2460
ANKRD9-transcript1      ACGTGGCCTGTGAGCTGGCGCGCCCCGAGTGCCTCTTCCTGCTGCTGGGCCACGGCGCCT 2452
ANKRD9-transcript3      ACGTGGCCTGTGAGCTGGCGCGCCCCGAGTGCCTCTTCCTGCTGCTGGGCCACGGCGCCT 1478

ANKRD9-transcript4      CGCCCGGTCTGCGGGACGGCGGCGGCCTCACGCCTCTCGAGCTGCTGCTGCGCCAGCTGG 1956
ANKRD9-transcript5      ------------------------------------------------------------
ANKRD9-transcript2      CGCCCGGTCTGCGGGACGGCGGCGGCCTCACGCCTCTCGAGCTGCTGCTGCGCCAGCTGG 2520
ANKRD9-transcript1      CGCCCGGTCTGCGGGACGGCGGCGGCCTCACGCCTCTCGAGCTGCTGCTGCGCCAGCTGG 2512
ANKRD9-transcript3      CGCCCGGTCTGCGGGACGGCGGCGGCCTCACGCCTCTCGAGCTGCTGCTGCGCCAGCTGG 1538

ANKRD9-transcript4      GCCGCGACGCCGGGGCCACTCCCTCCGCCGCCGGAGCCCCCGCCTCAGCTCCCGGGGAGC 2016
ANKRD9-transcript5      ------------------------------------------------------------
ANKRD9-transcript2      GCCGCGACGCCGGGGCCACTCCCTCCGCCGCCGGAGCCCCCGCCTCAGCTCCCGGGGAGC 2580
ANKRD9-transcript1      GCCGCGACGCCGGGGCCACTCCCTCCGCCGCCGGAGCCCCCGCCTCAGCTCCCGGGGAGC 2572
ANKRD9-transcript3      GCCGCGACGCCGGGGCCACTCCCTCCGCCGCCGGAGCCCCCGCCTCAGCTCCCGGGGAGC 1598

ANKRD9-transcript4      CGCGCCAGCGCCGCCTGCTGCTGCTGGACCTCCTGGCGCTGTACACCCCCGTGGGTGCCG 2076
ANKRD9-transcript5      ------------------------------------------------------------
ANKRD9-transcript2      CGCGCCAGCGCCGCCTGCTGCTGCTGGACCTCCTGGCGCTGTACACCCCCGTGGGTGCCG 2640
ANKRD9-transcript1      CGCGCCAGCGCCGCCTGCTGCTGCTGGACCTCCTGGCGCTGTACACCCCCGTGGGTGCCG 2632
ANKRD9-transcript3      CGCGCCAGCGCCGCCTGCTGCTGCTGGACCTCCTGGCGCTGTACACCCCCGTGGGTGCCG 1658

ANKRD9-transcript4      CCGGCTCGGCCCGCCAGGAGCTGCTGGGCGACCGGCCGCGCTGGCAGCG---------- 2125
ANKRD9-transcript5      ------------------------------------------------------------
ANKRD9-transcript2      CCGGCTCGGCCCGCCAGGAGCTGCTGGGCGACCGGCCGCGCTGGCAGCGGCTGCTGGGTG 2700
ANKRD9-transcript1      CCGGCTCGGCCCGCCAGGAGCTGCTGGGCGACCGGCCGCGCTGGCAGCGGCTGCTGGGTG 2692
ANKRD9-transcript3      CCGGCTCGGCCCGCCAGGAGCTGCTGGGCGACCGGCCGCGCTGGCAGCGGCTGCTGGGTG 1718
```

```
ANKRD9-transcript4      ------------------------------------------------------------
ANKRD9-transcript5      ------------------------------------------------------------
ANKRD9-transcript2      AGGACAAGTTCCAGTGGCTGGCGGGCCTGGCGCCGCCCTCGCTCTTCGCGCGCGCCATGC 2760
ANKRD9-transcript1      AGGACAAGTTCCAGTGGCTGGCGGGCCTGGCGCCGCCCTCGCTCTTCGCGCGCGCCATGC 2752
ANKRD9-transcript3      AGGACAAGTTCCAGTGGCTGGCGGGCCTGGCGCCGCCCTCGCTCTTCGCGCGCGCCATGC 1778

ANKRD9-transcript4      ------------------------------------------------------------
ANKRD9-transcript5      ------------------------------------------------------------
ANKRD9-transcript2      AGGTGCTGGTCACCGCCATCTCTCCAGGCCGCTTCCCCGAGGCCCTGGACGAGCTGCCGC 2820
ANKRD9-transcript1      AGGTGCTGGTCACCGCCATCTCTCCAGGCCGCTTCCCCGAGGCCCTGGACGAGCTGCCGC 2812
ANKRD9-transcript3      AGGTGCTGGTCACCGCCATCTCTCCAGGCCGCTTCCCCGAGGCCCTGGACGAGCTGCCGC 1838

ANKRD9-transcript4      ------------------------------------------------------------
ANKRD9-transcript5      ------------------------------------------------------------
ANKRD9-transcript2      TGCCCCCATTCCTGCAGCCGTTGGACCTCACTGGCAAAGGCTAGGCCCGGAGCACCCTAG 2880
ANKRD9-transcript1      TGCCCCCATTCCTGCAGCCGTTGGACCTCACTGGCAAAGGCTAGGCCCGGAGCACCCTAG 2872
ANKRD9-transcript3      TGCCCCCATTCCTGCAGCCGTTGGACCTCACTGGCAAAGGCTAGGCCCGGAGCACCCTAG 1898

ANKRD9-transcript4      ------------------------------------------------------------
ANKRD9-transcript5      ------------------------------------------------------------
ANKRD9-transcript2      GCGCTGGATTTTGGGACAAAACTATTTTTCAGAGCGTTGTACCG---------------- 2924
ANKRD9-transcript1      GCGCTGGATTTTGGGACAAAACTATTTTTCAGAGCGTTGTACCGGCACTTTATATATATT 2932
ANKRD9-transcript3      GCGCTGGATTTTGGGACAAAACTATTTTTCAGAGCGTTGTACCGGCACTTTATATATATT 1958

ANKRD9-transcript4      ------------------
ANKRD9-transcript5      ------------------
ANKRD9-transcript2      ------------------
ANKRD9-transcript1      GATCTCTGTACGGCACAA 2950
ANKRD9-transcript3      GATCTCTGTACGGCACAA 1976
```

Figure 6-2. Multiple sequence alignment of ANKRD9 splice variants. Sequences obtained from ENSEML database; ankyrin repeat domain 9 [Source:HGNC Symbol;Acc:20096] were aligned using Clustal W. Intron sequences are marked with green. Bold corresponds to translated protein coding regions. The rest of the sequence is untranslated regions (UTRs). The following colors are used to mark the siRNA targeted regions (yellow-ANKRD9 siRNA#1, blue- ANKRD9 siRNA#2, green- ANKRD9 siRNA#3, and pink- ANKRD9 siRNA#4). The region amplified with the ANKRD9 primer sets for qPCR is underlined.

Table 6-1. Downregulation of most ankyrin repeat proteins has no significant effect on copper levels. Shown are ICPMS data from the ionome database (Malinouski et al., 2014), in bold are the genes which upon downregulation result in statistically significant increase of copper levels **(z-score>4).**

Gene name	Protein name	Cu-fold change	Cu-z score
ANKRD9	**Ankyrin repeat domain 9**	**1.703**	**7.184**
AGAP2	**ArfGAP with GTPase domain, ankyrin repeat and PH domain 2**	**1.425**	**5.2**
ANKS3	**Ankyrin repeat and sterile alpha motif domain containing 3**	**1.485**	**4.403**
ASB13	**Ankyrin repeat and SOCS box-containing 13**	**1.412**	**4.066**
SOWAHC	sosondowah ankyrin repeat domain family member C	1.241	3.985
ASB14	Ankyrin repeat and SOCS box-containing 14	1.299	3.282
ASB5	Ankyrin repeat and SOCS box-containing 5	1.308	3.016
ASB9	Ankyrin repeat and SOCS box-containing 9	1.305	2.988
ASB16	Ankyrin repeat and SOCS box-containing 16	1.195	2.974
ANKRD11	Ankyrin repeat domain 11	1.148	2.925
ANKDD1A	Ankyrin repeat and death domain containing 1A	1.201	2.878
ANKS4B	Ankyrin repeat and sterile alpha motif domain containing 4B	1.217	2.793
AGAP3	ArfGAP with GTPase domain, ankyrin repeat and PH domain 3	1.202	2.439
ANKRD7	Ankyrin repeat domain 7	1.261	2.115
ANKRD33	Ankyrin repeat domain 33	1.118	1.968
KANK4	Homo sapiens KN motif and ankyrin repeat domains 4	1.002	0.029
ASZ1	Ankyrin repeat, SAM and basic leucine zipper domain containing 1	1.012	0.085
ANKMY1	Ankyrin repeat and MYND domain containing 1	1.07	1.905
ANKRD23	Ankyrin repeat domain 23	1.005	0.098
ANKRD44	Ankyrin repeat domain 44	1.02	0.193
ANKRD46	Ankyrin repeat domain 46	1.024	0.219
ASAP2	ArfGAP with SH3 domain, ankyrin repeat and PH domain 2	1.018	0.249
ARAP3	ArfGAP with RhoGAP domain, ankyrin repeat and PH domain 3	1.017	0.327
ASB17	Ankyrin repeat and SOCS box-containing 17	1.046	0.367
ANK3	Ankyrin 3, node of Ranvier (ankyrin G)	1.024	0.371
ASB6	Ankyrin repeat and SOCS box-containing 6	1.048	0.43
ANKHD1	Ankyrin repeat and KH domain containing 1	1.02	0.461
ANKRD13D	Ankyrin repeat domain 13 family, member D	1.1	1.468
ANKRD5	Ankyrin repeat domain 5	1.037	0.533
NRARP	NOTCH-regulated ankyrin repeat protein	1.046	0.555
ABTB1	Ankyrin repeat and BTB (POZ) domain containing 1	1.039	0.564
BANK1	B-cell scaffold protein with ankyrin repeats 1	1.026	0.591
ACAP1	ArfGAP with coiled-coil, ankyrin repeat and PH domains 1	1.053	0.618
ANKS1B	Ankyrin repeat and sterile alpha motif domain containing 1B	1.078	1.374
ANKRD30A	Ankyrin repeat domain 30A	1.059	0.662
ANKRD54	Ankyrin repeat domain 54	1.017	0.679
ANKRD32	Ankyrin repeat domain 32	1.131	1.305
ASB10	Ankyrin repeat and SOCS box-containing 10	1.127	1.296
ANKRD1	Ankyrin repeat domain 1 (cardiac muscle)	1.049	0.71
ANKS6	Ankyrin repeat and sterile alpha motif domain containing 6	1.065	0.723
RFXANK	Regulatory factor X-associated ankyrin-containing protein	1.045	0.747
ANKRD13B	Ankyrin repeat domain 13B	1.086	0.755
ASAP3	ArfGAP with SH3 domain, ankyrin repeat and PH domain 3	1.06	1.201
KANK1	KN motif and ankyrin repeat domains 1	1.049	0.81
ASB15	Ankyrin repeat and SOCS box-containing 15	1.076	0.816
ANKRD13A	Ankyrin repeat domain 13A	1.087	1.066
ANKS1A	Ankyrin repeat and sterile alpha motif domain containing 1A	1.071	0.935
AGAP1	ArfGAP with GTPase domain, ankyrin repeat and PH domain 1	1.09	1.049
ASB3	Ankyrin repeat and SOCS box-containing 3	1.04	1.038
AGAP4	ArfGAP with GTPase domain, ankyrin repeat and PH domain 4	1.087	1.019
POTE15	POTE ankyrin domain family, member B	0.841	-2.384

Table 6-2. Glycosyltransferases which upon downregulation do not alter the copper levels significantly. Shown are ICPMS data from the ionome database, **(z-score<2)** (Malinouski et al., 2014).

UGT1A1(NM_000463)	UGT1A10 (NM_019075),	UGT1A3 (NM_019093)	UGT1A5 (NM_019078)
UGT1A6 (NM_001072)	UGT1A7 (NM_019077)	UGT1A8 (NM_019076)	UGT2A1 (NM_006798)
UGT2A3 (NM_024743)	UGT2B10 (NM_001075)	UGT2B11 (NM_001073)	UGT2B15 (NM_001076)
UGT2B17 (NM_001077)	UGT2B28 (NM_053039)	UGT2B4 (NM_021139)	UGT2B7 (NM_001074)
UGT3A2(NM_174914)	HAS1 (NM_001523)	HAS2 (NM_005328)	HAS3 (NM_005329)
GYS1 (NM_002103)	GYS2 (NM_021957)	ALG2 (NM_033087)	GLT1D1 (NM_144669)
GTDC1(NM_001006636)	PIGA (NM_002641)	ABO (NM_020469)	GBGT1 (NM_021996)
B4GALNT4 (NM_178537)	B4GALT2 (NM_003780)	B4GALT3 (NM_003779)	B4GALT4 (NM_003778)
B4GALT6 (NM_004775)	CHPF (NM_024536)	CHPF2 (NM_019015)	CHSY1 (NM_014918)
CSGALNACT1 (NM_018371)	CSGALNACT2 (NM_018590)	XXYLT1 (NM_152531)	GLT8D1 (NM_018446)
GLT8D2 (NM_031302)	GYG1(NM_004130)	GYG2 (NM_003918)	GYLTL1B (NM_152312)
FUT4 (NM_002033)	FUT5 (NM_002034)	FUT6 (NM_000150)	FUT7 (NM_004479)
FUT9(NM_006581)	FUT10(NM_032664)	FUT1 (NM_000148)	FUT2 (NM_000511)
B4GALNT1(NM_001478)	B4GALNT2 (NM_153446)	MGAT1 (NM_002406)	POMGNT1 (NM_017739)
RTFDC1 (NM_016407)	GCNT1(NM_001490)	GCNT2 (NM_001491)	GCNT3 (NM_004751)
GCNT4 (NM_016591)	GCNT7 (XM_001723344)	XYLT1(NM_022166)	XYLT2 (NM_022167)
UGCG (NM_003358)	ALG9 (NM_024740)	PIGB (NM_004855)	PIGZ (NM_025163)
FUT8 (NM_178154)	UGCGL1 (NM_020120)	UGCGL2 (NM_020121)	GLT25D1 (NM_024656)
GALNT2 (NM_004481)	GALNT3(NM_004482)	GALNT5 (NM_014568)	GALNT6 (NM_007210)
GALNT8 (NM_017417)	GALNT10 (NM_198321)	GALNT11 (NM_022087)	GALNT12 (NM_024642)
GALNT13 (NM_052917)	GALNT14 (NM_024572)	GALNTL2 (NM_054110)	GALNTL3 (NM_022479)
ST3GAL1 (NM_003033)	ST3GAL2 (NM_006927)	ST3GAL3 (NM_006279)	ST3GAL5 (NM_003896)
ST3GAL6 (NM_006100)	ST6GALNAC1 (NM_018414)	ST6GALNAC2 (NM_006456)	ST6GALNAC3 (NM_152996)
ST6GALNAC4 (NM_014403)	ST6GALNAC5 (NM_030965)	ST6GALNAC6 (NM_013443)	ST8SIA1 (NM_003034)
ST8SIA2 (NM_006011)	ST8SIA3 (NM_015879)	ST8SIA4 (NM_005668)	ST8SIA5 (NM_013305)
B3GALNT2 (NM_152490)	B3GALT1 (NM_020981)	B3GALT2 (NM_003783)	B3GALT3 (NM_003781)
B3GALT4 (NM_003782)	B3GALT6 (NM_080605)	B3GNT2 (NM_006577)	B3GNT4 (NM_030765)
B3GNT5 (NM_032047),	B3GNT7 (NM_145236)	B3GNT8 (NM_198540)	B3GNT9 (NM_033309)
C1GALT1 (NM_020156)	C1GALT1C1 (NM_152692)	LFNG (NM_001040167)	RFNG (NM_002917)
A4GNT (NM_016161)	A4GALT (NM_017436)	PYGB (NM_002862)	PYGL (NM_002863)
PYGM (NM_005609)	POMT1 (NM_007171)	POMT2 (NM_013382)	B3GAT1 (NM_018644)
B3GAT2 (NM_080742)	MGAT4A (NM_012214)	MGAT4B (NM_014275)	MGAT5 (NM_002410)
ALG6 (NM_013339)	ALG8 (NM_024079)	ALG3 (NM_005787)	ALG10 (NM_032834)
AER61 (NM_173654)	EXT1 (NM_000127)	EXT2 (NM_000401)	EXTL1 (NM_004455)
EXTL2 (NM_001439)	EXTL3 (NM_001440)	POFUT1 (NM_015352)	STT3A (NM_152713)
STT3B (NM_178862)	POFUT2 (NM_015227)	KDELC1 (NP_076994)	KTELC1 (NM_020231)

Table 6-3. Glycosyltransferases which upon downregulation do alter the copper levels. Shown are ICPMS data from the ionome database, in bold are the genes which upon downregulation result in statistically significant increase of copper levels **(z-score>4 or z-score<-4)** (Malinouski et al., 2014).

gene name	Protein name	Cu-fold change	Cu-z score
MGAT3 (NM_002409)	**Mannosyl (beta-1,4-)-glycoprotein beta-1,4-N-acetylglucosaminyltransferase**	**1.349**	**4.754**
GALNT4 (NM_003774)	**N-acetylgalactosaminyltransferase 4**	**1.42**	**4.867**
GALNT1 (NM_020474)	**N-acetylgalactosaminyltransferase 1**	**1.281**	**4.4**
ALG12 (NM_024105)	**Alpha-1,6-mannosyltransferase**	**1.352**	**4.254**
GALNTL4 (NM_198516)	N-acetylgalactosaminyltransferase 18	1.215	3.824
ST3GAL4 (NM_006278)	ST3 beta-galactoside alpha-2,3-sialyltransferase 4	1.303	3.365
GLT6D1 (NM_182974)	Glycosyltransferase 6 domain containing 1	1.186	3.309
AGO61 (NM_032806)	O-linked mannose N-acetylglucosaminyltransferase 2 (beta 1,4-) (POMGNT2)	1.268	3.1
UGT1A9 (NM_021027)	UDP glucuronosyltransferase 1 family, polypeptide A9	1.17	3.083
PIGV (NM_017837)	Phosphatidylinositol glycan anchor biosynthesis, class V	1.149	3.04
B3GNT6 (NM_138706)	UDP-GlcNAc:betaGal beta-1,3-N-acetylglucosaminyltransferase 6 (core 3 synthase)	1.212	2.933
B3GAT3 (NM_012200)	Beta-1,3-glucuronyltransferase 3 (glucuronosyltransferase I)	1.239	2.832
CERCAM (NM_016174)	Cerebral endothelial cell adhesion molecule	1.356	2.823
ALG1 (NM_019109)	chitobiosyldiphosphodolichol beta-mannosyltransferase	1.166	2.745
GALNTL5 (NM_145292)	N-acetylgalactosaminyltransferase-like 5	1.223	2.636
GALNT9 (NM_021808)	N-acetylgalactosaminyltransferase 9	1.101	2.595
UGT1A4 (NM_007120)	UDP glucuronosyltransferase 1 family, polypeptide A4	1.136	2.471
ALG14 (NM_144988)	UDP-N-acetylglucosaminyltransferase subunit	1.189	2.333
ALG5 (NM_013338)	Dolichyl-phosphate beta-glucosyltransferase	1.136	2.267
MGAT2 (NM_002408)	mannosyl (alpha-1,6-)-glycoprotein beta-1,2-N-acetylglucosaminyltransferase	1.175	2.392
OGT (NM_003605)	O-linked N-acetylglucosamine (GlcNAc) transferase (OGT), transcript variant 1	1.145	2.253
UGT8 (NM_003360)	UDP glycosyltransferase 8	1.12	2.168
DPM1 (NM_003859)	Dolichyl-phosphate mannosyltransferase polypeptide 1, catalytic subunit	1.135	2.134
B4GALT5 (NM_004776)	UDP-Gal:betaGlcNAc beta 1,4- galactosyltransferase, polypeptide 5	1.204	2.073
LARGE (NM_004737)	Like-glycosyltransferase	1.12	2.071
FUT3 (NM_000149)	Fucosyltransferase 3 (galactoside 3(4)-L-fucosyltransferase	1.246	2.053
UGT3A1 (NM_152404)	**UDP glycosyltransferase 3 family, polypeptide A1**	**0.433**	**-4.772**
B4GALNT3	**Beta-1,4-N-acetyl-galactosaminyl transferase 3**	**0.489**	**-4.614**

(NM_173593)			
GLT25D2 (NM_015101)	collagen beta(1-O)galactosyltransferase 2	0.753	-3.961
B3GALTL (NM_194318)	beta 1,3-galactosyltransferase-like (B3GALTL)	0.665	-3.502
B3GNT3 (NM_014256)	UDP-GlcNAc:betaGal beta-1,3-N-acetylglucosaminyltransferase 3	0.809	-3.409
B3GALT5 (NM_006057)	UDP-Gal:betaGlcNAc beta 1,3-galactosyltransferase, polypeptide 5	0.779	-2.75
MGAT4C (NM_013244)	mannosyl (alpha-1,3-)-glycoprotein beta-1,4-N-acetylglucosaminyltransferase, isozyme C	0.806	-2.664
B4GALT7 (NM_007255)	UDP-Gal:betaGlcNAc beta 1,4- galactosyltransferase, polypeptide 7	0.857	-2.567
FUT11 (NM_173540)	Fucosyltransferase 11 (alpha (1,3) fucosyltransferase)	0.797	-2.455
ST6GAL1 (NM_003032)	ST6 beta-galactosamide alpha-2,6-sialyltranferase 1	0.86	-2.304
GALNT7 (NM_017423)	N-acetylgalactosaminyltransferase 7	0.916	-2.271
MGAT5B (NM_144677)	mannosyl (alpha-1,6-)-glycoprotein beta-1,6-N-acetyl-glucosaminyltransferase, isozyme B	0.791	-2.191
B4GALT1 (NM_001497)	UDP-Gal:betaGlcNAc beta 1,4- galactosyltransferase, polypeptide 1	0.879	-2.163
ALG11 (NM_001004127)	Alpha-1,2-mannosyltransferase	0.87	-2.155
ST6GAL2 (NM_032528)	ST6 beta-galactosamide alpha-2,6-sialyltranferase 2	0.807	-2.068
MFNG (NM_002405)	MFNG O-fucosylpeptide 3-beta-N-acetylglucosaminyltransferase (MFNG)	0.717	-2.005

Reference List

Leettola, C.N., Knight, M.J., Cascio, D., Hoffman, S., and Bowie, J.U. (2014). Characterization of the SAM domain of the PKD-related protein ANKS6 and its interaction with ANKS3. BMC Struct. Biol. *14,* 17-6807-14-17.

Malinouski, M., Hasan, N.M., Zhang, Y., Seravalli, J., Lin, J., Avanesov, A., Lutsenko, S., and Gladyshev, V.N. (2014). Genome-wide RNAi ionomics screen reveals new genes and regulation of human trace element metabolism. Nat. Commun. *5,* 3301.

Wu, Y., Zhao, Y., Ma, X., Zhu, Y., Patel, J., and Nie, Z. (2013). The Arf GAP AGAP2 interacts with beta-arrestin2 and regulates beta2-adrenergic receptor recycling and ERK activation. Biochem. J. *452,* 411-421.

VII. Appendix 2: ATP7B Forms Oligomers in a Cell

Introduction

ATP7B is a P-type ATPase that uses ATP hydrolysis to transport copper across membranes; mutations result in copper accumulation in the body (Wilson's disease) (Gupta et al., 2011). ATP7B has a dual localization in hepatocytes. Under basal conditions ATP7B transports copper into the TGN (trans Golgi network) and under elevated copper conditions ATP7B traffics from the TGN to endocytic vesicles, which accumulate copper and then fuse with the apical plasma membrane to excrete copper out of the cell (Roelofsen et al., 2000). Thus, ATP7B trafficking is essential for the regulation of intracellular copper levels. The mechanism that controls the copper-dependent exit of ATP7B from the TGN is not yet fully characterized. Copper-binding, kinase mediated phosphorylation levels, changes in inter-domain interactions, and interactions with accessory proteins play a role in facilitating the exit of ATP7B from the TGN; however the exact mechanism and sequence of events is not yet fully understood (Guo et al., 2005; Lim et al., 2006a; Lim et al., 2006b; Materia et al., 2012; Tao et al., 2003; Tsivkovskii et al., 2001; Vanderwerf et al., 2001).

Protein dimerization/oligomerization may enhance recruitment of trafficking machinery and be part of the mechanism that governs the TGN exit of ATP7B. A bacterial homologue of ATP7B (CopA) forms dimers as demonstrated by cryoelectron microscopy and reconstitution (Wu et al., 2008); existence of P-type ATPases (such as Na,K-ATPase and H+-ATPase) as oligomeric structures has been actively discussed in the literature. Whether mammalian ATP7B can form dimers, and whether these dimers are

physiologically relevant was unknown. This section describes experiments testing oligomerization state of ATP7B in mammalian cells.

Results

ATP7B exists in multimeric complexes in cells

We hypothesized that dimerization/oligomerization might be a novel mechanism regulating ATP7B trafficking. We analyzed the possibility of endogenous ATP7B forming higher molecular weight complexes in cells under native conditions. First we determined the apparent molecular mass of ATP7B following solubilization with mild detergent that retains tetrameric protein organization. The membranes obtained from HepG2 cells were resuspended using n-Dodecyl β-D-maltoside (DDM) and run on blue native gels (BN-PAGE). BN-PAGE is an electrophoretic technique that allows separation of multiprotein complexes in a native conformation (Schagger and von Jagow, 1991).

Our results suggested that the endogenous ATP7B exists in at least two forms: a monomeric form (around 230kDa) and in a higher molecular weight complex (around 480kDa), which could be a dimeric form of ATP7B (Fig. 7-1). We used three different antibodies of ATP7A to determine the size of ATP7B under native conditions. The dimeric structure was recognized primarily by the NBD-antibody, directed against the central portion of the molecule (Fig. 7-1b) and anti-C-terminus antibody (Fig. 7-1c). Staining of the high-molecular weight band with the anti-N-terminal antibody was weak implying that the N-terminus of ATP7B might be at the interface of the dimeric structures. We have shown for the first time that ATP7B can exist as multimeric

complexes in cells and we are interested in determining the role of the dimeric ATP7B complexes in cells.

Transfected wt-ATP7B and mutated-ATP7B can bind to each other and influence their localization

We tested whether the recombinant ATP7B variants that usually localize to different parts of the cell can colocalize in the same compartment as a result of interaction during co-transfection/co-expression. For these experiments, Hek293T cells were cotransfected with WT GFP-ATP7B (normally localized in TGN) (Fig. 7-2a) and Flag-ATP7B$^{R875,S340/341G}$ (normally localized in vesicles) (Fig. 7-2b) and the localization of both proteins was assessed. We observed that in the majority of cotransfected cells, both proteins colocalize, strongly suggesting their interaction. The localization pattern showed staining of both TGN or to vesicles, implying that two ATP7B variants not only interact but alter each other's localization in cells (Fig. 7-2c). In 30-40% of the cells, no significant colocalization was observed, suggesting that the level of expression and ratio of the proteins might be important for the multimer formation. To further verify potential interaction we performed immunoprecipitation experiments. GFP-ATP7B was co-immunoprecipitated with Flag-ATP7B in cotransfected cells, suggesting that ATP7B proteins do interact with each other.

Discussion

We have shown for the first time that ATP7B can exist in dimeric forms in cells using blue native-PAGE and cotransfection studies. Future studies will be focused on

determining whether the dimer formation depends on the copper-dependent trafficking of ATP7B to vesicles in cells and to identify the regions involved in dimer formation.

The mechanism of ATP7B trafficking to vesicles in response to copper has not been identified yet. We would like to determine if the dimer formation of ATP7B is physiologically relevant and how it affects dimer formation of ATP7B affects copper homeostasis. The dimer formation of ATP7B can be a novel mechanism, which might be involved in regulating the trafficking and/or copper transport function of ATP7B.

Materials and Methods

Cell lines: HepG2 cells (obtained from ATCC) were maintained in DMEM supplemented with 10 % FBS and 1 % pen/strep at 37 ºC in a 5% CO_2 incubator. Hek293TRex cells were maintained in MEM supplemented with 10 % FBS, 1 % pen/strep, 1 % non-essential amino acids, 12.5 μg/mL blasticidin and 100 μg/mL zeocin. During experiments media without blasticidin and zeocin was used.

Analysis of cell lysates using BN-PAGE: Cells were harvested, homogenized in a homogenizing buffer (25 mM imidazole, 0.25 M sucrose, 1 mM AEBSF and protease inhibitor tablets (Roche)) using a Dounce homogenizer with 40 strokes of a tight-fitting pestle. The lysate was centrifuged at 700 g for 10 min at 4°C to pellet cell debri and nuclei. The postnuclear supernatant was centrifuged at 3,000 g for 10 min at 4°C to pellet mitochondria. The resulting supernatant was then centrifuged at 20,000 g for 30 min at

4°C to pellet down the microsomal membranes. Protein concentration of the microsomal membranes was determined using a Bradford assay (Pierce). 15 µg of the pellet was resuspended in solubilizing buffer (1%DDM, 50mM Bis-Tris, 50mM NaCl, 10% w/v glycerol, 0.001% Ponceau S, pH 7.2) in a total volume of 15 µl and incubated for 1 h on ice. 1X of 10X loading dye (5% coomassie G250, 500mM aminocaproic acid) was added to the mixture, and it was loaded to 4-16% native gradient gel (Invitrogen). Proteins were transferred to a PVDF membrane using CAPS buffer, pH 11.0. The membrane was probed using rat anti N-terminus antibody (1:3000), rabbit- anti-NBD (nucleotide binding domain) antibody (1:3000) or an guinea pig anti C-terminus antibody (1:3000) of ATP7B. Goat anti rat Igg-HRP (1:10000, Santa Cruz), donkey anti rabbit Igg-HRP (1:10000, Santa Cruz), or donkey anti guinea pig Igg-HRP (1:10000, Santa Cruz) was used as a secondary antibody and the membranes were developed using a SuperSignal West Pico Substrate (Thermo Scientific).

Immunofluorescence microscopy: Hek293TRex cells on coverslips were transiently transfected with the wt GFP-ATP7B or mutant Flag-ATP7B$^{R875,S340/341G}$ using Turbofect. Protein expression of Flag-ATP7B$^{R875,S340/341G}$ was induced with 40 ng/ml DOX for 16 h in basal conditions. Cells were rinsed with PBS and fixed with in cold acetone-methanol mixture (1:1) for 30 sec. The cells were blocked in blocking buffer (1 % gelatin, 1 % BSA in PBS) and then incubated with appropriate primary and secondary antibodies diluted in blocking buffer. (Primary antibody: mouse anti-Flag antibody 1:250 (Sigma) and rabbit anti-TGN 46 1:300 (Genetex). Secondary antibody: Alexa Fluor 488 Goat anti mouse antibody 1:500 (Invitrogen) and Alexa Fluor 555 goat anti sheep 1:500 (Invitrogen)). Coverslips were mounted onto glass slides using

Vectashield w/DAPI (Vector Laboratories). Images were taken using a Zeiss PALM confocal microscope and a 100x oil immersion objective.

Co-immunuprecipitation of GFP-ATP7B: Hek293Trex cells were transiently transfected with the wt GFP-ATP7B or mutant Flag-ATP7B$^{R875,S340/341G}$ using Turbofect. Protein expression of Flag-ATP7B$^{R875,S340/341G}$ was induced with 40 ng/ml DOX for 16 h in basal conditions. Cells were rinsed with PBS and microsomal membranes were isolated as described above. The pellet was resuspended in 100 µl of IP buffer (150 mM NaCl, 10 mM Tris-HCl, 2 mM EDTA (pH 7.5), 1 % *n*-Dodecyl β-D-maltoside (DDM) (Sigma), protease inhibitor tablets (Roche)). 200 µl of blocking buffer (3 % BSA in PBST) was added. After 5 min, 2.5 µl of anti-Flag antibody (Sigma) was added and rotated for 1 h at room temperature. 55 µl of pre-equilibrated protein G resin (Thermo Scientific) was added and rotated for 1 h at RT. The resin was washed with 20 column volumes of PBS and the bound protein was eluted using 60 µl of elution buffer (0.17 M Tris, pH 6.8, 6.8 % SDS, 2.7 M urea, 1:100 β-mercaptoethanol). 24 µl of the eluted protein was loaded to a 4-20% TGX gel (Bio-Rad). The proteins were transferred to PVDF membrane using a 10 mM CAPS, pH 11 transfer buffer. Immunoblotting was done using rabbit anti-GFP antibody (1:2000 Invitogen) as primary antibody, and HRP-conjugated goat anti-rabbit IgG (1:10,000) (Santa Cruz) as a secondary antibody. The membranes were developed using a SuperSignal West Pico Substrate (Thermo Scientific).

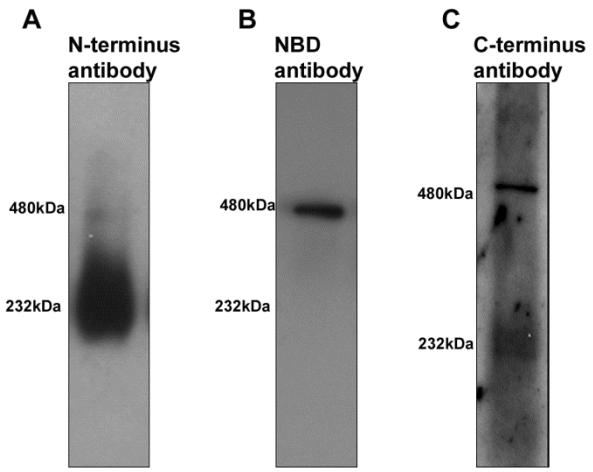

Figure 7-1. ATP7B exists in high molecular weight complexes. Membrane preparations from HepG2 cells were solubilized with 1% DDM and run on a blue native gel. The Western blot was immunoblotted using an anti N-terminus antibody (a), anti-NBD (nucleotide binding domain) antibody (b) or an anti C-terminus antibody of ATP7B.

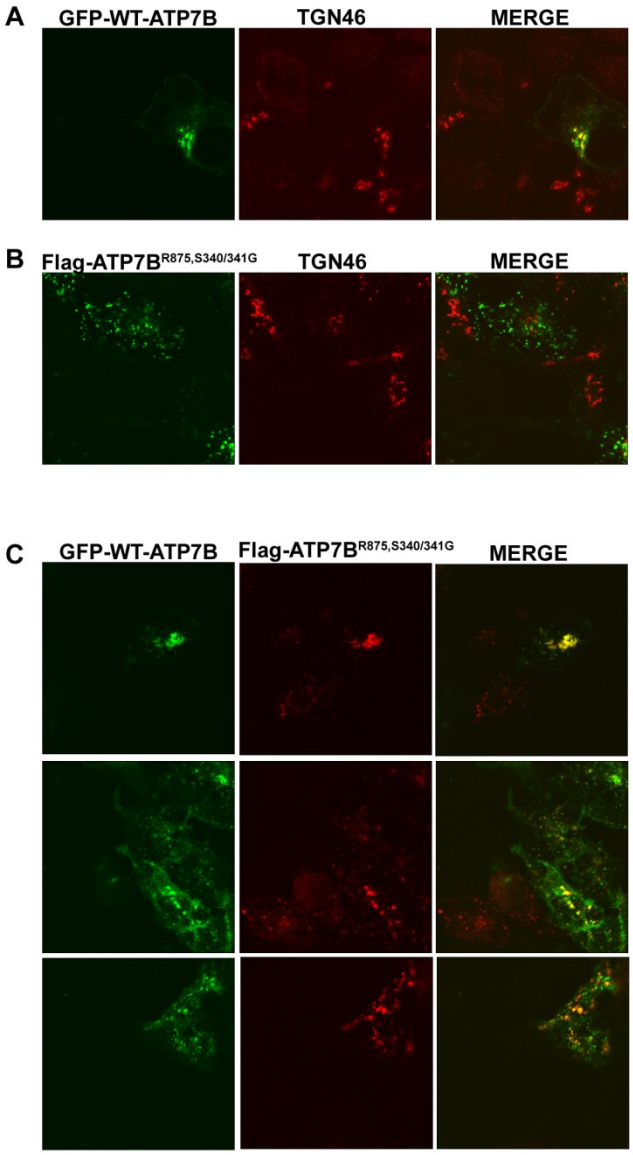

Figure 7-2. ATP7B can form dimers in cells. Hek293Trex cells were transfected or cotransfected with WT-GFP ATP7B and Flag-ATP7B$^{R875,S340/341G}$. Cells were fixed and immunostained using anti-Flag and anti-TGN46 antibody. (a) WT-GFP ATP7B localizes to TGN. (b) Flag-ATP7B$^{R875,S340/341G}$ localizes to vesicles. (c) Representative images of cells cotransfected with both WT-GFP ATP7B (green) and Flag-ATP7B$^{R875,S340/341G}$ (red). In most cells both ATP7B constructs colocalize either at the TGN region (upper panel) or in vesicles (middle, low panel).

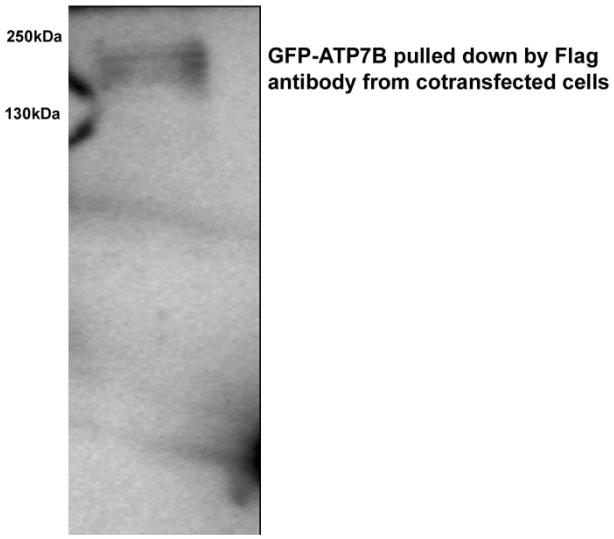

Figure 7-3. A. GFP-ATP7B interacts with Flag-ATP7B. Hek293Trex cells were cotransfected with GFP-ATP7B and Flag-ATP7B ATP7B. Membrane preparations were co-immunoprecipitated using anti-Flag antibody. Shown is a Western blot blotted with anti-GFP antibody.

Reference List

Guo, Y., Nyasae, L., Braiterman, L.T., and Hubbard, A.L. (2005). NH2-terminal signals in ATP7B Cu-ATPase mediate its Cu-dependent anterograde traffic in polarized hepatic cells. Am. J. Physiol. Gastrointest. Liver Physiol. *289,* G904-16.

Gupta, A., Bhattacharjee, A., Dmitriev, O.Y., Nokhrin, S., Braiterman, L., Hubbard, A.L., and Lutsenko, S. (2011). Cellular copper levels determine the phenotype of the Arg875 variant of ATP7B/Wilson disease protein. Proc. Natl. Acad. Sci. U. S. A. *108,* 5390-5395.

Lim, C.M., Cater, M.A., Mercer, J.F., and La Fontaine, S. (2006a). Copper-dependent interaction of dynactin subunit p62 with the N terminus of ATP7B but not ATP7A. J. Biol. Chem. *281,* 14006-14014.

Lim, C.M., Cater, M.A., Mercer, J.F., and La Fontaine, S. (2006b). Copper-dependent interaction of glutaredoxin with the N termini of the copper-ATPases (ATP7A and ATP7B) defective in Menkes and Wilson diseases. Biochem. Biophys. Res. Commun. *348,* 428-436.

Materia, S., Cater, M.A., Klomp, L.W., Mercer, J.F., and La Fontaine, S. (2012). Clusterin and COMMD1 independently regulate degradation of the mammalian copper ATPases ATP7A and ATP7B. J. Biol. Chem. *287,* 2485-2499.

Roelofsen, H., Wolters, H., Van Luyn, M.J., Miura, N., Kuipers, F., and Vonk, R.J. (2000). Copper-induced apical trafficking of ATP7B in polarized hepatoma cells provides a mechanism for biliary copper excretion. Gastroenterology *119,* 782-793.

Schagger, H., and von Jagow, G. (1991). Blue native electrophoresis for isolation of membrane protein complexes in enzymatically active form. Anal. Biochem. *199,* 223-231.

Tao, T.Y., Liu, F., Klomp, L., Wijmenga, C., and Gitlin, J.D. (2003). The copper toxicosis gene product Murr1 directly interacts with the Wilson disease protein. J. Biol. Chem. *278,* 41593-41596.

Tsivkovskii, R., MacArthur, B.C., and Lutsenko, S. (2001). The Lys1010-Lys1325 fragment of the Wilson's disease protein binds nucleotides and interacts with the N-terminal domain of this protein in a copper-dependent manner. J. Biol. Chem. *276,* 2234-2242.

Vanderwerf, S.M., Cooper, M.J., Stetsenko, I.V., and Lutsenko, S. (2001). Copper specifically regulates intracellular phosphorylation of the Wilson's disease protein, a human copper-transporting ATPase. J. Biol. Chem. *276,* 36289-36294.

Wu, C.C., Rice, W.J., and Stokes, D.L. (2008). Structure of a copper pump suggests a regulatory role for its metal-binding domain. Structure *16,* 976-985.

VIII. Curriculum Vitae

CURRICULUM VITAE

Nesrin Hasan

08/05/2014

Education:

Ph.D. expected	2014	Cellular and Molecular Physiology Graduate Program (Mentor: Dr. Svetlana Lutsenko)	Johns Hopkins University, Baltimore MD, USA
M.S.	2008	Biological Recognition Program	Jacobs University Bremen, Germany
B.S.	2006	Molecular Biology and Genetics, Minor degree in Chemistry	Middle East Technical University, Ankara, Turkey

Research Experience:

Graduate Student	2008-2014	Mentor: Dr. Svetlana Lutsenko, Department of Physiology, School of Medicine, Johns Hopkins University, Baltimore MD, USA
Research Trainee	2007-2008	Mentor: Dr. Kristine Glunde, Department of Radiology, School of Medicine, Johns Hopkins University, Baltimore MD, USA
Graduate Student	2006-2008	Jacobs University Bremen, Bremen, Germany
Intern	2005	Department of Biochemistry, Pharmacology and Toxicology of Leipzig University, Leipzig, Germany

Academic Honors, Scholarships and Awards:

Graduate Student Travel Award, Johns Hopkins School of Medicine, 2010

Full term tuition waiver by Johns Hopkins University, 2008-2014

Full term tuition waiver by Jacobs University Bremen for M.Sc. studies, 2006-2008

Nominated for and attended the 57th Meeting of Nobel Laureates in Physiology or Medicine, Germany, 2007

Publications:

Malinouski, M, **Hasan, NM**, Zhang, Y, Seravalli J, Lin, J, Avanesov, A, Lutsenko, S, Gladyshev, VN. (2014) Genome-Wide RNAi Ionomics Screen Reveals New Genes and Regulation of Human Trace Element Metabolism *Nat Commun.* Feb 13;5:3301

Hasan, NM, Gupta, A, Polishchuk, E, Yu, CH, Polishchuk, R, Dmitriev, OY, and Lutsenko, S. (2012) Molecular Events Initiating Exit of a Copper-transporting ATPase ATP7B from the Trans-Golgi Network. *J Biol Chem.* 287(43):36041-50.

Hatori, Y, Clasen, S, **Hasan, NM**, Barry, AN, and Lutsenko, S. (2012) Functional partnership of the copper export machinery and glutathione balance in human cells. *J Biol Chem.* 287, 26678-26687

Book Chapters:

Hasan NM, Lutsenko S. (2012) Regulation of copper transporters in human cells. *Curr Top Membr.* 69:137-61.

Abstracts:

Hasan, NM., Gupta, A., Polishchuk, E., Yu, CH., Polishchuk, R., Dmitriev, OY., and Lutsenko, S., (2012) Molecular Events Initiating Exit of a Copper-transporting ATPase ATP7B from the Trans-Golgi Network, Federation of American Societies for Experimental Biology (FASEB) New Frontiers in Transport ATPases: From Mechanistic to Therapeutic Concepts, Snowmass Village CO, USA

Hasan NM., Gupta A., Lutsenko S., (2010) The role of Serine residues in the loop connecting MBDs 3 and 4 in phosphorylation and intracellular targeting of the copper transporter ATP7B, 2010 American Society for Cell Biology (ASCB) Annual Meeting, Philadelphia PA, USA

Hasan NM., Greenwood T., Glunde K., (2008) V-ATPase inhibition results in lysosome swelling followed by lysosomal membrane permeabilization in breast cancer cells, Invasion and Metastasis Conference, Berlin, Germany

Conference Presentations:

Molecular Events Initiating Exit of a Copper-transporting ATPase ATP7B from the Trans Golgi Network, Federation of American Societies for Experimental Biology (FASEB) New Frontiers in Transport ATPases: From Mechanistic to Therapeutic Concepts, June 2012, Snowmass Village CO, USA (selected for oral presentation from the submitted abstracts)

Teaching Experience:

Completed the 'Preparing Future Faculty Teaching Academy Program' offered at Johns Hopkins University, Baltimore MD, USA (2013-2014)

Participated in 'Inaugural Science of Learning Symposium and 3rd Annual Symposium on Excellence in Teaching and Learning in the Sciences', Johns Hopkins University, Baltimore MD, USA (January 2014)

Participated in 'Summer Teaching Camp' organized by Institute for Excellence in Education (IEE) and the School of Medicine of Johns Hopkins University, Baltimore MD, USA (July 2013)